Physical consequences of black holes in non-perturbative quantum gravity and inflationary cosmology

Physical consequences of black holes in non-perturbative quantum gravity and inflationary cosmology

Paul Reska

Ph.D. Thesis Utrecht University, February 2011
ISBN: 978-94-610-8145-2

Physical consequences of black holes in non-perturbative quantum gravity and inflationary cosmology

Fysische gevolgen van zwarte gaten in niet-perturbatieve kwantumgravitatie en kosmologische inflatie

(met een samenvatting in het Nederlands)

Proefschrift

ter verkrijging van de graad van doctor aan de Universiteit Utrecht op gezag van de rector magnificus, prof.dr. J.C. Stoof, ingevolge het besluit van het college voor promoties in het openbaar te verdedigen op maandag 28 februari 2011 des ochtends te 10.30 uur

door

Paul Marek Reska

geboren op 4 mei 1981
te Katowice, Polen

Promotor: Prof.dr. R. Loll

The work described in this thesis was partially funded through the European Network on Random Geometry ENRAGE, contract MRTN-CT-2004-005616.

Contents

Chapter 1

Introduction

General Relativity

The formulation of Einstein's General Theory of Relativity in 1915 was a milestone in the history of physics. Not only does it reproduce Newtonian gravity in the limit of weak fields but it also makes several predictions of effects which cannot be explained by Newtonian gravity and which have been successfully tested (see [1] for a review). Einstein's field equations relate the stress-energy tensor of matter to the curvature of space-time. By 1916 a very important solution had been found by Schwarzschild under the assumption of spherical symmetry and in vacuum. The Schwarzschild solution allowed the first important test of the theory which is the bending of light by the gravitational field of our sun. Only in 1958 was it realized that the full extension of this solution describes what is known today as a black hole [2]. It has been shown that black holes generically form from the collapse of matter and that a space-time singularity in the center is created where the curvature becomes infinite [3, 4].

Applying the laws of General Relativity to the universe as a whole leads to the conclusion that its overall scale is dynamical. The expansion of this scale is usually described in terms of a time-dependent scale factor. In the first years after the formulation of Einstein's theory it was assumed that the universe is static. It is a curious fact that Einstein introduced the cosmological constant to try to allow for static solutions of his equations. Observations of the redshift of light from distant galaxies in the years 1910 to 1924, however, gave evidence for an expansion of the universe[1] [5]. The experimental and theoretical study of this expansion has grown into the rich field of cosmology. It has been a longstanding goal to trace back the history of the universe all the way from today to the first moments after the Big Bang. Cosmology has been further nourished by the discovery of the cosmic microwave background (CMB) radiation [6] which provides us with information about the state of the universe at a very

[1] As a reaction to this discovery, Einstein dismissed the cosmological constant term.

early stage. Precision measurements of the CMB have shown that the early universe was homogeneous to a very high degree [7]. It is generally believed that small field fluctuations around an otherwise homogeneous background during an early period of rapid expansion called inflation are the seeds of the large scale structure that we observe today [8]. A simplified description for the inflationary universe is given in terms of de Sitter space which exhibits an exponential expansion.

A general lesson from General Relativity is that space-time is dynamical and described by a local field. The space-time geometry is determined by the matter distribution in the universe via Einstein's equations. On the other hand, we know that on a fundamental level matter is best described by a quantum field theory. This quantum mechanical treatment of matter does not seem to make it possible to take into account its backreaction on the classical space-time in Einstein's theory. In particular, the field equations are inconsistent if the Einstein tensor that determines the classical geometry is equated to the operator-valued stress-energy tensor of quantum fields. One option is to simply substitute the stress-energy of the quantum fields by its expectation value [9]. However, this semiclassical approach is rather a mean field approximation and is not likely to be fundamental. In view of these problems, a unified description of space-time and matter thus seems to require a quantization of gravity. This implies that space-time exhibits a non-trivial quantum behavior on short scales which can be probed by high energies. A natural scale for quantum gravity is set by combining the speed of light c, Planck's constant $\hbar$ and Newton's constant G to the Planck mass $m_P = \sqrt{\hbar c/G} \simeq 1.2 \times 10^{19}\,\mathrm{GeV}/c^2$. It is expected that, in the first moments after the Big Bang, the universe was in an ultra-hot state where energies of this magnitude played a role and quantum gravity effects were indeed important. Furthermore, indirect evidence that gravity should be quantized is provided by scalar cosmological perturbations produced during inflation (this will be discussed below). As the universe expanded it cooled down and entered a subsequent phase in which particles are generally described in a Grand Unified Theory (GUT) [10, 11]. Today's standard model of particle physics is assumed to result from symmetry breaking that occurred during a phase transition as the universe cooled down even more.

Quantum gravity

Research in quantum gravity has so far been only theoretical because the necessary energy scale is out of reach. Currently, the most powerful accelerator experiment is the Large Hadron Collider (LHC) at CERN which will achieve a total collision energy of up to 14 TeV. This is still 16 orders of magnitude below the Planck scale. It is also not realistic that any new generation of accelerators will come even close to this scale. Rather, it is expected that quantum gravity effects might become important in the

setting of cosmology and astrophysics. One example of an effect where both gravity and quantum matter play a role is the evaporation of black holes and was proposed by Hawking in [12]. In this work quantum field theory is studied on a fixed curved background space-time, namely, that of a Schwarzschild black hole. However, this approach has to be regarded as an effective description of the combined matter-gravity system rather than genuine quantum gravity, since the backreaction of the quantum field on the geometry is neglected. Other conjectured phenomenological consequences of quantum gravity include violations of Lorentz invariance (see [13] for a recent overview).

While input from observations is pending, a lot of progress has been made in the theoretical understanding of quantum gravity. Linearized gravity on a fixed background space-time with scalar matter has been shown to define a non-renormalizable quantum field theory at one-loop level [14, 15]. In addition, the non-renormalizability of pure gravity at two-loop level was demonstrated in [16, 17] (see also [18] for a pedagogical review). It is possible to work with such a theory as an effective field theory without having access to the physics in the far UV [19]. But, in order to define a theory that is valid even at the Planck scale, several other approaches have been developed. The most popular theory that is expected to describe gravity in a quantum mechanical setting is string theory (for common textbooks see [20, 21] and [22, 23]). In string theory the assumption is made that matter consists of extended objects whose different vibrational modes correspond to elementary particles. The presence of a massless spin-2 particle in the spectrum strongly suggests that string theory actually incorporates General Relativity. Another well-known approach is loop quantum gravity which is background-independent. In this approach space-time is split into space and time within a first-order formalism using Ashtekar connection variables which obey first-order equations [24]. The rules of canonical quantization are then applied to obtain a quantum theory of gravity [25]. Moreover, attempts have also been made to study gravity in a non-perturbative and background independent way by lattice methods. One example is the application of Regge calculus [26] to perform a non-perturbative sum ("path integral") over piecewise flat geometries which differ only by the lengths of the links of the lattice [27]. While Regge calculus arises from the discretization of the metric formulation of General Relativity, the discretization of the first-order formalism is the starting point of spin foam models [28]. Yet another possibility is to consider a lattice discretization of space-time with all link lengths being equal, but summing over different ways of gluing the flat fundamental building blocks, which are taken to be four-simplices. In this way, the physical degrees of freedom are encoded in the connectivity of the triangulation. This defines the dynamical triangulations approach which we are now going to discuss in more detail.

Dynamical triangulations

Lattice methods have initially been developed and used for quantum chromodynamics (QCD) which is strongly coupled at low energies and is difficult to deal with perturbatively [29]. One implementation of a lattice regularization adapted to the case of gravity is given by the dynamical triangulations approach to quantum gravity and has been developed first in form of two-dimensional random surface models [30, 31, 32]. In contrast to the rigid lattice that is used for studying QCD, the lattice used for gravity implements different geometric configurations and, therefore, is dynamical. In early works on dynamical triangulations an ensemble of *Euclidean* geometries has been taken as the starting point. Thus, the sum over geometries is simply a partition function as we know it from statistical physics. This makes it possible in principle to determine numerically the expectation values of geometric observables which are the objects of interest in quantum gravity and which currently cannot be determined with perturbative methods. One such observable is the spectral dimension, which is a measure of the local properties of space-time and can be obtained from the return probability of a random walk on the simplicial manifold [33]. The method of dynamical triangulations has the nice property of being manifestly coordinate invariant which means that one does not have to deal with unphysical gauge degrees of freedom. Of course, all physical quantities have to be independent of arbitrary discretization details. This can only be achieved if the lattice spacing is seen as a UV cut-off rather than the scale of fundamental discreteness. It has been shown, however, that in the four-dimensional dynamically triangulated Euclidean model none of the two existing phases resembles on large scales a classical four-dimensional space-time. In one of them, the crumpled phase, space-time is effectively infinite-dimensional due to the presence of singular vertices with a very high connectivity. In the other phase, the branched polymer phase, space-time is effectively two-dimensional [34, 35].

In order to cure these deficiencies, a new model of dynamical triangulations which excludes causality violating geometries from the sum has been developed in [36, 37]. In the continuum, causality is violated if, e.g., during time evolution the universe splits into several pieces, thereby creating so-called baby universes. In this case there necessarily exist space-time points where the light-cone (and therefore the causal structure of space-time) becomes degenerate. On the lattice side the restriction translates into the requirement that the triangulated geometries which are summed over in the path integral have a time-slicing and fixed spatial topology. Numerical simulations of Causal Dynamical Triangulations (CDT) in four dimensions have exhibited a different and richer phase structure as compared to the Euclidean model. In fact, an additional phase is present with four-dimensional extended universes that appear to be classical on large scales. The large-scale shape of the emergent background geometry turns out

to be that of a de Sitter space [38, 39]. More specifically, measuring the expectation value of the spatial volume (after Wick rotation) at different time steps yields a volume profile which shows that the background is the round four-sphere, or, equivalently, Euclidean de Sitter space.

Matter-coupling with dynamical triangulations

The insight that the pure gravity CDT model has a good classical limit allows us to take a further step and ask the same question for the matter-coupled model. Since quantization of gravity is a challenging task in itself, most models are studied without taking matter degrees of freedom into account. Of course, to achieve a realistic picture of our world these degrees of freedom have to be included. Matter coupling in form of a scalar field has been studied in the non-perturbative setting of loop quantum gravity in [40]. On the other hand, in the framework of dynamical triangulations, dynamical, coupled gravity-matter systems are set up by simply extending the sum over all geometries to a double-sum over all geometrical *and* matter field configurations (for a spin, scalar or gauge field, say). This has already been demonstrated in the corresponding *Euclidean* quantum gravity models in four dimensions. In [41], for instance, the phase structure of the model is explored for the case of matter-coupling in form of an Ising spin and a Gaussian scalar field. The original hope of an interesting continuum limit at the transition point between the two phases described above could not be confirmed. In this sense, the inclusion of the matter field does not change the geometry in a significant way. In [42] the effect of $U(1)$ gauge fields on the geometry was found to be strong. For more than two gauge fields, the branched polymer phase seems to be substituted by a phase with Hausdorff dimension close to four. This was determined from the scaling of the average distance between simplices with their total number. However, this effect was attributed later to a change in the path integral measure and considered as irrelevant to IR physics [43].

Obviously, an analogous procedure for matter coupling can be set up in the model of *causal* dynamical triangulations where in addition a time slicing is available for studying the properties of the geometry. In order to include a scalar field, for instance, one simply has to add the discretized version of the scalar field action to the gravitational action. This way its influence on the geometry can be tested. The presence of a matter field should not change the spectral dimension on large scales if the classical limit is correct. By the same reasoning, looking at global properties of the average geometry, the volume profile obtained from CDT should match with the volume profile of the corresponding Euclideanized solution to Einstein's equations. In this thesis, a particular situation is studied in which, instead of a scalar field, a localized mass distribution is considered. Compared with the matter-free case, the mass introduces an

inhomogeneity in the geometry of the spatial slices, but preserves spherical symmetry. This situation is of great physical relevance because it corresponds to the gravitational field of any spherically symmetric mass distribution in a universe with a positive cosmological constant. The latter is inherent in the CDT model. We shall call such a mass distribution a point-like mass. The corresponding classical solution to Einstein's equations is the Schwarzschild-de Sitter space. While being described by a simple metric this solution entails other difficulties. Namely, taking the radius of the mass distribution to be sufficiently small forces us to deal with the presence of an event horizon which means that we are considering a black hole. The goal is then to determine the effect of a black hole on meaningful and computationally accessible observables in non-perturbative quantum gravity.

Unlike the previously mentioned work on dynamical matter fields, very little is known about the coupling of point or point-like masses to quantum gravity in four dimensions. Inclusion of point particles is common in discussions of both classical and quantum three-dimensional gravity [44]. The three-dimensional theory has no local degrees of freedom and therefore is significantly different from the four-dimensional one, already at the classical level. The inclusion of point particles is simplified by the fact that their presence only creates conical defects [45, 46], and not stronger curvature singularities like in higher dimensions. Quantization of three-dimensional gravity with point particles has been discussed early on in [47, 48] and more recently in the contexts of loop quantum gravity [49] and the Ponzano-Regge spin foam model [50].

One focus of the work presented in this thesis is the identification of an observable that is sensitive to the mass and the derivation of its classical properties. With these results the classical limit of the CDT model coupled to the mass-line can actually be tested. We emphasized already that this model aims at describing the physics in the very early universe where quantum gravity effects play a major role. As cosmic time moves on, the temperature decreases and such effects become more and more subdominant. The physically relevant question becomes how inflation was initiated and how field fluctuations caused the formation of structure that we observe in the universe today. While these so-called cosmological perturbations are usually studied on a homogeneous background, inhomogeneities from monopoles and black holes might also play an important role. The appropriate description for the case of black holes in inflation is again the Schwarzschild-de Sitter space. Monopoles in inflation, on the other hand, are asymptotically well described by the Reissner-Nordström-de Sitter space. The second part of this thesis deals with the effect of small inhomogeneities of this kind on cosmological perturbations.

Cosmological perturbations

It is generally believed that the early universe underwent a very short period of nearly exponential expansion called inflation. The original motivation for this scenario was the claim that it solves a number of puzzles in cosmology: the flatness problem, the horizon problem and the magnetic monopole problem [51, 52]. In a universe that is always dominated by matter or radiation we would expect a high spatial curvature in the present state of our universe, large inhomogeneities and a possible abundance of monopoles. The absence of large inhomogeneities in the cosmic microwave background (CMB) radiation, for instance, cannot be explained if different regions on the CMB sky have never been in causal contact. According to the inflationary scenario, all of the universe that we can observe was contained inside of a region that was smaller than the horizon size and thus could homogenize due to interactions. It should be emphasized, however, that inflationary scenarios suffer from fine tuning problems [53]. This has led to a different view on the inflationary paradigm, namely, the main motivation has become the explanation that inflation offers concerning the properties of small temperature fluctuations in the CMB and the formation of large scale structure [54, 8].

Most models of inflation are realized by a scalar field, the inflaton[2], which slowly rolls down a potential[3] [52, 55, 56]. From the Friedmann equations that describe the evolution of a homogeneous universe in time it can be seen that the large potential energy of the inflaton generates a rapid expansion which is well-approximated by de Sitter space. A semiclassical treatment of the inflaton field allows us to split it into a mean field configuration and field fluctuations which are dynamical and quantized. In addition to the fluctuations of the inflaton also metric perturbations play an important role in inflation. According to the decomposition theorem, the scalar, vector and tensor modes decouple on a homogeneous background [57]. In fact, only the tensor modes and a gauge invariant scalar, the Sasaki-Mukhanov field or scalar cosmological perturbation $\mathcal{R}$ [54, 58], are dynamical. This scalar field is a combination of the scalar gravitational potential and the fluctuation in the inflaton field.

It is convenient to look at these perturbations in momentum space and associate physical wavelengths to their Fourier modes. These physical wavelengths grow with the scale factor and during inflation the modes are stretched and exit the horizon, which remains at an almost constant physical scale. After this short period of inflation the universe enters a phase of radiation domination, which is followed by matter domination

[2]The inflaton particles have by now decayed into particles of the standard model.

[3]In contrast to this slow-roll inflation scenario stands Guth's initial proposal [51] which is now referred to as 'old inflation' and involves a tunneling process for the inflaton from a false vacuum phase to a true vacuum phase. Today's view on the initial proposal is that such a phase transition would lead to a highly inhomogeneous and anisotropic universe that we do not observe.

and the physical scale of the horizon grows. Thus, eventually, the modes re-enter the horizon and become observable to us.

The power spectrum $\mathcal{P}_\mathcal{R}(k)$ of the scalar cosmological perturbation $\mathcal{R}$ is defined from the two-point correlation function

$$\langle\Omega|\mathcal{R}(\vec{x},\eta)\mathcal{R}(\vec{x}',\eta)|\Omega\rangle = \int \frac{dk}{k}\,\mathcal{P}_\mathcal{R}(k,\eta)\,\frac{\sin(kr)}{kr}\,, \tag{1.1}$$

where $r = \|\vec{x}-\vec{x}'\|$ and $|\Omega\rangle$ is a suitably chosen vacuum state. In fact, the measured CMB anisotropies are directly related to this power spectrum. The spectral index n_s measures the scale dependence of the power spectrum

$$n_s(k) - 1 = \frac{d\log\mathcal{P}_\mathcal{R}(k)}{d\log k} \tag{1.2}$$

and is itself in general scale dependent. Assuming that the spectral index is constant (or taking its IR limit $k \to 0$), there are only two free parameters that specify the power spectrum: its amplitude $\Delta_\mathcal{R}$ and the spectral index. If one makes this assumption then the best fit to the WMAP seven-year data [59] gives a value of

$$n_s = 0.963 \pm 0.014\,(1\sigma)\,, \tag{1.3}$$

for the spectral index and $\Delta_\mathcal{R} = (2.43 \pm 0.11)\times 10^{-9}$ for the amplitude. Hence, there is indeed a small deviation from scale-invariance, $n_s = 1$, as predicted by inflation [60, 54].

In order to derive the power spectrum from theory, one has to take into account that the field fluctuations are quantized. Therefore, the quantum expectation value of fields evaluated at different positions but at equal time has to be determined, or, equivalently, we have to calculate the propagator with respect to a specific vacuum state. For a curved background, however, there is no unique choice of a vacuum state. In the case of cosmological perturbations the Bunch-Davies vacuum appears to be physically the most sensible choice because it minimizes the energy in the field fluctuations in the infinite past and reduces to the Minkowski vacuum [61].

The spectrum of scalar cosmological perturbations dominates over the spectrum of tensor perturbations in a slow-roll inflation scenario. However, tensor perturbations might provide invaluable insight regarding polarizations in the CMB. Indeed, it is the goal of the Planck mission to observationally verify the presence of anisotropies in parity violating B-modes and thus, indirectly, of tensor perturbations [62].

When studying field fluctuations on a curved background, the backreaction of the fields on the geometry is usually not taken into account in the literature on cosmological perturbations. This is justified as long as the local matter density is small. But the gravitational attraction of the perturbations might lead to a large local density which causes a gravitational collapse and the formation of black holes [63]. In this case the homogeneity assumption is strongly violated and the backreaction cannot be

neglected. These primordial black holes (PBHs) are presumably rather microscopic for two reasons. Firstly, by causality, the formation of large PBHs is prevented since only perturbations within a Hubble volume can contribute to the collapse. Secondly, the inhomogeneities on the CMB sky are very small which empirically excludes the presence of heavy objects during the inflationary era.

In the second part of this thesis, the effect of the presence of PBHs on the power spectrum of scalar cosmological perturbations will be studied. This may serve as a possibility to detect them from CMB anisotropies or simply to rule out their existence. Furthermore, breaking of homogeneity in the early universe could also be due to other relics like heavy particles or monopoles. In order to take their effect on cosmological perturbations, one has to determine the gravitational field they generate. This has been studied in [64] for the case of a monopole with the result that the field is regular in the interior and well-approximated by the Reissner-Nordström-de Sitter geometry in the asymptotic regime. Taking this fact as a starting point, the correction to the spectrum of scalar cosmological perturbations from the charge of a monopole will be investigated towards the end of this thesis.

An outline

This thesis is organized as follows. In Chapter 2 an introduction to Causal Dynamical Triangulations is given. It is argued that the four-dimensional model has a good classical limit in the absence of matter. Furthermore, we discuss the emergent background geometry arising from the non-perturbative sum over causal triangulations which on large scales can be identified with de Sitter space. For this the proper-time slicing present in CDT is translated to a proper-time slicing on the continuum de Sitter manifold. This slicing can be achieved by introducing Gaussian normal coordinates. We derive the volume profile of de Sitter space with respect to this slicing, which can be compared to the profile measured in numerical simulations of CDT.

In Chapter 3 we discuss matter coupling in CDT in form of a point-like mass. We focus on the derivation of the correction to the volume profile that is expected to be generated by this mass source. On the classical level the background geometry in the exterior region of such an object is given by the Schwarzschild-de Sitter solution. Unlike the de Sitter case, the proper-time slicing that is obtained by introducing Gaussian normal coordinates does not cover the entire space-time manifold. Indeed, close to the massive object the proper-time coordinates develop caustics and cannot be used to determine the volume profile exactly. An approximation scheme is presented in which the vicinity of the source is neglected. We derive a mass bound below which this approximation is valid and present the volume profiles for these small masses. Moreover, a possible implementation of the point-like particle in CDT in form of a

mass-line (representing the world-line of the mass) is discussed.

Chapter 4 deals with metric fluctuations on a homogeneous space-time manifold. The dynamics of these fluctuations is determined by expanding the Einstein-Hilbert action to quadratic order. Decomposing the metric perturbation into scalar, vector and tensor degrees of freedom it is seen that the modes decouple. In fact, it turns out that there are no physical degrees of freedom in the scalar and vector sector. The two physical degrees of freedom are the gauge invariant tensor modes and represent the two polarization states of the graviton. We canonically quantize these modes on a de Sitter background and derive the graviton spectrum from the two-point correlation function for the Bunch-Davies vacuum state.

In Chapter 5 the correction to the spectrum of scalar field fluctuations due to the presence of a primordial black hole is determined. These fluctuations can be used to determine scalar cosmological perturbations in the zero curvature gauge which cause the observed temperature fluctuations in the CMB. We estimate the formation probability of small black holes from Gaussian density fluctuations in the early universe. These black holes lose their mass during inflation as a result of Hawking radiation but for a certain range of small masses this effect can be neglected. Starting with the full Schwarzschild-de Sitter metric, coordinates are chosen such as to generalize the conformally flat de Sitter metric, and we then expand the resulting metric in a small mass parameter. The Keldysh propagator of a scalar field on this perturbed background is computed in momentum space to first order in this parameter. In order to regulate the Bunch-Davies vacuum state in the IR we consider the universe to be in a comoving box whose natural scale is set by the size of the horizon at the beginning of inflation. Taking the equal-time limit of the propagator we determine the correction to the spectrum and analyze it at different scales and for different choices of the position of the black hole from us.

Finally, chapter 6 contains the case of a charged massive object which breaks the translation invariance of de Sitter space and introduces a correction to the Keldysh propagator not only from its mass but also from its charge. The gravitational field is described by the metric in the interior of the 't Hooft-Polyakov monopole. Away from the origin it is given to very good approximation by the Reissner-Nordström-de Sitter solution. We derive the charge correction in momentum space to first order in a dimensionless charge parameter and the correction from the monopole interior. The relevance of these corrections for the spectrum is estimated from the suppression by different powers of small perturbation parameters present in the calculation.

Chapter 2

Quantum gravity from Causal Dynamical Triangulations

2.1 Causal Dynamical Triangulations

There has been growing interest in a non-perturbative formulation of quantum gravity in the last decades. Several candidate theories have emerged, among which is the Causal Dynamical Triangulations (CDT) programme. This approach implements a non-perturbative path integral quantization of gravity, where each contributing spacetime history carries a well-defined causal structure. In one of the phases of the underlying statistical model of 'random geometry' one has observed the formation of an extended universe with good classical properties. More specifically, it has been shown that both its Hausdorff [65] and spectral dimension [33] are four on large scales. Furthermore, the large-scale shape of this dynamically generated background geometry matches to great accuracy that of a de Sitter universe [38], corresponding to a universe with a positive (renormalized) cosmological constant, and the quantum fluctuations around it agree with predictions from a mini-superspace model [39].

The dynamics of CDT quantum gravity is defined directly on the space of geometries (in a continuum language: the space of metrics modulo diffeomorphisms) and forces one to tackle the issue of observables head-on, by giving measuring prescriptions for geometric observables whose expectation values with respect to the ensemble average over all spacetime geometries give nontrivial results. Examples of this are the dynamical dimensions mentioned above. In the CDT setting, another class of geometric quantities is accessible relatively easily, namely, those referring to the proper-time slicing that comes with the formulation.[1] This has been used previously in the pure-gravity theory

[1] One should keep in mind that geometric quantities associated with a spatial slice in Monte Carlo simulations of CDT will in general not correspond directly to properties of classical three-geometry; for this, they will usually need to be smeared out (coarse-grained) over some finite time-extension,

to study both the *volume profile* (the development $V_3(\tau)$ of the spatial three-volume as function of proper time τ) and the correlator of quantum fluctuations in the three-volume around the dynamically generated de Sitter background spacetime [38, 39].

After summarizing the main features of the CDT model we focus on an explicit derivation of the volume profile for Euclidean de Sitter space. For this we start with the metric in static coordinates and introduce Gaussian normal coordinates from a specific hypersurface. This work will be generalized in the following chapter which contains the derivation of such coordinates in the case that a mass is present.

2.1.1 Regularization of the gravitational path integral

Let us briefly review the motivation, implementation and the main results that the quantization programme of Causal Dynamical Triangulations has produced to date (for more in-depth reviews, see [67, 68, 69, 70, 71]).

Building on insights from general relativity and (canonical) quantum gravity, this approach uses nothing but standard quantum-field theoretic principles and methods, adapted to the situation where geometry is no longer part of a fixed background structure, but is itself dynamical. The basic quantum-dynamical principle it implements is the Feynman path integral, the "superposition of gravitational amplitudes" or "sum over histories"

$$Z = \int\limits_{[g]\in\mathcal{G}} \mathcal{D}g \; \mathrm{e}^{iS^{\mathrm{EH}}[g]}, \quad \text{with} \quad S^{\mathrm{EH}} = \frac{1}{G_N}\int d^4x\sqrt{-g}(R-2\Lambda)\,, \tag{2.1}$$

where each history is a spacetime geometry (a diffeomorphism equivalence class $[g]$ of metrics on a fixed manifold M, with $\mathcal{G}$ the space of all such equivalence classes), weighted with the exponential of i times its Einstein-Hilbert action. Because of the nonrenormalizability of gravity as a perturbative quantum field theory on a Minkowskian background, such a path integral necessarily has to be non-perturbative, which means that it must include spacetime configurations "far" from any classical solution. The evaluation of the ensuing, highly non-Gaussian path integral is technically challenging, and in the CDT approach is addressed by using powerful lattice methods, borrowed from the non-perturbative treatment of QCD. Adapting them to gravity implies that the rigid lattices of gauge theory become themselves dynamical, and actually take the form of *dynamical triangulations*, because of the way the infinitely many geometric/curvature degrees of freedom of the theory are regularized.

Namely, the gravitational path integral is regularized by summing over a class of piecewise flat four-manifolds, which can be thought of as being assembled from (two

cf. [66]. However, the spatial three-volume considered below is a sufficiently robust quantity, for which this turns out not to be necessary.

types of) four-dimensional simplices, which are simply triangular building blocks cut out of Minkowski space. They are individually flat, but can pick up nontrivial deficit angles after being glued together pairwise along three-dimensional subsimplices (tetrahedra), with curvature concentrated at two-dimensional subsimplices (triangles) where tetrahedra meet. This does not imply that spacetime is conjectured to consist of (Planck-sized) triangular building blocks. On the contrary, the edge length of the simplices serves as a short-distance cut-off and we are only interested in the *universal* properties of the model as this cut-off is sent to zero.

When evaluating the path integral, these simplicial geometries are taken to be Euclidean, like those that are summed over in the Euclidean gravitational path integral in its standard definition [72]. In contrast to previous Euclidean quantum gravity work, the triangulations used in CDT have a preferred, discrete notion of time $\tau = 1, 2, 3, \ldots$ inherited from a class of triangulated Lorentzian piecewise flat spacetimes by explicit Wick rotation [37, 73]. In the Lorentzian regime, the triangulations are restricted to those consisting of a sequence of slices with (discrete) proper-time thickness $\Delta\tau = 1$ and fixed topology. Links that lie in a spatial hypersurface of constant integer τ are spacelike and links connecting two adjacent spatial slices of this kind are timelike. The restriction on the path integral histories is motivated by the desire to eliminate the causality-violating 'baby universes' produced in *Euclidean* dynamical triangulations [35], which lead to an incorrect classical limit because of the absence of an extended four-dimensional geometry on large scales. After discretization and Wick rotation, the path integral becomes a statistical sum with Boltzmann weights using the Regge action [26], which is the discretized version of the Einstein-Hilbert action. The first major result of the CDT formulation was to show in exactly solvable two-dimensional quantum gravity that the signature, i.e., sum over Lorentzian as opposed to Euclidean geometries in the path integral, leads to genuinely different properties of the model (different intrinsic Hausdorff dimension, for instance) [36].

In dimension four, the regularized path integral can no longer be evaluated by exact methods, but Monte Carlo methods must be used to explore its continuum limit. This has led to a number of unexpected and new results. Since the curvature is allowed to fluctuate strongly on short scales, and since a nontrivial limiting process is involved, it turns out that the dimensionality of the "quantum geometry" generated by the path integral is not necessarily four. Only when the summed triangulations have the causal structure described above, and the (bare) coupling constants are chosen appropriately, does a four-dimensional universe emerge from the quantum theory [65, 66]. This is the first instance in which a classical-looking universe has been obtained from first principles within a non-perturbative formulation of quantum gravity. Moreover, as already mentioned in the introduction, this dynamically generated universe macroscopically resembles a de Sitter universe, with matching quantum fluctuations [38, 39].

2.1.2 Time slicing and classical limit of CDT

The classical limit of the CDT model is considered good if, when the length scale is large and quantum fluctuations are small, the continuum limit of the regularized path integral reproduces the observable predictions of classical general relativity. In order to compare the two, one needs to phrase their respective results in a common language, that of geometric *observables*. These are generally hard to come by, but in the case of CDT quantum gravity there is an extra structure that comes to our help. Each sample CDT geometry in the regularized path integral carries a discrete time label. Since this labelling is respected by the quantum superposition, a (possibly rescaled) version of the discrete time parameter labelling the slices is still available in the continuum. The reason for calling this a *proper* time comes from the fact that (i) at the discretized level, inside each flat four-simplex one can introduce a proper-time slicing (with respect to the Minkowskian metric of the simplex) in a way that after gluing all of them together, the triangulated "sandwich geometry" between integer times τ_0 and $\tau_0 + 1$ can be foliated into hypersurfaces $\tau = const$, $\tau_0 \leq \tau \leq \tau_0 + 1$ [74], (ii) in the continuum limit, the volume profile of the extended universe emerging in the 'well-behaved' phase of CDT quantum gravity matches that of a continuum Euclidean de Sitter space as a function of cosmological proper time, if the bare τ of the regularized geometries is rescaled by a finite constant. More precisely, the expectation value of the volume profile behaves to a very good approximation as

$$\langle V_3(\tau)\rangle = A\cos^3(\tau/B)\ , \tag{2.2}$$

for some constants A and B depending on the bare coupling constants and geometric parameters of the triangulation (see [39] for further details). The volume profile of Euclidean de Sitter space has exactly the same shape [cf. Eq. (2.16) below].

The latter is of course a highly nontrivial result, however, one needs to keep in mind that the role of τ as (constant multiple of) proper time—in the way this notion is used in the classical continuum theory—emerges unambiguously from CDT only on sufficiently large scales and in the sense of a quantum average (of a particular quantum observable). In order to understand better the relation with the continuum situation, recall that in the classical theory geometries with a time foliation are naturally described in the ADM formalism [75]. Labelling the spatial slices of the foliation as hypersurfaces of constant time t, and choosing coordinates x^i on each of them, the geometry is specified by writing the metric in the ADM form,

$$ds^2 = -N(t,x)^2dt^2 + h_{ij}(t,x)(dx^i + N^i(t,x)dt)(dx^j + N^j(t,x)dt)\,, \tag{2.3}$$

with lapse function $N(t,x)$, shift vector $N^i(t,x)$ and spatial metric $h_{ij}(t,x)$. The

volume profile of the spacetime with respect to this foliation is then given by

$$V_3(t) = \int d^3x \, \sqrt{\det h} \, . \tag{2.4}$$

A metric in proper-time form is one where $N = const.$ Requiring in addition the shift vector N^i to vanish, so that there are no cross terms $dx^i dt$ and the gauge is essentially fixed, one obtains a metric in *proper-time gauge* [76, 77]. The associated coordinates are the same as Gaussian normal coordinates [78, 75] with respect to any of the spatial hypersurfaces. Although such coordinate systems can always be set up in the neighbourhood of a hypersurface, they rarely exist globally because of the formation of caustics.[2] Therefore, taking a path integral only over those smooth metrics which globally can be put into proper-time gauge would appear far too restrictive.

However, this is not what is done in CDT quantum gravity, assuming we identify the time t in (2.3) with CDT's τ-parameter. Firstly, the ADM-decomposition (2.3) for differentiable, metric manifolds cannot in general be extended beyond a single four-simplex in piecewise flat simplicial geometries; they are neither smooth nor differentiable. (The same holds for individual CDT three-slices.) Secondly, when one follows the geodesics of freely falling, initially hypersurface-orthogonal observers in CDT (which are still well defined in open neighbourhoods not containing curvature singularities), one finds that they generically form caustics within a single time step $\Delta\tau = 1$. From this point of view, CDT histories are indeed full of caustics (and curvature singularities), whose density only increases as the lattice cut-off is taken to zero. Since individual path integral histories are *not* physical, this in no way contradicts the possibility that their *non-perturbative superposition* can be a quantum geometry which on large scales behaves classically. As we have seen for the case of Euclidean de Sitter space (EdS), the ground state of the empty universe emerging from CDT, it is also no obstacle to the existence of a well-defined global description in proper-time gauge. The fact that Euclidean de Sitter space possesses a global proper-time form which moreover has a direct Lorentzian interpretation under the straightforward substitution $\tau \to -i\tau$ is in a way a fortunate circumstance. If we want to use CDT quantum gravity to describe different physical situations, associated with a specific matter content and/or boundary conditions, we would in general expect that making a link to Lorentzian continuum physics will be (much) more difficult. As we will see in the next chapter, the inclusion of a mass distribution already presents challenges of this kind.

Let us now comment on spacetime topology. Computer simulations of CDT in four dimensions are performed with compact manifolds of product topology $I \times \Sigma^{(3)}$ or, if for

[2] Even in flat Minkowski space, by choosing an initial hypersurface $\tau = 0$ with typical extrinsic curvature K, caustics will form after a typical evolution time $\tau \sim K^{-1/2}$. For instance, a sphere of radius R has $K \sim 1/R^2$, while Gaussian normal coordinates, extended to the interior, become singular at its centre.

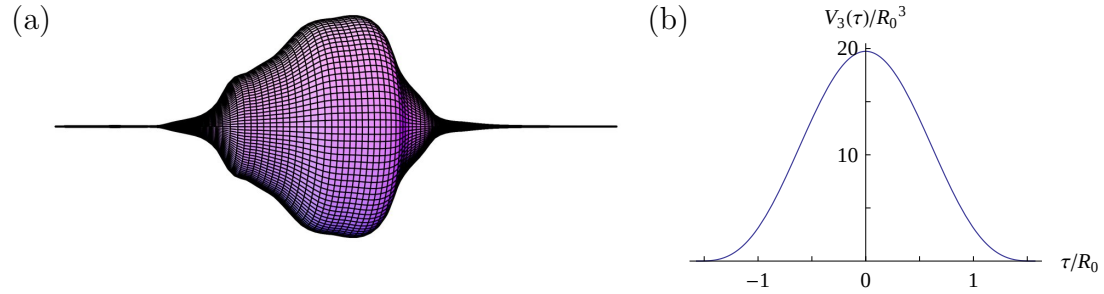

Figure 2.1: (a) Volume profile of a typical CDT universe that contributes to the sum over triangulations, made into a solid of revolution by rotation about the proper-time axis. It consists of an extended region, the 'blob', and a degenerate tube. (b) Normalized volume profile $V_3(\tau)/R_0^3$ for EdS space, cf. equations (2.2) and (2.16), which after a constant rescaling of τ matches that of the expectation value $\langle V_3(\tau)\rangle$ determined in CDT simulations [38, 39].

simplicity the time direction is compactified, $S^1 \times \Sigma^{(3)}$. In simulations considered so far, the spatial slices were chosen to be topological three-spheres, $\Sigma^{(3)} = S^3$. Interestingly, in the pure-gravity case, despite fixing the topology to $S^1 \times S^3$ at the outset, the system is driven dynamically to a state which is as close to a four-sphere as allowed by the kinematical constraints (minimal, nonvanishing spatial diameter at each time step). This is illustrated in Fig. 2.1(a), which shows the volume profile $V_3(\tau)$ of a typical sample geometry from the regularized path integral. It consists of an extended universe which forms a 'blob' and a thin degenerate tube or 'stalk' of minimal extension. After subtracting the minimal stalk-volume from the data, the average volume profile can be matched to that of EdS space (the "round four-sphere"), shown in Fig. 2.1(b), with great accuracy. In simulations, the period of the time identification is much larger than the time extension of the universe, such that this result is unaffected by the periodic boundary conditions.

2.2 Euclidean de Sitter space

2.2.1 Metric in static form

Written in the static form of the metric, the line element of Euclidean de Sitter (EdS) space is

$$ds^2 = f(R)dT^2 + f(R)^{-1}dR^2 + R^2 d\Omega^2(\theta,\phi)\,, \tag{2.5}$$

where $f(R) = 1 - R^2/R_0^2$, and the coordinates T and R are referred to as static or Schwarzschild coordinates. There is a cosmological horizon at the Hubble radius $R_0 = \sqrt{3/\Lambda}$ with $\Lambda > 0$ being the cosmological constant. The metric has Euclidean signature in the static region $0 \leq R < R_0$.

The topology of Euclidean de Sitter space is S^4. Suppressing the two angular variables θ and ϕ in (2.5), we see that the two-dimensional sheet spanned by T and

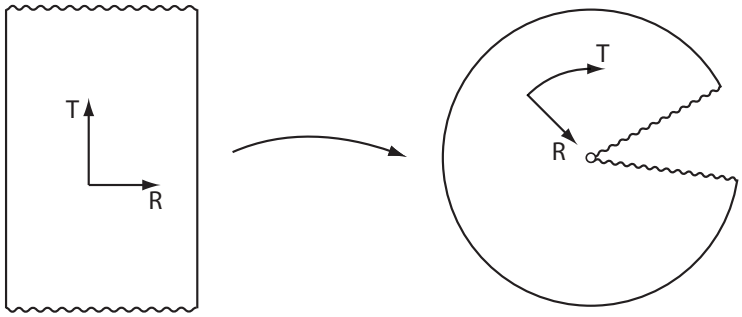

Figure 2.2: Euclidean de Sitter space can be compactified by taking the Schwarzschild time coordinate T to be periodic. The geometry can be smoothed out in the central point $R = R_0$ (the location of the cosmological horizon in Lorentzian signature) by adjusting the periodicity of T. The compactified, closed geometry is the four-sphere S^4 with radius R_0.

$0 \leq R < R_0$ can be wrapped by taking T to be periodic, as displayed in Fig. 2.2. The resulting punctured disc has a potential conical singularity at its center, $R = R_0$, which is smoothed out by a specific choice of the T-period, namely $T_P = 2\pi R_0$. One obtains the complete Euclidean manifold by gluing a two-sphere of radius R_0 to the puncture boundary.

2.2.2 Metric in proper-time form

As has been pointed out already, the explicit derivation of the volume profile has to be done by adopting a proper-time gauge. In order to achieve this form, we construct comoving or Gaussian normal coordinates (cf. [78, 75]) from the $T = 0$ surface, which coincides with half of the 'equator' of S^4 and will in general form a time-symmetric hypersurface (see also Fig. 2.3(a)). This procedure has been previously carried out, in Lorentzian signature, for the de Sitter case in [79] and for the Schwarzschild case in [80].

To obtain proper-time coordinates one has to integrate the radial geodesic equations and take initial conditions that guarantee that the geodesics are perpendicular to the $T = 0$ hypersurface. Then one chooses the proper time of these radial geodesics as a new time coordinate τ and requires $\tau = 0$ on that hypersurface. The comoving radial coordinate, R_i (the subscript i stands for *initial*), can be introduced as the position $R(T = 0)$, i.e. labelling each geodesic with the value of R at which it intersects the $T = 0$ hypersurface.

Let us now derive explicitly the line element on Euclidean de Sitter space in terms of Gaussian normal coordinates starting from the static form, Eq. (2.5). The Killing vector $\xi = \partial/\partial T$ yields a conserved quantity along the geodesics,

$$E = g_{\mu\nu}\xi^\mu \frac{dx^\nu}{d\tau} = f(R)\dot{T}\,, \tag{2.6}$$

where the dot refers to differentiation with respect to τ. We will refer to E as the energy parameter. The geodesic equations are then

$$\frac{dR}{d\tau} = m\sqrt{f(R) - E^2}, \qquad \frac{dT}{d\tau} = \frac{E}{f(R)}\,, \tag{2.7}$$

where $m = \pm 1$ distinguishes motion in Euclidean proper-time τ with increasing and decreasing R. Combining the two geodesic equations we find the proper time element along each geodesic,

$$d\tau = EdT + m\frac{\sqrt{f(R) - E^2}}{f(R)}dR\,. \tag{2.8}$$

While E is constant on a given geodesic, it may assume different values on different geodesics. For now, we take it as a yet to be specified function of coordinates $E(T, R)$. If we consider the two-dimensional R-T-plane to be foliated by non-intersecting geodesics, we can eliminate the T-coordinate in favour of their proper time τ and obtain the metric [81]

$$ds^2 = d\tau^2 + \frac{1}{E(T(\tau, R), R)^2}\left(dR - m\sqrt{f(R) - E(T(\tau, R), R)^2}d\tau\right)^2 + R^2 d\Omega^2\,. \tag{2.9}$$

Note that the metric is already in proper-time form. To set the shift vector to zero, and obtain a Gaussian normal coordinate system, we replace the R-coordinate by a comoving radial coordinate. We introduce the comoving radial coordinate by first observing that radial geodesic motion of a test body in EdS space corresponds to motion in the effective potential

$$V_{\text{eff}}(R) = \frac{R^2}{2R_0^2} \tag{2.10}$$

with total energy $E_{\text{tot}} = (1 - E^2)/2$. This is easily seen from writing the equation (2.7) in the form $\frac{1}{2}\dot{R}^2 + V_{\text{eff}}(R) = E_{\text{tot}}$. The turning radius, R_i, will be our comoving radial coordinate. For the maximal energy $E_{\text{tot}} = 1/2$ the turning radius is the cosmological horizon, $R = R_0$. Hence, for the construction of coordinates in proper-time gauge we look at geodesic motion of test bodies with initial positions $0 \leq R_i < R_0$ and zero initial velocity. The synchronization condition that each geodesic passes through its turning point at $T = \tau = 0$ completes the specification of the proper-time coordinates (τ, R_i). In terms of the new coordinates, the energy parameter is specified simply as $E = \sqrt{f(R_i)}$.

Integration of the radial geodesic equation yields

$$\tau(R, R_i) = -m\int_R^{R_i} \frac{dy}{\sqrt{f(y) - f(R_i)}}\,, \tag{2.11}$$

which can be solved explicitly and inverted to give

$$R(\tau, R_i) = R_i \cos\left(\tau/R_0\right)\,. \tag{2.12}$$

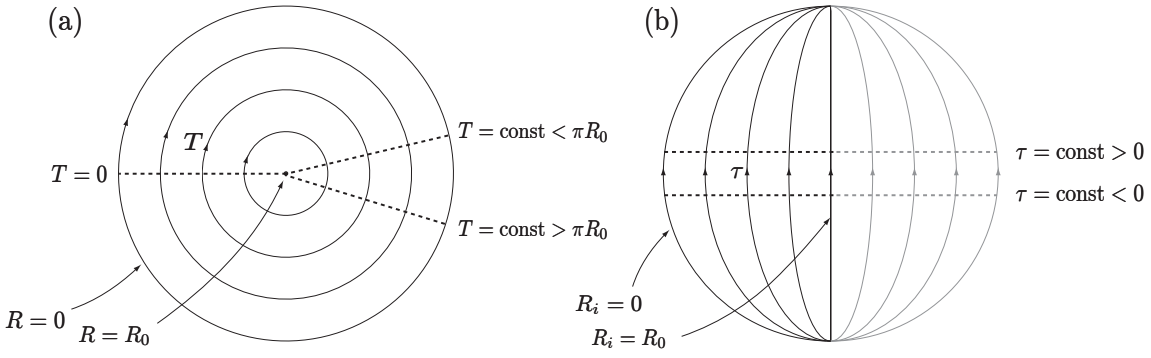

Figure 2.3: Euclidean de Sitter space (after periodically identifying the static time T, with angular variables θ, ϕ suppressed), described in terms of (a) static and (b) proper-time coordinates. In static coordinates, lines $R = const$ are concentric circles, with mid point $R = R_0$ and outermost circle $R = 0$. In the proper-time coordinates, the lines $R_i = const$ converge at $\tau = \pm\pi R_0/2$. Only one half of the disc is covered by Gaussian normal coordinates emanating from the $T = 0$ surface (dark curves). The other half (which is of a lighter shade in the figure) can be covered by reflecting the (τ, R_i) coordinates about the middle line $R_i = R_0$ or, equivalently, by constructing Gaussian normal coordinates from the $T = \pi R_0$ surface, which smoothly joins the $T = 0$ one.

This results in the metric line element

$$ds^2 = d\tau^2 + R_0^2 \cos^2(\tau/R_0) \left[\frac{dR_i^2}{R_0^2 - R_i^2} + (R_i/R_0)^2 d\Omega^2 \right] . \tag{2.13}$$

The global proper-time coordinate system on de Sitter space is introduced by extending the range of the radial coordinate by introducing an angle ψ, $0 \leq \psi < \pi$, where

$$R_i = R_0 \sin\psi \, . \tag{2.14}$$

The relationship between static (T, R) and comoving (τ, R_i) coordinates is illustrated in Fig. 2.3. The disc depicted in Fig. 2.3(a) is formed from R-T-space by periodically identifying the static time T such that $0 \leq T \leq 2\pi R_0$. The static coordinates (T, R) cover the entire disc. Fig. 2.3(b) depicts the same disc, but now with dark vertical lines representing constant R_i (radial geodesics) and dashed horizontal lines representing constant τ. On the left half of the disc a $R_i = const$ line is represented by an angle $\psi < \pi/2$ and on the right half by $\psi > \pi/2$, with the middle line given by $R_i = R_0$ or $\psi = \pi/2$. The line element written in terms of τ and ψ becomes

$$ds^2 = d\tau^2 + R_0^2 \cos^2(\tau/R_0) \left(d\psi^2 + \sin^2\psi \; d\Omega^2 \right) . \tag{2.15}$$

Note that this is the line element of the round four-sphere, where the geodesic $R_i = 0$ has become the location of the coordinate singularity $\psi = 0$. Spatial sections of this four-dimensional Euclidean geometry are three-spheres, which is consistent with CDT simulations. From this metric, or already from the line element (2.13), we can

immediately derive the volume profile

$$V_3(\tau) = 2\pi^2 R_0^3 \cos^3(\tau/R_0) \tag{2.16}$$

for EdS space, which we have referred to earlier in equation (2.2).

Chapter 3

Coupling a point-like mass to quantum gravity with CDT

3.1 CDT with a localized mass

Let us now move on to the case that a localized or point-like mass is included in the CDT model. The classical solution to the Einstein equations outside the source is then given by the Schwarzschild-de Sitter (SdS) metric. In this chapter, we address the question of how to detect the presence—on sufficiently large scales—of this particular background geometry in CDT quantum gravity coupled to a point-like mass. This implies finding a quantum observable that is well defined in the non-perturbative, background-independent setting of the full path integral, is sensitive to the presence of the mass, and is potentially measurable in the computer simulations.

As we shall see, the volume profile is a geometric quantity that is modified by the presence of the mass. We will focus in this chapter on the derivation in the continuum of the volume profile of the Euclidean Schwarzschild-de Sitter (ESdS) solution in a proper-time slicing. The resulting curves can be used to test whether the classical limit of CDT coincides with the Euclidean Schwarzschild-de Sitter geometry by measuring the average volume profile in simulations of CDT with a mass line representing the point-like source. To our knowledge, no background-independent approach to quantum gravity has so far succeeded in generating a Schwarzschild-de Sitter geometry in the classical limit. The volume profiles we derive can be used as a criterion to identify this spacetime in any background-independent approach to quantum gravity in four spacetime dimensions, when using a suitable proper-time slicing.

The particular Gaussian normal coordinate system we work with in the continuum, in order to mimic the CDT set-up, exhibits caustics in the vicinity of the mass, which cannot be eliminated by extending the coordinates to the matter region. Nevertheless, by requiring the mass distribution to be sufficiently compact (point-like), the total

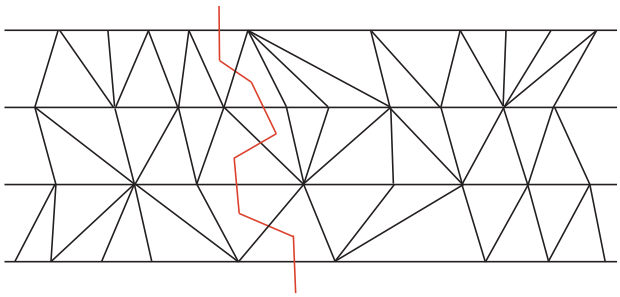

Figure 3.1: Mass line on the dual lattice of a triangulation in CDT, for simplicity demonstrated in two dimensions, representing the worldline of a point-like mass.

mass M to be small and treating the situation as a one-parameter family deviating from the known, pure-gravity case $M = 0$, we are able to quantify the consequences of $M \neq 0$ for the physical volume profile. For the numerical derivation of the volume profiles, we neglect the problematic region by cutting out a tube from the Euclidean Schwarzschild-de Sitter space whose spatial slices are balls of constant Schwarzschild radius. This procedure gives rise to an upper bound for the mass under consideration. The profiles for masses below this bound are the ones that should be compared with those coming from CDT simulations to test for the possible presence of a Euclidean Schwarzschild-de Sitter ground state. A mass propagating in triangulated spacetime can be represented by a timelike mass line on the lattice dual to the triangulation.

The concept of a point mass is already problematic in classical general relativity, in the sense of including it consistently as a distributional source in the Einstein equations (for a recent overview, see [82] and references therein). In addition, an important piece of work in this context is [83] where a spherical shell with a finite bare mass was considered. It was shown that taking the limit of zero radius of the spherical shell results in a zero ADM mass. Therefore, it is necessary to assume an *infinite* bare mass in order to obtain a finite ADM mass. For these reasons, we will refrain from making the point mass idealization and assume an extended, but localized, spherically symmetric mass source, mostly without discussing its internal structure. An exception is section 3.3, where we consider the extension of the proper-time coordinates in the exterior to a simple interior matter distribution. In any case, from the point of view of the regularized geometries used in the simulations, one cannot really distinguish between a point mass and a compact, massive object that fits inside a single spatial simplex. In this context, we call a compact mass distribution *point-like* if its spatial extent does not exceed that of a single triangulation simplex.

In CDT simulations, the worldline of such a mass is naturally represented by a time-like path, transverse to the foliation, on the dual lattice of the triangulation, as illustrated in Fig. 3.1. The (Euclidean) action associated with this mass line is

$S_p = ML$, where M is the bare mass, and L is the (positive) total length of the line in units of the lattice spacing a. This is the regularized version of the continuum action associated to a localized mass M, $S_p = M \int d\tau$, integrated with respect to the proper time along its world-volume, which in turn depends on the spacetime geometry containing the mass line. The action S_p gives an extra contribution to the Boltzmann weight of each path-integral configuration and therefore changes the expectation value of geometric quantities under consideration. In particular, the volume profiles are expected to be modified.

3.2 Euclidean Schwarzschild-de Sitter space

3.2.1 Metric in static form

As in section 2.2 we start by writing down the line element of Euclidean Schwarzschild-de Sitter (ESdS) space in its static form,

$$ds^2 = f(R)dT^2 + f(R)^{-1}dR^2 + R^2 d\Omega^2(\theta, \phi)\,, \tag{3.1}$$

where now $f(R) = 1 - 2M/R - R^2/R_0^2$ with the mass of the source M. For a given cosmological constant, there is an upper limit for the mass of the Schwarzschild black hole, given by $M_N = 3^{-3/2}R_0$, the Nariai mass [84], because the static region disappears in this limit. We recover Euclidean de Sitter space for $M = 0$, and the Euclidean Schwarzschild metric for $\Lambda = 0$. The metric has Euclidean signature in the static region $R_+ < R < R_{++}$, where

$$R_+ = 6M_N \cos\left(\frac{\alpha + 4\pi}{3}\right), \quad R_{++} = 6M_N \cos\left(\frac{\alpha}{3}\right), \tag{3.2}$$

are the locations of the black hole horizon and the cosmological horizon, respectively, and $\alpha = \arccos(-M/M_N)$.

For the Lorentzian version of the solution (3.1), the event horizon only forms if the object that generates the gravitational field is sufficiently dense. We shall consider a mass distribution that is glued to the exterior vacuum region such that no event horizon is present. For now we will focus solely on the properties of the vacuum region.

Wrapping the two-dimensional sheet spanned by T and $0 < R < R_{++}$ like in the EdS case by taking T to be periodic we obtain a punctured disc which has a potential conical singularity at its center, $R = R_{++}$, as displayed in Fig. 3.2. This singularity is smoothed out by choosing the T-period to be $T_P = 4\pi/|f'(R_{++})|$.

The maximal Euclidean vacuum region is spanned by $R_+ < R < R_{++}$. Periodic compactification along the T-direction introduces a different global topology and two potential conical singularities at R_+ and R_{++}, which cannot be smoothed out simultaneously [85]. Fortunately, the new topology and the ambiguity in periodicity need

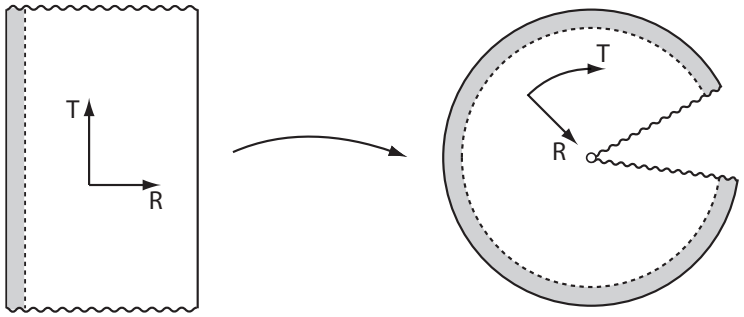

Figure 3.2: Euclidean Schwarzschild-de Sitter space can be compactified in a similar way as Euclidean de Sitter case, Fig 2.2, by taking the Schwarzschild time coordinate T to be periodic. The center of the disc is now given by $R = R_{++}$ and the periodicity of T is $T_P = 4\pi/|f'(R_{++})|$. The shaded region represents the matter region and contains no conical singularities. It is glued to the exterior vacuum solution at a constant Schwarzschild radius $R = R_S > R_+$, outside the horizon. The compactified, closed geometry has topology S^4.

not be dealt with if the manifold consists of an ESdS exterior and an interior matter region (shaded in Fig. 3.2), without an inner horizon.

As a consequence of the compactification, the mass line closes to a contractible loop on the S^4. If one wants to compare with the calculations presented here, this should be taken into account when implementing the mass line in CDT simulations, rather than using a noncontractible loop which winds around the compactified time direction, say.

3.2.2 Metric in proper-time form

The line element for Euclidean Schwarzschild-de Sitter space in terms of Gaussian normal coordinates can be derived in analogy with the Euclidean de Sitter case in section 2.2.2. For this we first determine the radial geodesics in ESdS space.[1] The effective potential for radial geodesic motion is given in this case by

$$V_{\text{eff}}(R) = M/R + R^2/2R_0^2\,, \tag{3.3}$$

It is displayed in Fig. 3.3 for $M = 0$ and $M = M_N/10$. The potential has a minimum at $R = R_* = M^{1/3}R_0^{2/3}$ and there are two turning points for a test body moving in the potential which are given by the roots of the equation $f(R) = E^2$. The larger turning radius, R_i, will be our comoving radial coordinate. For the maximal energy the turning radii are the two horizons, $R = R_+$ and $R = R_{++}$. To construct the proper-time coordinates for this general case we only have to consider initial positions $R_* < R_i < R_{++}$ and zero initial velocity.

[1] The complete analytic solution for geodesics in Schwarzschild-de Sitter space was constructed in [86, 87].

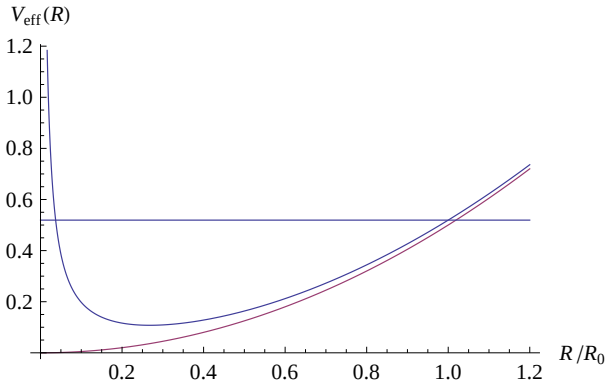

Figure 3.3: The effective potential for radial geodesic motion in ESdS space for $M = M_N/10$ (upper curve with horizontal line to illustrate turning points for the maximum total energy) and for $M = 0$ (lower curve). These potentials determine the evolution of the $R_i = const$ geodesics which form the proper-time coordinate system.

Integration of the radial geodesic equation yields

$$\tau(R, R_i) = -m \int_R^{R_i} \frac{dy}{\sqrt{f(y) - f(R_i)}} = -mR_0 \int_\rho^1 d\xi \sqrt{\frac{\xi}{P(\xi)}}\,, \tag{3.4}$$

with the dimensionless quantities $\xi = y/R_i$, $\rho = R/R_i \leq 1$, $\beta = 54MM_N^2/R_i^3$ and

$$P(\xi) = -\xi^3 + (\beta + 1)\xi - \beta = (1 - \xi)(\xi - \xi_+)(\xi - \xi_-)\,, \tag{3.5}$$

$$\xi_\pm = -\frac{1}{2} \pm \Delta, \quad \Delta = \sqrt{\frac{1}{4} + \beta}. \tag{3.6}$$

In terms of special functions the above integral becomes

$$\tau = -mR_0\sqrt{2/\Delta}\left[(1 - \xi_-)\Pi(\mu, \frac{\xi_+ - 1}{2\Delta}, r) + \xi_- F(\mu, r)\right]\,, \tag{3.7}$$

where

$$\mu = \arcsin\sqrt{\frac{2\Delta(1 - \rho)}{(1 - \xi_+)(\rho - \xi_-)}}, \quad r = \sqrt{\frac{(1 - \xi_+)(-\xi_-)}{2\Delta}}\,. \tag{3.8}$$

F and Π are the elliptic functions of the first and third kind, respectively [88, 3.167.15]. Equation (3.7) is an implicit definition of $R(\tau, R_i)$. This relation allows us to write the line element in terms of proper-time τ and comoving spatial coordinate R_i as

$$ds^2 = d\tau^2 + \frac{(\partial R/\partial R_i)^2}{f(R_i)} dR_i^2 + R(\tau, R_i)^2 d\Omega^2\,. \tag{3.9}$$

As we have seen in section 2.2.2 the expression for $R(\tau, R_i)$ is known explicitly for $M = 0$. When $M \neq 0$, the values of $R(\tau, R_i)$ can be obtained by numerically solving the implicit equation (3.7). Both cases are shown for comparison in Fig. 3.4. Note that the radial geodesics in EdS space, Fig. 3.4(a), do not intersect except for extreme values of τ, but those in ESdS space do, Fig. 3.4(b), that is, they form caustics. The implications of these caustics are discussed in the next section.

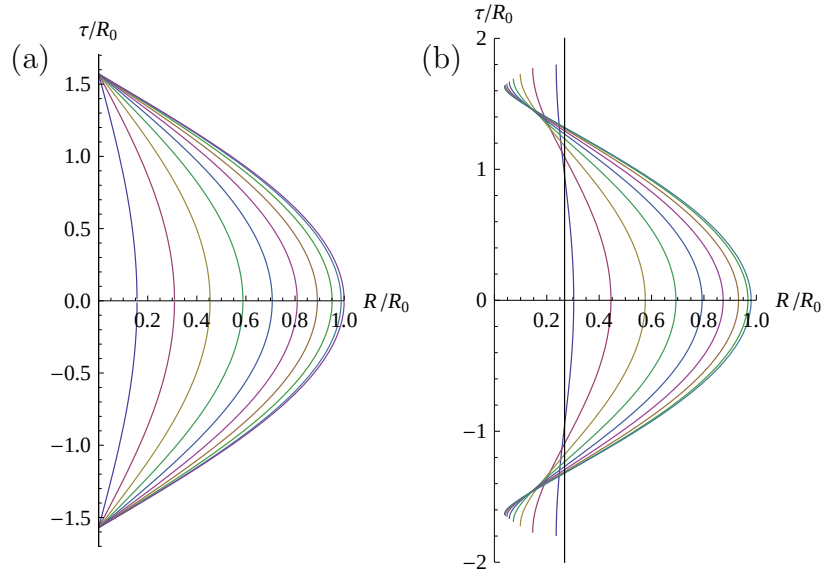

Figure 3.4: $R_i = const$ geodesics in (a) Euclidean de Sitter space and (b) Euclidean Schwarzschild-de Sitter ($M = M_N/10$) space. The outermost line is the $R_i = R_{++}$ geodesic. (a) All curves converge at $\tau = \pm\pi R_0/2$. (b) The vertical line marks $R = R_* \equiv M^{1/3}R_0^{2/3}$, the minimum of the effective potential. Geodesics, which at $T = 0$ are located to the right of the line start intersecting each other when entering the region $R < R_*$, forming caustics. There are no caustics in the region $R_* < R < R_{++}$.

3.2.3 Domain of comoving coordinates and caustics

It is well known that Gaussian normal coordinates in general fail to cover the entire underlying manifold. Below, we determine how much of ESdS space can be covered by the coordinates constructed in the previous section. Figs. 3.5(a) and 3.5(b) parallel the discussion of section 2.2.2, though the ranges of the static coordinates change to $0 \leq T \leq T_P$ and $0 < R < R_{++}$ in the ESdS case. Again, the right half of the disc in Fig. 3.5(b) can be covered by reflection of the (τ, R_i) coordinates or by constructing Gaussian normal coordinates from the $T = T_P/2$ surface. As explained in section 3.2.1 the geometry we are considering has no inner horizon since the exterior vacuum is matched to a static interior matter solution (shaded region) at $R_S > R_+$.

The comoving coordinate system breaks down at an intersection point of two radial geodesics, because it would associate two distinct labels (τ, R_i), (τ, R_i') with the same physical point. In contrast to the EdS case described in section 2.2.2, where geodesics in Fig. 2.3 intersect only at the poles, Fig. 3.5(b) shows that they intersect and thus form caustics already for $R < R_*$ in the ESdS case. Fig. 3.5 is schematic, the corresponding calculations are presented in the previous section for the vacuum region and in the following section for the matter region. Therefore, we can conclude that comoving coordinates (τ, R_i) cover EdS space in its entirety[2], while only a portion of ESdS space

[2]Strictly speaking, these coordinates fail to cover some lower-dimensional submanifolds. But, since

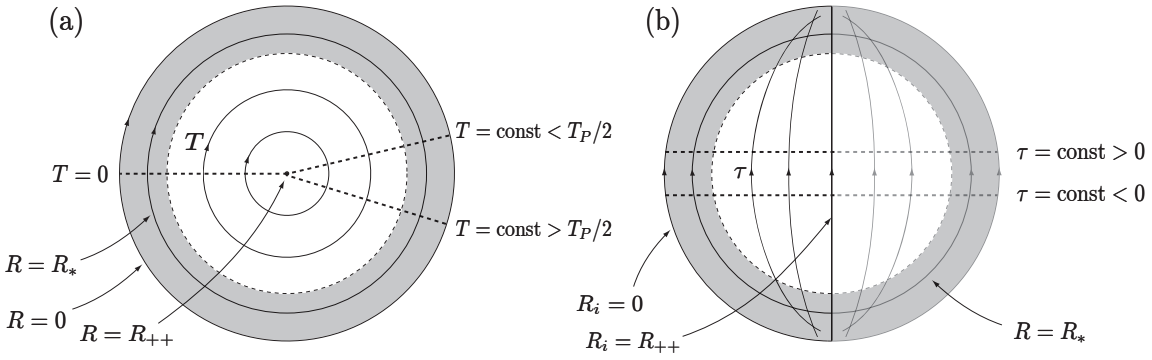

Figure 3.5: Euclidean Schwarzschild-de Sitter space (after periodically identifying the static time T, with angular variables θ, ϕ suppressed), described in terms of (a) static and (b) proper-time coordinates (cf. Fig. 2.3). The shaded region $R < R_S$ in (b) is occupied by matter. In static coordinates, lines $R = const$ are concentric circles, with mid point $R = R_{++}$ and outermost circle $R = 0$. In the proper-time coordinates, the lines $R_i = const$ start forming caustics in the region $R < R_*$. The middle line is $R_i = R_{++}$. Every $R_i = const$ appears once on the left half of the disc (dark curves, perpendicular to the $T = 0$ surface), and is mirrored on the right half of the disc (light curves, perpendicular to $T = T_P/2$).

is covered, namely for $R > R_*$, with R_* the boundary of the caustic region.

Caustics appear already in the ESdS exterior vacuum, in which case $R_* = (MR_0^2)^{1/3}$. Generically, caustics persist even if the vacuum exterior is glued to an interior matter solution of arbitrarily low density, as explicitly shown for a specific matter model in the next section. Thus, for convenience, from now on R_* will only refer to this *vacuum caustic boundary*. To ensure that the entire vacuum region is covered by comoving coordinates, we require that the matter-vacuum boundary satisfies the condition $R_S > R_*$, which puts an upper bound on the density of the mass distribution. We only consider densities below this critical value. This bound and the associated bound on the total mass are discussed in detail in sections 3.4.1 and 3.4.2.

We should emphasize that the occurrence of caustics does not imply any pathologies of the underlying spacetime, but is a consequence of the choice of a particular coordinate system. In order to calculate the volume profile, all we need is a proper-time slicing. Neither the vanishing of the shift vector nor the existence of a single, global coordinate system are in principle necessary. However, our (time-symmetric) choice of the Gaussian normal coordinates starting at $T = 0$ and $T = T_P/2$ has the advantage of being continuously connected to a globally well-defined coordinate system in the limiting case $M = 0$. That coordinate system was used to successfully compare classical, continuum volume profiles to those produced by CDT simulations. It is this successful case that we are 'perturbing' about.[3]

we are only interested in computing three- and four-volumes, they can be safely ignored.

[3]It is possible that there exist even more convenient coordinate choices for $M \neq 0$, which would

3.3 Caustic formation in an interior matter solution

We show here that gluing the vacuum ESdS solution to an interior solution of matter of constant density does not significantly improve on the situation found in vacuo with respect to the formation of caustics in a set of Gaussian normal coordinates. The matter distribution we are interested in is the Wick-rotated version of a simple model of a spherically symmetric relativistic star in the presence of a positive cosmological constant. The Euclidean stress-energy tensor can be taken to be the one of a perfect fluid with a uniform density ρ,

$$T^{\mu\nu} = -\left(p(R) + \rho\right) u^\mu u^\nu + p(R) g^{\mu\nu} \,. \tag{3.10}$$

Solving the Euclidean Einstein equations one finds that the line element inside the matter region written in Schwarzschild coordinates is [89] [4]

$$ds^2 = \left(A\, Y(R_S) - B\, Y(R)\right)^2 dT^2 + \frac{dR^2}{Y(R)^2} + R^2 d\Omega^2 \,, \tag{3.11}$$

where we denote the location of the surface of the matter distribution by $R_S > R_+$ (or $R_S > R_*$, as we restrict to later on) and define

$$Y(R) = \sqrt{1 - \frac{8\pi\rho + \Lambda}{3} R^2}, \quad A = \frac{9M}{6M + \Lambda R_S^3}, \quad B = \frac{3M - \Lambda R_S^3}{6M + \Lambda R_S^3}, \quad \rho = \frac{3M}{4\pi R_S^3} \,. \tag{3.12}$$

Setting $R = R_S$ in (3.11), we see that the interior matter solution is matched continuously to the exterior ESdS vacuum region. This implies that the correct matching condition for the radial timelike geodesics is that the first derivatives match at boundary.

For the case $R_S = R_* = M^{1/3} R_0^{2/3}$ we can determine the extension of radial geodesics to the interior region explicitly. This is depicted in Fig. 3.6(a). The geodesics intersect inside of the matter region and hence the formation of caustics persists.

This result is not specific to the choice $R_S = R_*$. In order to avoid a lengthy analysis we set up a simple criterion for the intersection of geodesics. We release two test bodies, one from $R_i = R_{++}$ and the other from $R_i = R_S$, with zero initial velocity and compare the proper time they take to arrive at $R = 0$, which is the center of the star. If the test body starting at the surface takes longer, then there must be an intersection. The arrival time for the test body starting from $R_i = R_{++}$ is given by

$$\tau(R_i = R_{++}) = \sigma \arcsin\left(R_S/\sigma\right) + \int_{R_S}^{R_{++}} \frac{dy}{\sqrt{f(y)}} \,, \tag{3.13}$$

avoid caustics altogether, but we have not found them.

[4] Some intermediate results in this reference contain typographical errors. However, we have verified that the formulas relevant for this work are correct.

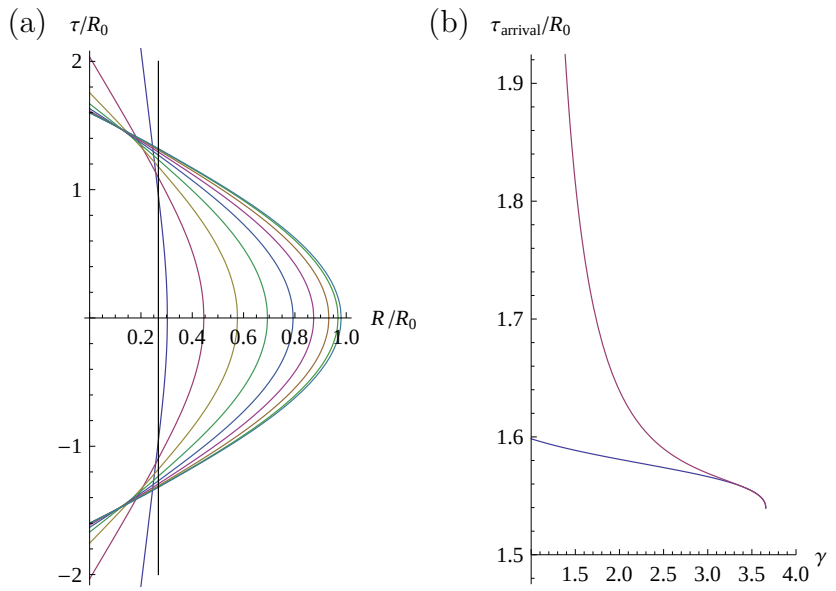

Figure 3.6: Gluing an interior uniform matter distribution to an external Euclidean Schwarzschild-de Sitter solution for $M = M_N/10$. (a) $R_i = const$ geodesics for the special case of gluing at the radius $R = R_*$ (vertical line). The curves intersect inside the matter region, illustrating the breakdown of the Gaussian normal coordinates. The outermost line is the $R_i = R_{++}$ geodesic. (b) For general gluing radius: proper time at $R = 0$ (arrival time) of the two radial geodesics, $R = R_{++}$ (lower curve) and $R = \gamma R_*$ (upper curve), as functions of $\gamma = R_S/R_*$, showing that adjusting the gluing condition does not prevent the breakdown of the Gaussian coordinates in the interior region.

with $1/\sigma^2 = (1 + 2/\gamma^3)/(27M_N^2)$ and $\gamma = R_S/R_*$. The first term in (3.13) constitutes the contribution of the matter region and the second constitutes that of the vacuum region. The integral in the second term is the same as that evaluated in (3.7).

For the test body starting with zero initial velocity at the star's surface, $R = R_S$, we have

$$\tau(R_i = R_S) = \int_0^{R_S} \frac{dy}{Y(y)\sqrt{1 - \frac{f(R_S)}{(AY(R_S) - BY(y))^2}}}\,, \tag{3.14}$$

where the constants $A, B, f(R_S)$ and $Y(R_S)$ all depend on γ. The resulting arrival times are plotted in Fig. 3.6(b), where the upper curve represents the $R_i = R_S$ case and was found by numerical integration. The arrival times are equal only when the trajectories coincide, i.e. when the star surface reaches the cosmological horizon. Therefore, we conclude that the Gaussian normal coordinates are not well defined in the interior region for any choice of radius and density of the mass distribution. We have not investigated whether fine-tuning of the internal structure of the matter model (e.g. by considering inhomogeneous or anisotropic fluids) could help in preventing the occurrence of caustics. However, such a possibility appears unlikely to us.

3.4 Volume profiles

3.4.1 Cutting out the vicinity of the mass-line

In computer simulations, the volume profile is determined by counting spatial simplices per slice of constant proper time for the individual sample geometries and taking the average value over the ensemble. For simulations with a mass line, the average of the discrete geometries should approximate the Euclidean Schwarzschild-de Sitter space well away from the mass, but poorly close to it. Thus it makes sense to discard the simplices pierced by the mass line and to excise a corresponding thin 'tube' surrounding the mass from the four-dimensional continuum geometry. Only the volume profiles of the remaining regions will be compared. On every spatial slice $\tau = const$ we choose to cut out the region inside of a ball of a certain Schwarzschild radius R, whose area is $4\pi R^2$. Of course, this choice of the radius depends on the mass and only for small masses can we expect a good match between the continuum and discrete picture. A more detailed analysis on the mass bound will be presented in the following section.

An important property of this prescription is that the surface of this region (which has topology $S^2 \times S^1$ for compactified Schwarzschild time) is invariantly defined, and mapped into itself under the flow of the time-like Killing vector. This agrees with the discrete picture, where the sequence of four-simplices cut out of the four-geometry representing the mass line has the topology of a tube. A strict implementation of the classical continuum set-up on the simplicial lattice would allow only for mass lines whose boundary is everywhere time-like, which would limit the types of tube geometry that can occur in a single time step. This would be associated with an excised region per time step of some typical, average surface area $O(1)$ in discrete units, even though the internal geometry of the excised region is considered unspecified. Other prescriptions for cutting out the matter region in the classical continuum geometry are in principle possible. However, they must not deviate from the Schwarzschild prescription more than the scale set by the discretization (the lattice spacing) which is the size of the error already inherent in the triangulation procedure.

In view of the quantum nature of the CDT path integral, simulations may have to include more general mass lines, which can wind around longer in a given time step or are even allowed to run backwards in time.

3.4.2 Derivation of a mass bound

We emphasized that due to caustic formation in the continuum picture it is necessary to cut out a certain region of the Euclidean manifold. Now, it is important to carefully translate the excised region from the continuum picture to the discrete one in order

to reliably compare the volume profiles. For this we relate the physical parameters on both sides. In the continuum there are only two parameters, the mass M and the cosmological constant Λ, which sets the cosmological radius $R_0 = \sqrt{3/\Lambda}$. Newton's constant G_N has been set to one. In CDT simulations performed so far, the directly specifiable parameters[5] are the bare Newton's constant, the mass, and the number of four-simplices N. The lattice spacing a is introduced to relate dimensionless simulation parameters to dimensionful physical parameters. We relate simulation and continuum parameters by comparing geometric observables in the continuum limit. For instance, for Euclidean de Sitter space, the total four-volume is $V_4 = \frac{8\pi^2}{3} R_0^4$, from (2.16), while on the triangulation side we have $V_4 = \frac{\sqrt{5}}{96} a^4 N$ [39], leading to the relationship

$$a/R_0 = \left(\frac{8 \cdot 96\pi^2}{3\sqrt{5}}\right)^{1/4} N^{-1/4} \sim 5.8 N^{-1/4} \,. \tag{3.15}$$

Typical values of $N \sim 3 \times 10^5$ give $a/R_0 \sim 1/4$.

Another important relationship is between the lattice spacing a and the maximum mass M accessible to simulations. To find the possible range of masses we recall that the vacuum caustic boundary $R_* = 3M^{1/3}M_N^{2/3}$ must fall within the matter region, $R_* < R_S$. On the other hand, in order to compare directly with the calculations presented here, one should consider mass distributions that are sufficiently compact to fit inside a region of the same size as the simplex whose volume we neglect, that is, $R_S < a$. The resulting condition $R_* \leq a$ can be expressed as an upper bound on the mass M:

$$M \;\leq\; 3^{3/2}\left(\frac{a}{R_0}\right)^3 M_N \;=\; \frac{1}{3}a^3\Lambda \;\sim\; 33.6\frac{a}{\sqrt{N}} \,. \tag{3.16}$$

The first is the most useful form of the bound for the numerical calculations carried out in the following section, where, as we shall see, the dimensionless parameter $\epsilon = M/M_N$ determines the shape of the volume profiles. The last form gives an estimate for the maximum accessible mass in terms of simulation parameters, with the approximation coming from direct use of equation (3.15). Since a/R_0 is expected to be small, the deviations of the volume profile from the Euclidean de Sitter case for accessible masses are also likely to be small.

3.4.3 Derivation of the volume profiles

Having discussed the range of validity of the excision we can move on to the derivation of the volume profile which can be used to test the classical limit of matter-coupled

[5] Another parameter specifiable in simulations is the directional asymmetry parameter Δ, though its value is not accessible in a classical geometry. For the discrete computations presented in this subsection, we will assume for definiteness that $\Delta = 0$, such that the Euclideanized four-simplices are all equilateral [73].

CDT quantum gravity and constitutes the main result of this chapter. From the line element (3.9) and definition (2.4) we obtain an integral expression for the total three-volume of the vacuum region,

$$V_3(\tau) = 8\pi \int_{R_i^{\min}(\tau)}^{R_{++}} dR_i \frac{R^2(\tau, R_i) R'(\tau, R_i)}{\sqrt{f(R_i)}}\,, \tag{3.17}$$

where $R' = \partial R/\partial R_i$, a factor of 4π comes from the angular integration, and an extra factor of 2 takes the doubling of the $R_i \leq R_{++}$ region into account, as explained in section 3.2.3. The function $R_i^{\min}(\tau)$ is the cut-off condition $R = a$ in proper-time coordinates.

In the continuum, increasing the mass while keeping R_0 (and therefore the cosmological constant Λ) fixed changes the total four-volume. In CDT simulations, however, the four-volume (that is, the number of four-simplices) is usually kept fixed for technical reasons.[6] In order to facilitate comparison with CDT results, we invert the relationship between R_0 and V_4 in the continuum for fixed mass M. First, note that the function R in the definition of the volume profile (3.17) and the four parameters τ, R_i, M and R_0 on which it depends all have the dimension of length. Hence, we can write

$$R(\tau, R_i, M, R_0) = R_0 F(\zeta, R_i/R_0, \epsilon)\,, \tag{3.18}$$

for some dimensionless function F that depends only on the dimensionless parameters $\zeta = \tau/R_0$, $\epsilon = M/M_N = 3^{3/2} M/R_0$ and the ratio R_i/R_0. The volume profile can therefore also be written as

$$V_3(\tau, \epsilon) = R_0^3 G(\tau/R_0, \epsilon)\,, \tag{3.19}$$

with another dimensionless function G whose explicit form is to be evaluated. Note that the lower integration limit in (3.17) introduces an additional dependence on the lattice length a that we suppress here. From equation (2.16) it follows that $G(\zeta, 0) = 2\pi^2 \cos^3\zeta$ for the case $M = 0$. In terms of the function G the four-volume is

$$V_4(\epsilon) = \int_{-\tau_{\max}(\epsilon)}^{\tau_{\max}(\epsilon)} d\tau\ V_3(\tau, \epsilon) = R_0^4 \int_{-\tau_{\max}(\epsilon)/R_0}^{\tau_{\max}(\epsilon)/R_0} d\zeta\ G(\zeta, \epsilon) \equiv R_0^4 H(\epsilon)\,. \tag{3.20}$$

In these expressions the integration limit is given by the time $\tau_{\max}(\epsilon)$ where the three-volume becomes zero. For Euclidean de Sitter space the value of the function $H(\epsilon)$ before cutting out the tube is $H(0) = 8\pi^2/3$. If V_4^* is the fixed four-volume used in a simulation, we have to adjust R_0 depending on the value of ϵ by setting $R_0(\epsilon) = (V_4^*/H(\epsilon))^{1/4}$. The rescaled four-volume $H(\epsilon)$ can be easily evaluated analytically in

[6] The path integrals for fixed four-volume and fixed cosmological constant are related by a Laplace transformation [66].

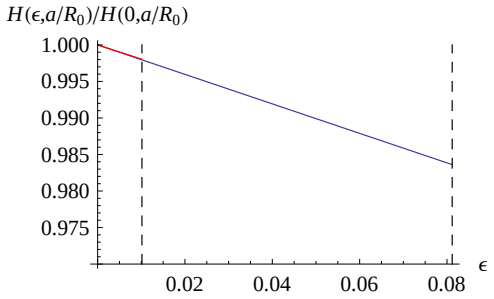

Figure 3.7: Plots of the dependence of the scaled total four-volume on the parameter ϵ for the two cut-off values $a/R_0 = 1/8$ [red line, ranging from zero to the first vertical line at $\epsilon = 3^{3/2}(1/8)^3$] and $a/R_0 = 1/4$ [blue line, ranging from zero to the second vertical line at $\epsilon = 3^{3/2}(1/4)^3$]. Both functions are normalized to one at $\epsilon = 0$. In the displayed region the curves are linear to very good approximation; the cut-off dependence is essentially negligible.

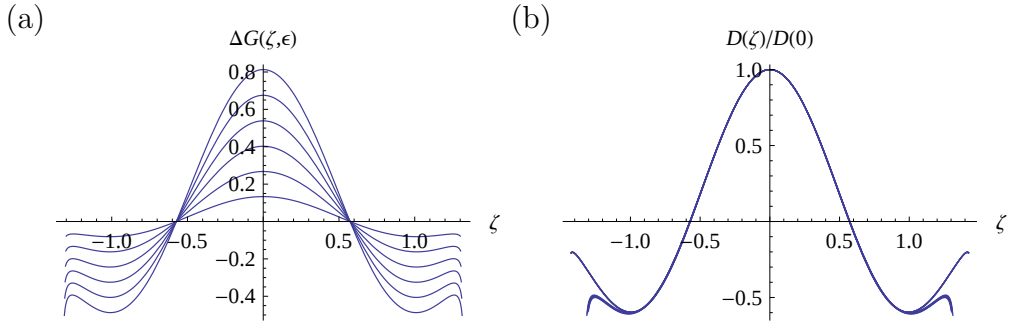

Figure 3.8: (a) Difference, $\Delta G(\zeta, \epsilon) = G(\zeta, 0) - G(\zeta, \epsilon)$, between the pure EdS volume profile rescaled to a fixed four-volume and the rescaled volume profiles for $\epsilon = \epsilon_{\max}/7, \ldots, 6\epsilon_{\max}/7$, with cut-off at $R = a = R_0/4$ and $\epsilon_{\max} = 3^{3/2}(a/R_0)^3$. (b) Repeating the difference measurements of (a) for both $a/R_0 = 1/4$ and $a/R_0 = 1/8$ yields a total of 12 curves, which we have normalized by letting them all go through the point $(0, 1)$. We observe that they are multiples of a single universal curve, modulo some weak cut-off artifacts near $\zeta = \pm\pi/2$ that quickly disappear for smaller values of a/R_0.

static coordinates:

$$H(\epsilon, a/R_0) = \frac{4\pi}{R_0^4}\int_0^{T_P} dT \int_a^{R_{++}} dR R^2 = \frac{8\pi^2}{3}\frac{8\cos^3(\alpha(\epsilon)/3) - 3^{3/2}(a/R_0)^3}{\left|\frac{3\epsilon}{4\cos^2(\alpha(\epsilon)/3)} - 6\cos(\alpha(\epsilon)/3)\right|}\,, \tag{3.21}$$

where $f(R)$, R_{++}, T_P, and $\alpha(\epsilon) = \arccos(-\epsilon)$ were introduced in section 3.2.1. We checked the numerical evaluation of the volume profiles $V_3(\tau, \epsilon)$, as described below, by comparing the value of $H(\epsilon, a/R_0)$ obtained from numerical quadrature of (3.20) to its exact value in (3.21) and found that our numerics are reliable.

For small a/R_0, and over the correspondingly small range of ϵ, the total four-volume is well approximated by

$$\frac{H(\epsilon, a/R_0)}{H(0, a/R_0)} \sim 1 - 3^{-3/2}\left[1 + 3(a/R_0)^3\right]\epsilon\,, \tag{3.22}$$

as can be seen from Fig. 3.7.

In Fig. 3.8(a) we have plotted the difference between the rescaled pure Euclidean de Sitter profile $G(\zeta, 0)$ and the rescaled profiles $G(\zeta, \epsilon)$ for different values of $\epsilon > 0$, with the same interior region cut out, in the mass range given by (3.16) and for same fixed four-volume. They were obtained in Mathematica by first dividing the positive region of the τ-interval into 200 equidistant parts. For each τ the integral (3.17) is computed by numerical quadrature with the integrand given by cubic spline interpolation over 400 equidistant points. These points are obtained by solving numerically the implicit relation (3.7) for R and by finite differences to find R'. Having obtained the points of the $V_3(\tau, \epsilon)$ curve, we perform another cubic interpolation and numerically integrate the resulting function to get $H(\epsilon)$, according to (3.20). This allows us to rescale the profiles and obtain $G(\zeta, \epsilon)$ from equation (3.19). The curves in Fig. 3.8(a) appear to scale linearly in ϵ. Indeed, after a rescaling linear in ϵ, all of them collapse onto the single curve (modulo cut-off artifacts) plotted in Fig. 3.8(b). Since we are restricted to small values of the parameter ϵ, it is not surprising that we are in the linear regime, where rescaled profiles are well approximated by the first two terms of the Taylor expansion in ϵ,

$$G(\zeta, \epsilon) = 2\pi^2 \cos^3 \zeta - \epsilon D(\zeta) + O(\epsilon^2)\,. \tag{3.23}$$

In Fig. 3.8(b) we show $D(\zeta)/D(0)$, that is, the linear coefficient in (3.23), normalized such that its value at $\zeta = 0$ is given by 1.

Numerical simulations produce volume profiles $V_3(\tau)$ in lattice units. Rescaling the range of τ to $[-\pi/2, \pi/2]$ fixes the value of R_0 in lattice units and defines the rescaled volume profile $G(\zeta)$ through equation (3.19). We believe that determining $G(\zeta)$ from numerical simulations of CDT with a mass-line, subtracting it from $2\pi^2 \cos^3 \zeta$ and normalizing this difference to be 1 at $\zeta = 0$ should reproduce the curve $D(\zeta)/D(0)$ plotted in Fig. 3.8(b), thereby establishing a good classical limit of the matter-coupled model. The corresponding value of ϵ can be obtained from comparing the normalized simulation four-volume V_4^*/R_0^4 to $H(\epsilon)$ in (3.21) or (3.22).

3.5 Discussion

In any theory of quantum gravity, it is notoriously difficult to come up with "observables", that is, quantities with an invariant geometric meaning, which may eventually be related to physical observations. Besides their obvious use in bridging between theory and phenomenology, they play an important role at the current stage, when we are not yet in possession of a complete, non-perturbative formulation of quantum gravity. This role is at least two-fold. First, appropriately coarse-grained geometric observables can provide nontrivial tests of whether a proposed non-perturbative theory possesses a well-defined classical limit, and whether in this limit it reproduces the physics of

classical general relativity correctly. Second, evaluating an observable which explicitly probes the quantum regime of the theory can be a means of comparing different candidate theories of quantum gravity.

A prominent example of both of these uses is the so-called spectral dimension of spacetime, measured on short and large scales. Its expectation value was first studied in Causal Dynamical Triangulations [33, 66], exhibiting a characteristic scale dependence. On large scales, the expected classical value of four is reproduced, which decreases to two[7] when approaching the Planck scale, indicating strong deviations from classicality. This is a highly nontrivial result which has since been reproduced in at least two completely different formulations of quantum gravity [90, 91], stimulating further research into a common origin of this seemingly universal behaviour [92, 93].

This example illustrates how observables of this type can yield valuable information about the quantum theory. Unfortunately, they are rather rare. In this chapter, we have looked at another geometric quantity which has been studied previously in CDT, the three-volume profile, which makes explicit use of the proper-time foliation. In a first attempt to try and quantify the effects of matter on geometry in this framework, we have analyzed how the volume profile can be expected to change under insertion of a point-like mass, as a function of the particle mass M, if the corresponding ground state geometry which is generated dynamically by CDT is related to the Schwarzschild-de Sitter geometry.

As we have seen, the analysis involved several nontrivial steps, despite the relatively simple and static nature of the classical metric. The difficulties have to do with the nonlocal nature of the volume profile, which requires a careful treatment of boundary conditions and regions of validity of the coordinate systems one has to use in a continuum calculation. Another difficulty derives from having to define a quantity which is geometric, i.e. independent of any particular coordinate choice, to be able to compare with the (coordinate-free) set-up of the CDT simulations. Both of these issues are characteristic for quantum observables in gravity.

Our specific construction involved the use of a system of Gaussian normal coordinates. On the one hand, this gave us a relatively good control on some of the global properties of the Euclidean Schwarzschild-de Sitter space like at the (Euclideanized) cosmological horizon, on the other hand the coordinates do not cover the complete region outside the source. However, when restricting the mass to be small, the proper-time foliation is nearly global in the sense that neglecting the contribution to the spatial volume from the region inside of a certain small Schwarzschild radius, we obtain an approximation to the actual volume profiles while preserving their characteristic deviation from the Euclidean de Sitter profile. The approximation is equivalent to neglecting

[7] More precisely, a value compatible with two, taking into account the error bars of the Monte Carlo simulations.

those simplices that contain the mass-line when determining the average spatial volume in the computer simulations. Let us point out that the deviations we have computed are small and one will need good control of the numerical errors to measure them. We also found that the correct way of implementing the mass line in the simulations, if one wants to compare to our calculation, is by representing it by a contractible loop on the geometry which has a four-sphere topology.

We regard the work presented in this chapter as a step towards understanding the dynamics of coupled systems of matter and geometry in non-perturbative quantum gravity, about which there is currently little known, since most candidate theories have focussed their efforts on the pure-gravity situation. As we have already mentioned above, it is possible that our treatment can be improved, to cover a larger region of spacetime and/or the case of larger masses. In addition, it would be interesting to derive the volume fluctuations from a mini-superspace action in the same way as has been done for Euclidean de Sitter space [39] and check whether the agreement between the analytical and numerical calculations persists.

Chapter 4

Gravitational perturbations on a FLRW background

Having discussed matter-coupling in form of a point-like mass in the setting of non-perturbative quantum gravity in the previous chapter, we now move on to the discussion of the role of inhomogeneities from spherically symmetric objects of a similar type in inflationary cosmology. For this we first discuss cosmological perturbations on a homogeneous background in this chapter and then analyze the effect of primordial black holes and magnetic monopoles on their spectrum in the following two chapters.

4.1 Gravitational perturbations in cosmology

The main motivation for the inflationary paradigm is the elegant explanation it offers for the anisotropies in the cosmic microwave background (CMB) radiation and the formation of the large scale structure (see [8] for a review). Quantum fluctuations of matter and gravitational degrees of freedom generate scalar cosmological perturbations that are predicted to be responsible for the temperature fluctuations in the CMB and the structure we observe in the universe [54, 94, 95]. In inflationary models the existence of a scalar field (the inflaton) is usually assumed whose energy density is dominated by its potential which drives the rapid expansion. Besides the scalar cosmological perturbations also tensor perturbations of the metric are expected to play an important role during inflation. While predictions coming from scalar cosmological perturbations appear to be consistent with precision measurements of the COBE mission [7], the impact of tensor perturbations could so far not be experimentally tested due to their weak coupling to matter. However, tensor perturbations generated during inflation have been shown to source both types of polarizations in the CMB sky, the E- and B-modes, as opposed to scalar perturbations which do not source B-modes [96]. The detection of a B-mode anisotropy would not only be the strongest evidence for inflation

so far but even determine the scale of inflation. In fact, the Planck mission is designed to observe this effect [62].

We will focus in this chapter on the tensor perturbations of the metric and only briefly comment on the inclusion of the inflaton field in the final section. In general, field perturbations are characterized by their spectrum which is derived from the momentum space representation of the propagator. The derivation of the graviton spectrum requires an expansion of the Einstein-Hilbert action to quadratic order and an isolation of the physical degrees of freedom. Metric perturbations contain only two physical degrees of freedom, namely, the two polarization states of the tensor modes. In the following chapter we will see that in slow-roll inflation the graviton spectrum is suppressed as compared to the spectrum of scalar cosmological perturbations. This justifies the procedure of neglecting the tensor modes when computing corrections to the spectrum of scalar cosmological perturbations from a small black hole.

4.2 Metric perturbations of a general background

The basic assumption of cosmological perturbation theory is that we can split the matter fields and the metric into a background field and dynamical field fluctuations. The latter are considered to be small and their field equations can be linearized. We start with the metric perturbations but we will make a few comments about a minimally coupled scalar field later. In order to separate physical and gauge degrees of freedom we first derive the quadratic action for the metric perturbations by expanding the Einstein-Hilbert action around a fixed background. The metric can thus be written as

$$\hat{g}_{\mu\nu} = g_{\mu\nu} + h_{\mu\nu}\,, \tag{4.1}$$

where $\hat{g}_{\mu\nu}$ denotes the full metric, the background metric is $g_{\mu\nu}$ and the perturbation is $h_{\mu\nu}$. Quantities with a hat will always be computed using $\hat{g}_{\mu\nu}$ and all other quantities using $g_{\mu\nu}$. In D space-time dimensions the Einstein-Hilbert action with a cosmological term is given by

$$S[\hat{g}_{\mu\nu}] = \frac{1}{16\pi G}\int d^D x\sqrt{-\hat{g}}\left(\hat{R} - (D-2)\Lambda\right)\,. \tag{4.2}$$

Later we will set $D = 4$ but we keep the space-time dimension general for the moment since this does not complicate the calculations and the formulas can be used for dimensional regularization if necessary.

Let us now expand the metric determinant $\sqrt{-\hat{g}}$ and the Ricci tensor $\hat{R}_{\mu\nu}$ in the fluctuations. From $\hat{g}_{\mu\nu}\hat{g}^{\nu\alpha} = \delta^{\alpha}_{\ \mu}$ we find that

$$\hat{g}^{\mu\nu} = g^{\mu\nu} - h^{\mu\nu} + h^{\mu}_{\ \alpha}h^{\alpha\nu} + \mathcal{O}(h^3)\,, \tag{4.3}$$

where the cubic orders are dropped here and henceforth. All indices are lowered and raised with the background metric. For short, we denote the trace by $h \equiv g^{\mu\nu}h_{\mu\nu}$. Using the expression (4.3) we find that the expansion of the metric determinant is given by

$$\sqrt{-\hat{g}} = \sqrt{-g}\left(1 + \frac{1}{2}h + \frac{1}{8}h^2 - \frac{1}{4}h_{\mu\nu}h^{\mu\nu}\right) + \mathcal{O}(h^3) \tag{4.4}$$

and the Ricci tensor is

$$\hat{R}_{\beta\delta} = R_{\beta\delta} + R^{(1)}_{\beta\delta} + R^{(2)}_{\beta\delta} + \mathcal{O}(h^3)\,, \tag{4.5}$$

with

$$R^{(1)}_{\beta\delta} = \nabla^\alpha \nabla_{(\beta} h_{\delta)\alpha} - \frac{1}{2}\nabla_\delta\nabla_\beta h - \frac{1}{2}\Box h_{\beta\delta}, \tag{4.6}$$

$$\begin{aligned} R^{(2)}_{\beta\delta} = \frac{1}{2}\Big[& h^{\alpha\mu}\left(\nabla_\delta\nabla_\beta h_{\alpha\mu} + \nabla_\mu\nabla_\alpha h_{\beta\delta} - \nabla_\alpha\nabla_\delta h_{\mu\beta} - \nabla_\alpha\nabla_\beta h_{\mu\delta}\right) \\ & + \frac{1}{2}\nabla_\beta h_{\alpha\mu}\nabla_\delta h^{\alpha\mu} + \nabla^\mu h_\delta{}^\alpha\left(\nabla_\mu h_{\alpha\beta} - \nabla_\alpha h_{\mu\beta}\right) \\ & - \left(\nabla_\alpha h^{\mu\alpha} - \frac{1}{2}\nabla^\mu h\right)\left(\nabla_\delta h_{\mu\beta} + \nabla_\beta h_{\mu\delta} - \nabla_\mu h_{\beta\delta}\right)\Big]. \end{aligned} \tag{4.7}$$

The covariant d'Alembertian is defined as $\Box = g^{\mu\nu}\nabla_\mu\nabla_\nu$ and we have introduced the symmetrization $T_{(\mu\nu)} = \frac{1}{2}\left(T_{\mu\nu} + T_{\nu\mu}\right)$. Hence, we obtain the following expansion of the action

$$\begin{aligned} S &= S^{(0)} + S^{(1)} + S^{(2)} + \mathcal{O}(h^3) \\ &= \frac{1}{16\pi G}\Bigg\{ \int d^Dx\sqrt{-g}\Big[R - (D-2)\Lambda\Big] \\ &\quad + \int d^Dx\sqrt{-g}\Big[R^{(1)} - h^{\beta\delta}R_{\beta\delta} + \frac{1}{2}h\Big(R - (D-2)\Lambda\Big)\Big] \\ &\quad + \int d^Dx\sqrt{-g}\Big[R^{(2)} - h^{\beta\delta}R^{(1)}_{\beta\delta} + h^\beta{}_\alpha h^{\alpha\delta}R_{\beta\delta} + \frac{1}{2}h\Big(R^{(1)} - h^{\beta\delta}R_{\beta\delta}\Big) \\ &\qquad\qquad + \Big(\frac{1}{8}h^2 - \frac{1}{4}h_{\mu\nu}h^{\mu\nu}\Big)\Big(R - (D-2)\Lambda\Big)\Big] + \mathcal{O}(h^3)\Bigg\}. \end{aligned} \tag{4.8}$$

Note that

$$R^{(1)} \equiv g^{\mu\nu}R^{(1)}_{\mu\nu} = \nabla^\alpha\left(\nabla^\beta h_{\alpha\beta} - \nabla_\alpha h\right) \tag{4.9}$$

contributes only a boundary term to $S^{(1)}$. Such boundary terms can be neglected if the field falls off sufficiently fast at infinity. In particular, we will assume that the metric perturbation is irrelevant at the boundary. As usual, the linear order of the action is proportional to the equations of motion,

$$S^{(1)} = -\frac{1}{16\pi G}\int d^Dx\sqrt{-g}\,(EE)^{\mu\nu}\,h_{\mu\nu}\,, \tag{4.10}$$

with

$$(EE)^{\mu\nu} = R^{\mu\nu} - \frac{1}{2}g^{\mu\nu}\Big(R - (D-2)\Lambda\Big) \tag{4.11}$$

that vanishes if the background metric solves Einstein's equations for vacuum but in presence of a cosmological constant. In this case, the field equations can be simplified to

$$R_{\mu\nu} = \Lambda g_{\mu\nu}\,. \tag{4.12}$$

In order to achieve a simple form of the quadratic action, we introduce the trace reversed graviton $\tilde{h}_{\mu\nu} = h_{\mu\nu} - \frac{1}{2}g_{\mu\nu}h$ and find the final expression

$$\begin{aligned} S^{(2)} \;=\; \frac{1}{16\pi G}\int d^D x\sqrt{-g}\Big[&\frac{1}{4}\tilde{h}^{\mu\nu}\left(g_{\alpha\mu}g_{\beta\nu}\Box + 2R_{\alpha\mu\beta\nu}\right)h^{\alpha\beta} + \frac{1}{2}(\nabla_\mu\tilde{h}^{\mu\alpha})(\nabla^\nu\tilde{h}_{\nu\alpha}) \\ &+ \frac{1}{2}h_{\mu\alpha}\tilde{h}^{\alpha}{}_{\nu}\,(EE)^{\mu\nu}\Big]\,. \end{aligned} \tag{4.13}$$

4.3 Perturbations of a FLRW background

For the purpose of application to cosmology we now specialize to the case that the metric around which we are perturbing is the Friedmann-Lemaître-Robertson-Walker (FLRW) metric. The FLRW model describes a homogeneous universe which can expand/contract in cosmological time t with a scale factor $a(t)$. Homogeneity implies that the spatial curvature is constant. In fact, observations have shown that the spatial curvature is very close to zero. Therefore, we will only consider the case of a spatially flat universe with the line element

$$ds^2 = -dt^2 + a^2(t)d\vec{x}^2\,. \tag{4.14}$$

The matter content of the universe is described by the stress-energy tensor of a perfect fluid which is given by

$$T^{\mu\nu} = (p+\rho)\,u^\mu u^\nu + pg^{\mu\nu} \tag{4.15}$$

with the energy density ρ, the pressure p and the four-velocity of the fluid u^μ. The equation of state parameter w relates the fluid density to its pressure,

$$p = w\rho\,. \tag{4.16}$$

During inflation the universe is dominated by the energy density of the inflaton field. This implies that roughly $w = -1$. Non-relativistic matter (pressureless dust) and radiation domination are characterized by $w = 0$ and $w = 1/3$, respectively.

There are two important quantities that determine the evolution of the universe, the Hubble rate

$$H(t) = \frac{\dot{a}}{a} \tag{4.17}$$

and the deceleration parameter

$$\epsilon(t) = -\frac{\dot{H}}{H^2}\,. \tag{4.18}$$

Quantities with a dot are differentiated with respect to t. From Einstein's equations in $D = 4$ it follows that the Hubble rate and the deceleration parameter are related in a simple way to the energy density and pressure

$$H^2 = \frac{8\pi G}{3}\rho + \frac{\Lambda}{3} \tag{4.19}$$

$$(1-\epsilon)\,H^2 = -\frac{4\pi G}{3}\,(\rho + 3p) + \frac{\Lambda}{3}\,. \tag{4.20}$$

These are called the Friedmann equations which play a central role in cosmology.

Let us now proceed to the derivation of the equation of motion for metric perturbations on a FLRW background. For this we first show how the quadratic action decomposes into a scalar, a vector and a tensor sector for the case that no matter fields are present. To start, note that the metric and the curvature tensors of the FLRW geometry assume a particularly simple form if we introduce the conformal time η by setting $dt = ad\eta$. We can thus write the line element as

$$ds^2 = a^2(\eta)\left(-d\eta^2 + d\vec{x}^2\right)\,, \tag{4.21}$$

so the metric is given by $g_{\mu\nu} = a^2(\eta)\eta_{\mu\nu}$ with the Minkowski metric $\eta_{\mu\nu}$. For convenience, let us redefine the metric perturbation by setting $\hat{g}_{\mu\nu} = a^2(\eta)\,(\eta_{\mu\nu} + \psi_{\mu\nu})$, hence

$$h_{\mu\nu} = a^2\psi_{\mu\nu}, \quad \psi = g^{\mu\nu}\psi_{\mu\nu}, \quad \tilde{\psi}_{\mu\nu} = \psi_{\mu\nu} - \frac{1}{2}g_{\mu\nu}\psi\,. \tag{4.22}$$

Neglecting boundary terms, we find that the resulting action in terms of $\psi_{\mu\nu}$ is

$$\begin{aligned} S^{(2)} = \frac{1}{16\pi G}\int d^D x a^{D+4}\Bigg[&\frac{1}{4}\psi^{\mu\nu}\left(\partial^\alpha\partial_\alpha - (D-2)\frac{a'}{a^3}\partial_0\right)\psi_{\mu\nu} \\ &- \frac{1}{4}\psi\left(\partial^\alpha\partial_\alpha - (D-2)\frac{a'}{a^3}\partial_0 + 4\left(\frac{a'}{a^2}\right)^2\right)\psi - \frac{1}{2}(D-2)(D-1)\left(\frac{a'}{a^2}\right)^2\psi_{0\nu}\psi^{0\nu} \\ &+ \frac{1}{2}(D-2)\left((4-D)\left(\frac{a'}{a^2}\right)^2 - \frac{3}{2}\frac{a''}{a^3}\right)\psi\psi^0{}_0 + \frac{1}{2}(D-4)\frac{a'}{a}\psi^{0\alpha}\partial^\nu\psi_{\nu\alpha} \\ &- \frac{1}{2}\psi^{\alpha\lambda}\partial_\lambda\partial^\nu\psi_{\nu\alpha} - (D-1)\frac{a'}{a^3}\psi\partial^\alpha\psi_{0\alpha} + \frac{1}{2}\psi\partial^\alpha\partial^\nu\psi_{\nu\alpha}\Bigg]\,. \end{aligned} \tag{4.23}$$

A prime denotes a derivative with respect to η. Next, we split the metric perturbation $\psi_{\mu\nu}$ into scalar, vector and tensor degrees of freedom. The result is the following decomposition,

$$\begin{aligned} &\psi_{00}, \qquad \tilde{\psi} = \delta^{ij}\psi_{ij}, \qquad \psi_{0i} = F_i + \partial_i B, \\ &\psi_{ij} = \frac{\delta_{ij}}{D-1}\tilde{\psi} + \left(\partial_i\partial_j - \frac{\delta_{ij}}{D-1}\nabla^2\right)S + \partial_{(i}W_{j)} + \psi_{ij}^{TT}\,. \end{aligned} \tag{4.24}$$

Thereby, the ten degrees of freedom of the symmetric tensor field $\psi_{\mu\nu}$ become four scalars ψ_{00}, $\tilde{\psi}$, S and B, two transverse vectors F_i and W_i and a transverse traceless tensor ψ_{ij}^{TT}. There are two degrees of freedom (polarizations) in each transverse vector and two in the transverse traceless tensor. Plugging this decomposition into the action (4.23) yields the action for the scalar modes

$$\begin{aligned} S^S = \frac{1}{16\pi G}\int d^D x\; a^{D-2}\Bigg[& -\frac{1}{4}(D-2)(D-1)\frac{a'^2}{a^2}\psi_{00}^2 \\ & + \frac{1}{2}(D-2)\left(2\frac{a'^2}{a^2}-\frac{a''}{a}\right)(\partial_i B)^2 + \frac{1}{4}\frac{D-2}{D-1}\tilde{\psi}\left(-\overleftarrow{\partial_0}\overrightarrow{\partial_0}-\frac{D-3}{D-1}\nabla^2\right)\tilde{\psi} \\ & + \frac{1}{4}\frac{D-2}{D-1}\nabla^2 S\left(\overleftarrow{\partial_0}\overrightarrow{\partial_0}-\frac{D-3}{D-1}\nabla^2\right)\nabla^2 S - \frac{1}{2}\frac{D-2}{D-1}\psi_{00}\nabla^4 S \\ & + \frac{1}{2}(D-2)\tilde{\psi}\left(\frac{a'}{a}\partial_0+\frac{1}{D-1}\nabla^2+(D-4)\frac{a'^2}{a^2}+\frac{3}{2}\frac{a''}{a}\right)\psi_{00} + (D-2)\frac{a'}{a}\psi_{00}\nabla^2 B \\ & - \frac{D-2}{D-1}\nabla^2 B\partial_0\nabla^2 S + \frac{D-2}{D-1}\nabla^2 B\partial_0\tilde{\psi} + \frac{1}{2}\frac{(D-2)(D-3)}{(D-1)^2}\tilde{\psi}\nabla^4 S\Bigg], \end{aligned} \tag{4.25}$$

the action for the vector modes

$$\begin{aligned} S^V = \frac{1}{16\pi G}\int d^D x\; a^{D-2}\Bigg[& \frac{1}{2}F_i\left(-\nabla^2+(D-2)\left[2\frac{a'^2}{a^2}-\frac{a''}{a}\right]\right)F_i \\ & + \frac{1}{8}\partial_0(\partial_j W_i)\partial_0(\partial_j W_i) + \frac{1}{2}F_i\nabla^2(\partial_0 W_i)\Bigg] \end{aligned} \tag{4.26}$$

and, finally, the action for the tensor modes

$$S^T = \frac{1}{16\pi G}\int d^D x\; a^{D-2}\left[\frac{1}{4}\psi_{ij}^{TT}\left(\partial^2-(D-2)\frac{a'}{a}\partial_0\right)\psi_{ij}^{TT}\right], \tag{4.27}$$

with $\partial^2 = \eta^{\mu\nu}\partial_\mu\partial_\nu$. This result is very powerful since it tells us that the different modes decouple and evolve independently. In particular, we can completely disregard the scalar and vector sectors when computing the power spectrum for the graviton in section 4.5.

Defining the momenta that are canonically conjugate to the scalars[1],

$$\tilde{\pi} = \frac{\delta S^S}{\delta\partial_0\tilde{\psi}}, \quad \pi^{00} = \frac{\delta S^S}{\delta\partial_0\psi_{00}}, \quad \pi^S = \frac{\delta S^S}{\delta\partial_0 S}, \quad \pi^B = \frac{\delta S^S}{\delta\partial_0 B}, \tag{4.28}$$

and the momenta canonically conjugate to the vectors,

$$\pi_i^F = \frac{\delta S^V}{\delta\partial_0 F_i}, \quad \pi_i^W = \frac{\delta S^V}{\delta\partial_0 W_i}, \tag{4.29}$$

[1]In order to compute the momenta, one has to eliminate all second time derivatives by integration by parts.

one can show that they all can be expressed in terms of the fields without time derivatives acting on them. In this sense, there are no physical degrees of freedom in the scalar and vector sectors. On the other hand, we can derive the equation of motion for the dynamical tensor modes by varying the tensor action,

$$\frac{\delta S^T}{\delta \psi_{ij}^{TT}} = \frac{1}{32\pi G} a^{D-2} \left[\partial^2 - (D-2)\frac{a'}{a}\partial_0 \right] \psi_{ij}^{TT} = 0\,. \tag{4.30}$$

As we will see later, it is important for the derivation of the correct amplitude of the graviton spectrum to keep track of the factor $1/(16\pi G)$ that multiplies the tensor action.

4.4 Gauge invariant fields on a FLRW background

The presence of constraints in the phase space of the ten field degrees of freedom in $\psi_{\mu\nu}$ and their conjugate momenta reflects the gauge symmetry of the Einstein-Hilbert action which is invariant under the action of diffeomorphisms. In order to make a connection to measurable quantities, one has to find the gauge invariant fields. For this we determine how the metric perturbation $h_{\mu\nu}$ transforms under infinitesimal diffeomorphisms given by $x^\mu \to x^\mu + \xi^\mu$,

$$h_{\mu\nu} \to h_{\mu\nu} - 2\nabla_{(\mu}\xi_{\nu)} = h_{\mu\nu} - 2\partial_{(\mu}\xi_{\nu)} + 2\frac{a'}{a}\left(\xi_\mu \delta^0{}_\nu + \xi_\nu \delta^0{}_\mu + \xi_0 \eta_{\mu\nu}\right)\,. \tag{4.31}$$

The transformation rules for the scalar, vector and tensor fields are found by performing a decomposition of the vector ξ^μ that generates the gauge transformation. Let us write $\xi^\mu = (\xi^0, \xi^i)$ and $\xi^i = \xi^i_T + \partial_i \xi$, $\partial_i \xi^i_T = 0$. The scalar fields thus transform as

$$\begin{aligned} \psi_{00} &\to \psi_{00} + 2\left(\partial_0 + \frac{a'}{a}\right)\xi^0, \qquad \tilde{\psi} \to \tilde{\psi} - 2\left(\nabla^2 \xi + (D-1)\frac{a'}{a}\xi^0\right)\,, \\ B &\to B - \partial_0 \xi + \xi^0, \qquad S \to S - 2\xi\,, \end{aligned} \tag{4.32}$$

while the vectors transform as

$$F_i \to F_i - \partial_0 \xi^i_T, \qquad W_i \to W_i - 2\xi^i_T\,. \tag{4.33}$$

The tensor modes are found to be gauge invariant. It is now a simple task to construct two gauge invariant scalars, Φ and Ψ, and a gauge invariant vector V_i,

$$\begin{aligned} 2\Phi &= \psi_{00} + \left(\partial_0 + \frac{a'}{a}\right)(\partial_0 S - 2B)\,, \\ 2(D-1)\Psi &= \tilde{\psi} - \nabla^2 S + (D-1)\frac{a'}{a}(2B - \partial_0 S)\,, \\ V_i &= \partial_0 W_i - 2F_i\,, \end{aligned} \tag{4.34}$$

where Φ and Ψ are the Bardeen potentials.

4.5 The power spectrum of gravitons

So far, we have determined the equation of motion for the graviton and established its gauge invariance. Let us now proceed to the quantization of the tensor modes. This will allow us to derive the graviton spectrum that is obtained from the momentum space representation of the graviton propagator. We take the background to be de Sitter space in $D = 4$ although it would be more realistic to consider quasi-de Sitter space which has a small but non-zero deceleration parameter ϵ and describes power law inflation.

We canonically quantize the tensor modes by first defining the conjugate momentum of the tensor perturbation as

$$\pi_{ij}^{TT} = \frac{\delta S^T}{\delta \partial_0 \psi_{ij}^{TT}} = \frac{a^{D-2}}{32\pi G} \partial_0 \psi_{ij}^{TT} \,. \tag{4.35}$$

Since ψ_{ij}^{TT} is transverse and traceless, so is π_{ij}^{TT} and the equal-time Poisson brackets have to be consistent with this property. In addition, the symmetry of the indices has to be respected by the Poisson brackets. We thus make the following ansatz

$$\begin{aligned} &\{\psi_{ij}^{TT}(\vec{x},\eta), \pi_{kl}^{TT}(\vec{y},\eta)\} = \\ &\quad \frac{1}{2}\left(\delta_{ik}\delta_{jl} + \delta_{il}\delta_{jk} - \alpha\delta_{ij}\delta_{kl}\right)\delta^{D-1}(\vec{x}-\vec{y}) \\ &\quad + \frac{1}{2}\left[\omega\left(\delta_{ik}\partial_j\partial_l + \delta_{il}\partial_j\partial_k + \delta_{jl}\partial_i\partial_k + \delta_{jk}\partial_i\partial_l\right) + \beta\left(\delta_{ij}\partial_k\partial_l + \delta_{kl}\partial_i\partial_j\right)\right]\Delta_0(\vec{x},\vec{y}) \\ &\quad + \gamma \int d^{D-1}\vec{z}\left[\partial_i^z\partial_j^z\Delta_0(\vec{x}-\vec{z})\right]\left[\partial_k^z\partial_l^z\Delta_0(\vec{y}-\vec{z})\right] \,, \end{aligned} \tag{4.36}$$

where Δ_0 is a Green's function for the Poisson equation, $\nabla^2\Delta_0(\vec{x},\vec{y}) = \delta^{D-1}(\vec{x}-\vec{y})$. The coefficients α, β, ω and γ are determined from

$$\begin{aligned} \{\psi_{ii}^{TT}(\vec{x},\eta), \pi_{kl}^{TT}(\vec{y},\eta)\} &= 0 \\ \{\partial_i^x\psi_{ij}^{TT}(\vec{x},\eta), \pi_{kl}^{TT}(\vec{y},\eta)\} &= 0 \,, \end{aligned} \tag{4.37}$$

which yields $\alpha = \beta = \frac{2}{D-2}$, $\omega = -1$ and $\gamma = (D-3)/(D-2)$. It follows from (4.36) that the canonical equal time commutation relations are given by

$$[\psi_{ij}^{TT}(\vec{x},\eta), \pi_{kl}^{TT}(\vec{y},\eta)] = \frac{i}{2}\left(P_{ik}P_{jl} + P_{il}P_{jk} - \frac{2}{D-2}P_{ij}P_{kl}\right)\delta^{D-1}\left(\vec{x}-\vec{y}\right) \,, \tag{4.38}$$

with the transverse projector $P_{ij} = \delta_{ij} - \partial_i\partial_j/\nabla^2$. In order to determine the propagator, we still have to find the mode functions. For this we first redefine the field as $\chi_{ij} = a^{(D-2)/2}\psi_{ij}^{TT}$ to eliminate the single time derivative from the equation of motion (4.30). The result is

$$\left[\partial^2 + \frac{D-2}{2}\left(\frac{a''}{a} + \frac{D-4}{2}\frac{a'^2}{a^2}\right)\right]\chi_{ij}(\vec{x},\eta) = 0. \tag{4.39}$$

Next, we perform a Fourier transformation which makes it easier to solve for the mode functions. The quantum field χ_{ij} can be expanded as

$$\chi_{ij}(\vec{x},\eta) = \frac{2}{M_P}\sum_{\alpha=+,\times}\int\frac{d^{D-1}\vec{k}}{(2\pi)^{D-1}}\epsilon_{ij}^{\alpha}(k)\left[\chi(k,\eta)a_\alpha(\vec{k})e^{i\vec{k}\cdot\vec{x}}+\chi^*(k,\eta)a_\alpha^\dagger(\vec{k})e^{-i\vec{k}\cdot\vec{x}}\right], \tag{4.40}$$

where $a_\alpha(\vec{k})$ and $a_\alpha^\dagger(\vec{k})$ are the annihilation and creation operators for gravitons with polarization state α and obey the usual commutation relations

$$[a_\alpha(\vec{k}),a_\beta^\dagger(\vec{k'})] = (2\pi)^{D-1}\delta_{\alpha\beta}\delta^{D-1}(\vec{k}-\vec{k}')\,. \tag{4.41}$$

We have denoted the polarization tensor by ϵ_{ij}^{α}. It obeys the following summation rules,

$$\epsilon_{ij}^{\alpha}\epsilon_{ij}^{\beta} = \delta^{\alpha\beta}, \qquad \sum_\alpha \epsilon_{ij}^{\alpha}(\vec{k})\epsilon_{kl}^{\alpha}(\vec{k}) = \frac{1}{2}\left(P_{ik}P_{jl}+P_{il}P_{jk}-\frac{2}{D-2}P_{ij}P_{kl}\right), \tag{4.42}$$

where the momentum space representation of the transverse projector is $P_{ij}=\delta_{ij}-k_ik_j/k^2$. Specializing now to de Sitter space in $D=4$, we find from the Fourier decomposition (4.40) and from (4.39) that the mode function $\chi(k,\eta)$ satisfies

$$\left[\partial_\eta^2+\vec{k}^2-\frac{2}{\eta^2}\right]\chi(k,\eta)=0\,. \tag{4.43}$$

We have used here that the scale factor is given by $a(\eta)=-1/(H\eta)$ for de Sitter space. The solutions to this equation are given by

$$\chi(k,\eta) = N_k\left(1-\frac{i}{k\eta}\right)e^{-ik\eta} \tag{4.44}$$

and its complex conjugate $\chi^*(k,\eta)$. The normalization factor N_k can be found from the commutation relations (4.38) which yield

$$W[\chi,\chi^*] = \chi\partial_\eta\chi^*-\chi^*\partial_\eta\chi = i \tag{4.45}$$

for the Wronskian of the system of solutions of (4.43). Plugging the solutions $\chi(k,\eta)$ and $\chi^*(k,\eta)$ into this relation it follows that $N_k=1/\sqrt{2k}$.

Let us now move on to the derivation of the spectrum of gravitons on the de Sitter background by computing the two point correlation function. Recall that in $D=4$ we have $h_{ij}=a^2\psi_{ij}=a\chi_{ij}$. From equations (4.40), (4.41) and (4.42) we find that

$$\begin{aligned}&\langle\Omega|h_{ij}(\vec{x},\eta)h_{kl}(\vec{y},\eta)|\Omega\rangle \\ &\quad= \frac{4a^2}{M_P^2}\int\frac{d^3\vec{k}}{(2\pi)^3}\frac{1}{2}\left(\sum_\alpha\epsilon_{ij}^{\alpha}(\vec{k})\epsilon_{kl}^{\alpha}(\vec{k})\right)|\chi(\vec{k},\eta)|^2e^{i\vec{k}\cdot(\vec{x}-\vec{y})} \\ &\quad= \frac{1}{2}\int\frac{dk}{k}\mathcal{P}_g(k,\eta)\frac{\sin(kr)}{kr}\frac{1}{2}\left(P_{ik}P_{jl}+P_{il}P_{jk}-P_{ij}P_{kl}\right),\end{aligned} \tag{4.46}$$

where the vacuum state $|\Omega\rangle$ is the Bunch-Davies vacuum [61] which is annihilated by all $a_\alpha(\vec{k})$. From (4.44) we see that the Bunch-Davies vacuum reduces to the Minkowski or conformal vacuum in the infinite past ($\eta \to -\infty$) and in the UV limit $k \to \infty$. Note that we defined the graviton power spectrum in the last expression together with a factor 1/2 which accounts for the two polarizations of the graviton. Hence, the spectrum is given by

$$\mathcal{P}_g(k,\eta) = \frac{4k^3a^2}{\pi^2}\frac{|\chi_\alpha(k,\eta)|^2}{M_P^2} = \frac{2H^2}{\pi^2 M_P^2}\left(1+\frac{k^2}{(aH)^2}\right). \tag{4.47}$$

The first part dominates in the infrared limit $k \to 0$ (super-Hubble scale) and is physically interpreted as graviton production in de Sitter space. On the other hand, the spectrum reduces to the case of the conformal vacuum in the UV limit.

4.6 Including a minimally coupled scalar field

So far we have only considered gravitational degrees of freedom. Modelling the early universe, however, involves a scalar field whose potential energy drives inflation. A scalar field Φ, the inflaton, is minimally coupled to gravity by adding the matter action

$$S_M = \int d^4x\,\sqrt{-g}\left(-\frac{1}{2}\left(\partial_\mu\Phi\right)\left(\partial^\mu\Phi\right) - V(\Phi)\right) \tag{4.48}$$

to the Einstein-Hilbert action (4.2). By varying this action with respect to the metric we obtain the stress-energy tensor,

$$T_{\mu\nu} = -\frac{2}{\sqrt{-g}}\frac{\delta S_M}{\delta g^{\mu\nu}} = \left(\partial_\mu\Phi\right)\left(\partial_\nu\Phi\right) - g_{\mu\nu}\left(\frac{1}{2}\left(\partial_\alpha\Phi\right)\left(\partial^\alpha\Phi\right) + V(\Phi)\right). \tag{4.49}$$

In the case of homogeneous cosmology with metric (4.14) the field Φ can only be a function of time t. Then, from (4.15), we find that the energy density is $\rho = -T_0{}^0 = \frac{1}{2}\dot{\Phi}^2 + V(\Phi)$ and the pressure is $p = T_x{}^x = T_y{}^y = T_z{}^z = \frac{1}{2}\dot{\Phi}^2 - V(\Phi)$. Using the conservation of stress-energy $\nabla^\mu T_{\mu\nu} = 0$ we obtain the equation of motion for Φ,

$$\ddot{\Phi} + 3H\dot{\Phi} + \frac{dV}{d\Phi} = 0\,. \tag{4.50}$$

Note that slow-roll inflation implies that $\ddot{\Phi}$ can be neglected and that the kinetic energy of the inflaton is small compared to its potential energy, $\dot{\Phi} \ll V(\Phi)$. From the Friedmann equation (4.19) it follows that the Hubble rate in slow-roll inflation is nearly constant and given by

$$H^2 = \frac{8\pi G}{3}\rho = \frac{8\pi G}{3}V(\Phi)\,. \tag{4.51}$$

For the slow-roll parameter $\epsilon = -\dot{H}/H^2$ we find

$$\epsilon \approx \frac{1}{16\pi G V^2}\left(\frac{dV}{d\Phi}\right)^2 . \tag{4.52}$$

Thus, making the adiabatic approximation by neglecting slowly varying quantities is equivalent to the requirement of a flat potential for the inflaton.

When studying cosmological perturbation one should take into account that the universe's expansion is not exactly exponential, or equivalently, that the slow-roll parameter is not exactly zero. In geometrical terms this means that the background is not de Sitter space but quasi-de Sitter space. A rigorous study of cosmological perturbations in slow-roll inflation was presented in [54] and more recently, using the path integral formalism, in [97].

Chapter 5

Curvature perturbations from primordial black holes

5.1 Inhomogeneous cosmology

Precision measurements of the cosmic microwave background (CMB) have shown that the universe is isotropic to a very high degree. Indeed, the CMB radiation is an almost perfect black body [7] with a temperature of $T_0 = 2.725 \pm 0.001$ K [98], and tiny temperature fluctuations superimposed with an amplitude of the order $10^{-5}T_0$ [99]. The exception is the dipole, which is at the level of $10^{-3}T_0$, and can be explained by our motion with respect to the CMB rest frame. The assumption that measurements at any position in the universe would lead to the same result (the 'cosmological principle') implies that the universe is also homogeneous. Observations of the matter distribution in the universe show that it is homogeneous on scales of the order of 100 Mpc and thus support this assumption [100, 101].

On the other hand, certain anomalies (deviations from the ΛCDM model) have been found in the CMB data whose origin is presently not clear. Some of these anomalies are [102, 103]: anomalously small quadrupole and octupole moments, the north-south asymmetry, the peculiar alignment of the quadrupole and octupole [104], the curious lack of power in the temperature angular correlation function on large angular scales [102], etc. Different authors disagree, however, in what constitutes significant deviation from homogeneity and isotropy. For example, Bennett et al. [102] tend to tune down the statistical significance of these anomalies, and argue that they are the result of *a posteriori* selection. They also argue that, in the absence of a deep theoretical justification, which would make further tests possible, these anomalies will most likely remain curiosities. In addition to the CMB anomalies, there are also anomalies in the large scale structure of the universe. For example, observational evidence was reported that there are large scale (dark) flows of galactic clusters [105] which cannot be

explained by homogeneous, adiabatic, Gaussian, cosmological perturbations generated during inflation. Moreover, some authors [106, 107, 108, 109] offer an alternative to dark energy by considering the earth to be located near the center of a large void[1] [109], or by considering a randomly distributed collection of voids in the universe (the Swiss cheese universe) [111, 112].

The question that is posed in this chapter is whether some of these anomalies could be due to the presence of small black holes in the inflationary universe. While answering this question rigorously is hard, here a first step is made in addressing it. Namely, in order to model cosmological perturbations, we consider quantum fluctuations of a massless (or light) scalar field minimally coupled to gravity in Schwarzschild-de Sitter (SdS) space, and calculate the corresponding spectrum. Using the Sasaki-Mukhanov gauge invariant potential in zero curvature gauge, the spectrum of scalar cosmological perturbations is estimated. We make the assumption that the gauge invariant treatment also applies to the inhomogeneous cosmology at hand. However, this approach should be tested by a rigorous study of cosmological perturbations in inhomogeneous settings. Based on the analysis of the previous chapter, it is argued that the tensor perturbations can be ignored, since we expect that, just as in homogeneous cosmologies, their amplitude will be suppressed when compared to that of scalar perturbations.

It is an important question how to relate the results presented in this chapter for the correction to the spectrum of scalar cosmological perturbations for a primordial black hole to the CMB observables. An interesting study in this direction is Ref. [113], where the authors investigate how different types of violation of homogeneity and isotropy would affect the temperature fluctuations in the CMB. Based on symmetry considerations, the authors consider in particular how a point-like defect (particle), a line-like defect (cosmic string) or a plane-like defect (domain wall) would modify the observed temperature anisotropies. By symmetry a small black hole is closest to a point-like object, yet its event horizon makes it a more complex object to study.[2]

The main theoretical motivation for studying spectral inhomogeneities generated by a stationary black hole in inflation is that they yield results which can be tested against observations. In fact, the resulting spectrum can be viewed as a six parameter *template*. A good analogue are the gravitational wave templates provided by black hole binary systems. To illustrate more precisely what we mean, recall that homogeneous inflation produces a (power law) spectrum which, as a function of spatial momentum k, can be viewed as a two-parameter template, the parameters being the spectral amplitude ($\Delta_{\mathcal{R}}$) and its slope ($n_s - 1$), which have been by now tightly constrained

[1] It should be pointed out, however, that constraints on voids have been established recently in [110].

[2] A further complication lies in the fact that a black hole could rotate and/or move with respect to the inflaton's rest frame. The latter could in principle be related to the claimed large scale dark flows [105].

by CMB measurements [114]. When viewed as a template, the SdS spectrum contains four additional parameters. These constitute the black hole position $\vec{y}$ with respect to us and its mass M during inflation[3], which we parametrize by $\mu = (GMH_0/2)^{1/3}$. Here H_0 denotes the de Sitter Hubble parameter, and G is Newton's constant.[4] In the light of the upcoming CMB observatories, such as the Planck satellite, and ever increasing large scale galactic redshift surveys, the hypothesis of black holes in inflation can presumably be tested.

5.2 Inflaton field on Schwarzschild-de Sitter space

5.2.1 Background metric and equation of motion

A primordial black hole breaks the translational invariance of the background but does preserve rotational symmetry. The space-time metric of a black hole in an asymptotically homogeneous universe is the Schwarzschild-de Sitter (SdS) solution, giving rise to a line element which is usually written in static coordinates as

$$ds^2 = -f(\tilde{r})dt^2 + \frac{d\tilde{r}^2}{f(\tilde{r})} + \tilde{r}^2 d\Omega^2 \,, \tag{5.1}$$

with [5] $f(\tilde{r}) = 1 - 2GM/\tilde{r} - \Lambda\tilde{r}^2/3$. In these coordinates the three symmetries of the SdS space are manifest: the time translation invariance and the two spatial rotations. Using these coordinates, quantum fluctuations of a scalar field on the Schwarzschild background have been studied in Ref. [115, 116, 117]. It was found that the radial mode functions of a massless scalar field can be expressed in terms of Heun's functions. But the presence of a cosmological horizon complicates the analysis and the SdS case has only been investigated for an extremal black hole [118]. The reason for this is the difficult singularity structure of the d'Alembertian for (5.1).

For applications to cosmology, another form of the metric is more useful. In Appendix A we show by explicit coordinate transformations that the metric takes the form [6]

$$ds^2 = a^2(\eta)\left\{ -d\eta^2 + \left(1 + \frac{\mu^3\eta^3}{r^3}\right)^{4/3}\left[\left(\frac{1-\mu^3\eta^3/r^3}{1+\mu^3\eta^3/r^3}\right)^2 dr^2 + r^2 d\Omega^2\right]\right\}, \tag{5.2}$$

[3] Of course, the black hole has by now evaporated.

[4] If, in addition, the black hole is moving, three additional parameters are needed to specify its velocity; if it is rotating, three additional parameters are needed to specify its angular momentum; if it is charged, one more parameter is needed. Regarding the results presented in Ref. [105], it would be of particular interest to study the spectrum of a (slowly) moving black hole.

[5] In contrast to the previous chapters, Newton's constant $G = 6.674 \times 10^{-11}$ m^{3}kg^{-1}s^{-2} is not set to one.

[6] A similar form of the metric can be found in [119]. However, it has the disadvantage of being degenerate at the black hole horizon.

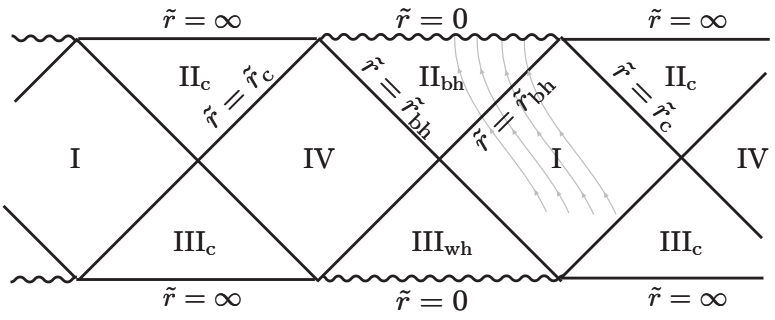

Figure 5.1: This plot shows the Carter-Penrose diagram of Schwarzschild-de Sitter space. It is an infinite sequence of black hole regions ($\mathrm{II_{bh}}$), white hole regions ($\mathrm{III_{wh}}$), static regions (I and IV) and cosmological regions ($\mathrm{II_c}$ and $\mathrm{III_c}$). The coordinates we use reach the black hole singularity as well as the cosmological regions. We show schematically some $r = \text{const.}$ lines (grey). In contrast to $\tilde{r} = \text{const.}$ lines, they are timelike everywhere, cross the black hole horizon and eventually reach the singularity. Arrows indicate the flow in conformal time η. Asymptotic future is given by $\eta \to 0$ and corresponds to the boundary $\tilde{r} = \infty$ in the diagram.

with $\mu = (GMH_0/2)^{1/3}$ and the scale factor a which is a simple function of the conformal time η, $a(\eta) = -1/(H_0\eta)$ ($\eta < 0$). Notice that the metric (5.2) exhibits a black hole singularity at a finite radius, $r_0 = -\mu\eta$ (see also Eq. (7.10)), such that in this metric $r_0 < r < \infty$ covers one half of SdS space. The Carter-Penrose diagram is plotted in Fig. 5.1 (see also [120]) which also shows (schematically) how the interior of the black hole is covered by our coordinates. The Hubble rate H_0 is related to the potential energy of the inflaton through the Friedmann equation, $H_0^2 = V(\phi_0)/(3M_P^2)$, with the reduced Planck mass $M_P = (8\pi G)^{-1/2} = 2.4 \times 10^{18}$ GeV. Here we assume that the inflaton potential energy $V(\phi_0)$ is constant, such that it can be related to the effective cosmological constant as $\Lambda = V(\phi_0)/M_P^2$.

The equation of motion for the massless inflaton field ϕ is the Klein-Gordon equation,

$$\Box\phi(x) = 0, \tag{5.3}$$

where the d'Alembertian $\Box$ acting on a scalar field is given by

$$\Box\phi(x) = g_{\mu\nu}\nabla^\mu\nabla^\nu\phi(x) = \frac{1}{\sqrt{-g}}\partial_\mu\sqrt{-g}g^{\mu\nu}\partial_\nu\phi(x). \tag{5.4}$$

One easily finds from the determinant g of the metric tensor,

$$\sqrt{-g} = a^4 r^2 \sin\theta \left(1 - \frac{\mu^6\eta^6}{r^6}\right), \tag{5.5}$$

and hence

$$\Box\phi(x) = \frac{1}{a^2}\Bigg[- \frac{1}{a^2\left(1-\frac{\mu^6\eta^6}{r^6}\right)}\partial_\eta a^2\left(1-\frac{\mu^6\eta^6}{r^6}\right)\partial_\eta \tag{5.6}$$
$$+ \frac{1}{r^2\left(1-\frac{\mu^6\eta^6}{r^6}\right)}\partial_r r^2 \frac{\left(1+\frac{\mu^3\eta^3}{r^3}\right)^{2/3}\left(1-\frac{\mu^6\eta^6}{r^6}\right)}{\left(1-\frac{\mu^3\eta^3}{r^3}\right)^2}\partial_r + \frac{1}{r^2\left(1+\frac{\mu^3\eta^3}{r^3}\right)^{4/3}}\nabla^2_{S^2}\Bigg]\phi(x),$$

where $\nabla^2_{S^2}$ is the Laplacian on the 2-dimensional sphere,

$$\nabla^2_{S^2} = \frac{1}{\sin(\theta)}\frac{\partial}{\partial\theta}\sin(\theta)\frac{\partial}{\partial\theta} + \frac{1}{\sin^2(\theta)}\frac{\partial^2}{\partial\phi^2}\,.$$

Because the CMB is highly isotropic, translation invariance in the early universe can be only weakly broken [102, 103]. Hence $\mu \ll 1$ and we can expand the metric in the parameter μ to first non-trivial order. The result is:

$$ds^2 = a^2\Bigg\{ - d\eta^2 + \left(1-\frac{8\mu^3\eta^3}{3r^3}\right)dr^2 + \left(1+\frac{4\mu^3\eta^3}{3r^3}\right)r^2 d\Omega^2\Bigg\} + \mathcal{O}\left(\mu^6\right) \tag{5.7}$$
$$\sqrt{-g} = a^4 r^2\sin\theta + \mathcal{O}\left(\mu^6\right)\,; \qquad \Box = \Box^{dS} + \delta\Box + \mathcal{O}\left(\mu^6\right)\,.$$

The differential operator $\Box^{dS}$ is the d'Alembertian on de Sitter space,

$$\Box^{dS} = \frac{1}{a^2}\left(-\frac{1}{a^2}\partial_\eta a^2\partial_\eta + \nabla^2\right) = \frac{1}{a^2}\left(-\frac{1}{a}\partial^2_\eta a + \nabla^2 + \frac{a''}{a}\right)\,, \tag{5.8}$$

and

$$\delta\Box = \frac{4\mu^3\eta^3}{3r^3}\left(\frac{2r}{a^2}\partial_r\frac{1}{r}\partial_r - \frac{1}{a^2r^2}\nabla^2_{S^2}\right) = -\frac{4\mu^3H_0^2\eta^5}{3r^3}\left(\nabla^2 - 3\partial_r^2\right), \tag{5.9}$$

with $a' = da/d\eta$ and $\nabla^2 = \partial_i\partial_i$ is the Cartesian Laplace operator in 3 dimensions.

5.2.2 An estimate of the perturbation parameter μ

The metric (5.2) contains the perturbation parameter $\mu = (GMH_0/2)^{1/3}$ as a constant. A more realistic point of view, however, is that a black hole of mass M decays due to an evaporation process and H_0 is a time-dependent expansion rate of the universe. Assuming a slow-roll inflationary scenario, i.e. small deceleration parameter

$$\epsilon = -\frac{\dot{H}}{H^2} \ll 1\,, \tag{5.10}$$

we can neglect the time-dependence of H_0 in the following discussion. Further comments on this approximation are made in section 5.4. For the rate of change of M we make the following estimate. The evaporation time of a black hole is known to be [63, 121]

$$T = \frac{30720\pi}{g_*}G^2M^3\,, \tag{5.11}$$

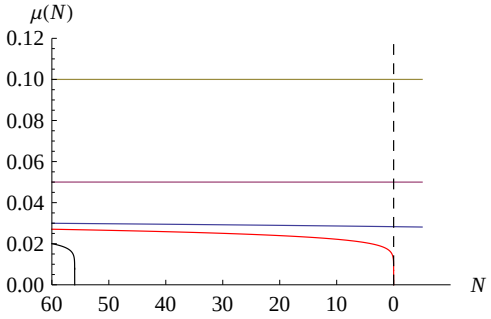

Figure 5.2: The dependence of μ on the number of e-foldings N is displayed here for different values μ_0 at the start of inflation. The red curve (second from below) corresponds to $\mu_{\rm crit} \approx 0.027$, the black hole evaporates after 60 e-foldings in this case. Below this critical value black holes evaporate before the end of inflation, black (lowest) curve. Above $\mu_{\rm crit}$ primordial black holes survive inflation. Their mass is seen to be constant to a very good approximation (blue, purple and brown curve).

where $g_* \sim 10^2 - 10^3$ is the number of relativistic degrees of freedom at the energy scale $\sim 1/(GM)$. The correction to the evaporation time (5.11) due to the Hubble horizon is negligible as long as $\mu \ll 1$ [121]. Assuming that the evaporation process takes longer than $N = 60$ e-foldings we get,

$$\mu > \mu_{\rm crit} = \left(\frac{1}{2} \left(\frac{NGH_0^2 g_*}{30720\pi} \right)^{1/3} \right)^{1/3} \simeq 0.027\,, \tag{5.12}$$

where we took $GH_0^2 \simeq 10^{-12}$ and $g_* \simeq 10^2$. In summary, for primordial black holes with a mass parameter $0.027 \lesssim \mu \ll 1$ we expect the SdS background to be a good realization of the inhomogeneous inflationary scenario. The constancy of μ is demonstrated in Fig. 5.2.

5.3 Formation probability for black holes

To assess the physical relevance of primordial black holes we first have to estimate the probability for their formation. For this we consider a pre-inflationary period dominated by heavy non-relativistic particles with a mass m smaller than the Planck mass $m_p = G^{-1/2} = 1.2 \times 10^{19}$ GeV and Hubble rate $H_* < m_p$ (here and henceforth an index $*$ refers to quantities evaluated at the initial time t_*). On not too small scales the matter distribution is well described by the local mass density $\rho(\vec{x}, t) = \rho_0(t)(1+\delta(\vec{x}, t))$. For the formation of a black hole we are interested in the growth of density fluctuations inside of a bounded region. Due to the universe's expansion it is natural to consider the number of particles $N(R, t)$ in a ball with *comoving* radius R and *comoving* volume V_R at time t. The initial statistical fluctuations for the particle number are assumed to be Gaussian, $\delta N(R, t) \sim \sqrt{N(R, t)}$ with variance $\sigma(R, t) = \langle \delta N(R, t)^2 \rangle = \langle N(R, t) \rangle$.

The mass density in the ball is linearly related to the local density,

$$\rho(R,t) = \frac{1}{V_R}\int_{\|\vec{x}\|<R} d^3\vec{x}\ \rho(\vec{x},t)\,, \tag{5.13}$$

which can also be written as $\rho(R,t) = mN(R,t)/V_R$. Fluctuations in the particle number are thereby easily translated into density fluctuations.

Black holes can potentially form from gravitational interaction due to gravitational attraction of such fluctuations [63]. To study their evolution we consider the classical equation of motion for $\delta(\vec{x},t) = \delta\rho(\vec{x},t)/\rho_0(t)$ [122]:

$$\ddot{\delta} + 2H\dot{\delta} - c_s^2\left(\frac{\nabla}{a}\right)^2\delta - 4\pi G\rho_0(1+w)(1+3w)\delta = 0\,, \tag{5.14}$$

with the speed of sound $c_s^2 = \partial p_0/\partial\rho_0 = w$, where p_0 is the background fluid pressure. We take the equation of state parameter $w = p_0/\rho_0$ to be constant. When the gravitational term dominates in the above equation the density perturbation becomes unstable. The critical scale for the perturbation is given by the Jeans momentum

$$\left(\frac{k}{a}\right)_J = \frac{\sqrt{4\pi G\rho_0(1+w)(1+3w)}}{c_s}, \tag{5.15}$$

which determines when thermal pressure is in balance with the gravitational force. The Jeans length $\lambda_J = 2\pi/(k/a)_J$ reaches the Hubble radius $R_H = 1/H$ if $w \approx 1/3$ but for $w \approx 0$ the Jeans length is very small compared to R_H and small black holes can form. We can solve Eq. (5.14) for $k/a \ll (k/a)_J$ (super-Jeans scale) by making the ansatz $\delta \propto t^\alpha$ and we find that

$$\delta(k,t) = \delta_*(k)\left(\frac{t}{t_*}\right)^{\frac{2(1+3w)}{3(1+w)}} + \overline{\delta}_*(k)\left(\frac{t}{t_*}\right)^{-1}. \tag{5.16}$$

We shall neglect the second mode which is always decaying. The first mode is growing in decelerating space-times ($w > -1/3$), whereas in accelerating space-times ($-1 \leq w \leq -1/3$) it also decays. The amplification actually increases with increasing w but, as mentioned before, we are only interested in the case $w \approx 0$ since in this case $\lambda_J/a \ll R_H$, which also has to be satisfied for the growing solution. The initial density perturbation is given by

$$\delta_*(k) \equiv \frac{\delta\rho_*(k)}{\rho_*(k)} \simeq \frac{\delta N_*(k)}{N_*(k)} \sim \frac{1}{\sqrt{N_*(k)}}. \tag{5.17}$$

Clearly, we have to look at large fluctuations away from the mean value $\langle N\rangle$ to find a significant probability of black hole formation. It is convenient to translate momentum space fluctuations $\delta\rho(k,t)$ to fluctuations in a ball of comoving radius R by writing

$$\frac{\delta N(R,t)}{\langle N(R,t)\rangle} = \frac{\delta\rho(R,t)}{\rho_0(t)} = \int_0^\infty dk\ \frac{\delta\rho(k,t)}{\rho_0(t)}W(kR)\,, \tag{5.18}$$

with $\delta\rho(k,t) = \langle\delta\rho(\vec{k},t)\rangle_{\theta,\phi}$ being the angle averaged momentum space mass density and

$$W(kR) = \frac{2}{\pi}\frac{\sin(kR) - kR\cos(kR)}{kR} \tag{5.19}$$

the *window function* for spherically distributed matter in a ball of radius R. From relation (5.18) we conclude that $\delta N(R,t)/\langle N(R,t)\rangle$ grows precisely as the momentum space fluctuations (5.16),

$$\frac{\delta N(R,t)}{\langle N(R,t)\rangle} = \frac{\delta N_*(R_*)}{\langle N_*(R_*)\rangle}\left(\frac{H_*}{H}\right)^{\frac{2(1+3w)}{3(1+w)}} . \tag{5.20}$$

Next, note that

$$\langle N(R,t)\rangle = \frac{m_p^2 H^2 R^3}{2m} , \tag{5.21}$$

which follows from the Friedmann equation, $H^2 = (8\pi/3)\rho_0(t)/m_p^2$ and from

$$\rho_0(t) = \frac{3}{4\pi}\frac{\langle N(R,t)\rangle m}{R^3} .$$

Now, from Eq. (5.17) and (5.21), we can write,

$$\sigma_*(R_*) = \langle\delta N_*(R_*)^2\rangle = \langle N_*(R_*)\rangle = \frac{m_p^2 H_*^2 R_*^3}{2m} \tag{5.22}$$

and hence

$$\sigma(R,t) \equiv \langle\delta N^2(R,t)\rangle = \frac{\langle N(R,t)\rangle^2}{\langle N_*(R_*)\rangle}\left(\frac{H_*}{H}\right)^{\frac{4(1+3w)}{3(1+w)}} = \frac{m_p^2 H^4 R^6}{2m H_*^2 R_*^3}\left(\frac{H_*}{H}\right)^{\frac{4(1+3w)}{3(1+w)}} . \tag{5.23}$$

The physical radius of the ball we consider is given by $R(t) = R_*(a/a_*)$ and thus $R(t) = R_*(H_*/H)^{\frac{2}{3(1+w)}}$ in (5.23). In a decelerating universe, $w > -1/3$, the comoving radius grows slower than the Hubble radius R_H, such that, if $R_* < 1/H_*$ initially at $t = t_*$, it will remain sub-Hubble at later times. This trend reverses during inflation, in which $w < -1/3$.

A black hole with Schwarzschild radius R_S forms if, due to statistical fluctuations, the number of particles in V_{R_S} becomes sufficiently large, $N(R_S,t) > R_S m_p^2/(2m)$. Using (5.21) and writing $N(R_S,t) = \langle N(R_S,t)\rangle + \delta N(R_S,t)$ one obtains the condition

$$\delta N > \delta N_{\rm cr} = \frac{m_p^2 R_S}{2m} - \langle N(R_S,t)\rangle = \frac{m_p^2 R_S}{2m}[1 - (HR_S)^2] . \tag{5.24}$$

Thus, using that the fluctuations δN are Gaussian distributed,

$$P(\delta N) = \frac{1}{\sqrt{2\pi\sigma}}\exp\left(-\frac{\delta N^2}{2\sigma}\right) ,$$

with $\sigma = \langle\delta N^2\rangle$, the probability that a black hole forms is found to be

$$P\big(\delta N(R_S,t) > \delta N_{\rm cr}(R_S,t)\big) = \int_{\delta N_{\rm cr}}^{\infty} d(\delta N)P(\delta N) \approx \frac{1}{2\sqrt{\pi}}\frac{\exp\Big(-\frac{\delta N_{\rm cr}^2}{2\sigma(R_S,t)}\Big)}{\delta N_{\rm cr}/\sqrt{2\sigma}}, \tag{5.25}$$

where, making use of Eqs. (5.23) and (5.24),

$$\frac{\delta N_{\rm cr}}{\sqrt{2\sigma(R_S,t)}} = \frac{m_p}{2H_*\sqrt{mR_*}}[1-(RH)^2] = \frac{m_p}{2H\sqrt{mR}}[1-(RH)^2]\left(\frac{H}{H_*}\right)^{\frac{2+3w}{3(1+w)}} \gg 1\,. \tag{5.26}$$

The inequality in (5.26) is needed to correctly evaluate the integral (5.25). Notice also that, when that inequality is met, the probability for black hole formation is (exponentially) suppressed. Clearly, the inequality is broken for super-Hubble scales, for which $RH > 1$. But at super-Hubble scales we do not expect the analysis to be valid anyway because of the suppression of statistical fluctuations (see also the comments further below). For later purposes it is useful to rewrite our result for the probability of black hole formation (5.25–5.26) as

$$P(\mu,m,H) = \frac{\mu^{3/2}}{1-16\mu^6}\sqrt{\frac{4mH}{\pi m_p^2}}\left(\frac{H_*}{H}\right)^{\frac{2+3w}{3(1+w)}}\exp\left(-\frac{m_p^2(1-16\mu^6)^2}{16mH\mu^3}\left(\frac{H}{H_*}\right)^{\frac{2(2+3w)}{3(1+w)}}\right), \tag{5.27}$$

where we made use of the mass parameter $\mu = (GMH/2)^{1/3}$. Obviously, $\mu < 4^{-1/3}$ must be satisfied in order for a black hole to be sub-Hubble. The question is then how to convert the probability (5.25) into the number of black holes formed before inflation and during inflation. The analysis presented above is meant to provide a rough estimate of the number of sub-Hubble black holes formed before inflation, and neither takes a proper account of causality, nor of nonlinear dynamics of over-densities. Staying within this type of reasoning, we propose to interpret (5.27) as an estimate for the probability that a black hole formed by the beginning of inflation in a comoving volume $V_R = (4\pi/3)R^3$. The expected number of black holes per Hubble volume $(4\pi/3)R_H^3$ at the beginning of inflation is then

$$\langle N_{\rm BH}(\mu,m,H)\rangle \approx \frac{P(\mu,m,H)}{(R_SH)^3} = \frac{P(\mu,m,H)}{64\mu^9}\,. \tag{5.28}$$

If that Hubble volume corresponds to X Hubble volumes today, then there will be about $X\langle N_{\rm BH}(\mu,m,H)\rangle$ pre-inflationary black holes within our past lightcone. A more detailed discussion on how to relate the number of black holes (5.28) to the number of (pre-)inflationary black holes potentially observable today is given in section 5.9. In Fig. 5.3 we show how the expected number of black holes (5.28) depends on the black hole mass parameter μ for different values of particle mass m and initial Hubble rate H_*. We emphasize, however, that in our analysis we make the assumption that the statistical fluctuations are normally distributed on all scales. This might not be true, as has been argued for example in [123], where fluctuations of other types are considered on super-Hubble scales. Causality can limit the size of these statistical fluctuations. It may be more realistic to assume that on super-Hubble scales surface

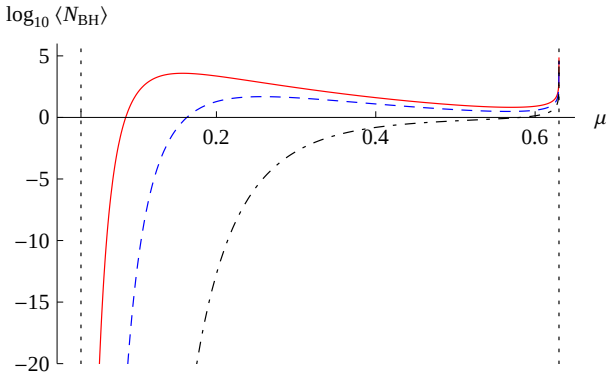

Figure 5.3: In this figure we display the formation probability of black holes per Hubble volume on a logarithmic scale as a function of the mass parameter $\mu = (GMH/2)^{1/3}$ for particle mass $m = 0.3\,m_p$ and initial Hubble parameter $H_* = 0.3\,m_p$ (solid curve, red), $m = 0.3\,m_p$ and $H_* = 0.1\,m_p$ (dashed, blue) and $m = 0.01\,m_p$ and $H_* = 0.3\,m_p$ (dot-dashed, black). The left vertical dashed line indicates the critical black hole mass $\mu_{\rm crit} = 0.03$ and the right one marks $\mu = 4^{-1/3}$. Black holes with mass parameter close to $\mu_{\rm crit}$ are seen to be Gaussian suppressed, whereas in the intermediate range their number can be $\mathcal{O}(1)$ per Hubble volume at the beginning of inflation.

fluctuations are dominant, $\delta N \propto \sqrt{S} \sim N^{1/3}$ and $\sigma \approx \langle N \rangle^{2/3}$, thus, suppressing the formation of black holes that are initially super-Hubble. The actual probability for black hole formation might therefore be smaller in the region $\mu \sim 4^{-1/3}$ than it is shown in Fig. 5.3. Moreover, the formation probability depends strongly on the mass m of the heavy particles, and yet we do not know much about it. Based on our current understanding of particle physics and gravity, it is reasonable to assume that m is limited from above by the Planck mass m_p. If $m \ll m_p$, however, the particles would start behaving relativistically, which would increase the Jeans length and further suppress, or even prevent, the formation of black holes.

5.4 From scalar fluctuations to scalar cosmological perturbations

5.4.1 Homogeneous background

Before discussing the effect of inhomogeneities on the scalar spectrum, we review the treatment of cosmological perturbations on homogeneous backgrounds, such as described the conformally flat background metric, $g^b_{\mu\nu} = a^2(\eta)\eta_{\mu\nu}$, that we considered already in the previous chapter. The physical situation we have in mind is a slow-roll inflationary model driven by a homogeneous inflaton field $\phi_0(t)$, where the Hubble parameter $H(t)$ is a slowly varying function of time and the de Sitter limit is obtained when $H \to H_0 = \text{const}$. Scalar perturbations in this model are induced by the quan-

tum fluctuations of the inflaton, while tensor perturbations are induced by the quantum fluctuations of the graviton. We have previously shown that in linearized perturbation theory the two decouple.

Let us consider again the decomposition of the inflaton Φ and the metric tensor $g_{\mu\nu}$ into the background fields ϕ_0, $g^b_{\mu\nu}$ and the fluctuations ϕ, $h_{\mu\nu}$,

$$\Phi(x) = \phi_0(t) + \phi(x)\,, \qquad g_{\mu\nu}(x) = g^b_{\mu\nu}(t) + a^2 h_{\mu\nu}(x)\,.$$

The background fields a and ϕ_0 are classical field configurations, whereas $h_{\mu\nu}$ and ϕ are dynamical quantum fields. A detailed study shows that (see e.g. [97]) there are only three physical degrees of freedom, two from the graviton and one from the scalar field. In homogeneous cosmology these can be expressed in terms of the gauge invariant tensor h^{TT}_{ij} and the gauge invariant Sasaki-Mukhanov field (curvature perturbation),

$$\mathcal{R} = \psi - \frac{H}{\dot\phi_0}\phi\,, \tag{5.29}$$

where ψ is the scalar gravitational potential defined by the scalar-vector-tensor decomposition of h_{ij}:

$$h_{ij} = 2\psi\delta_{ij} - 2\partial_i\partial_j E + 2\partial_{(i}F_{j)} + h^{TT}_{ij} \tag{5.30}$$

and ϕ is the inflaton fluctuation. When working with gauge invariant variables, such as $\mathcal{R}$ in (5.29), we are guaranteed to get observable CMB temperature fluctuations, since it is the gradient of $\mathcal{R}$ that sources photon number fluctuations through the photon Boltzmann equation. One can also get a physically sensible answer when one fixes a gauge. For example, in the comoving gauge, in which $\phi = 0 = E = F_i = 0$, it is the spatial gravitational potential ψ that determines the Sasaki-Mukhanov field, $\mathcal{R} = \psi$ (5.29). On the other hand, in the zero curvature gauge, in which $\psi = 0 = E = F_i = 0$, it is the inflaton fluctuation ϕ that determines $\mathcal{R}$ through (5.29),

$$\mathcal{R} = -\frac{H}{\dot\phi_0}\phi \qquad (\text{zero curvature gauge})\,. \tag{5.31}$$

This relation can be used to estimate the late time potential from the inflaton fluctuations $\phi(x)$. The spectrum of scalar cosmological perturbations $\mathcal{P}_\mathcal{R}$ in the zero curvature gauge ($\mathcal{P}_\mathcal{R}$ is conserved on super-Hubble scales) is related to the spectrum of scalar field fluctuations $\mathcal{P}_\phi$ as,

$$\mathcal{P}_\mathcal{R} = \frac{H^2}{\dot\phi_0{}^2}\mathcal{P}_\phi = \frac{1}{2\epsilon M_P^2}\mathcal{P}_\phi\,. \tag{5.32}$$

In order to get the latter identity, we used the second Friedmann equation, $-4\pi G\dot\phi^2 = \dot H$, and the definition for the slow-roll parameter, $\epsilon = -\dot H/H^2$.

Of course, there are two remaining degrees of freedom in the graviton which have not been taken into account. However, the graviton spectrum $\mathcal{P}_g$ is known to be suppressed

in slow-roll inflation [97, 114, 124] [cf. also (4.47)]

$$\mathcal{P}_g = \frac{2H^2}{\pi^2 M_P^2}, \qquad r \equiv \frac{\mathcal{P}_g}{\mathcal{P}_\mathcal{R}} = 16\epsilon \ll 1\,, \tag{5.33}$$

such that, to first approximation, we can neglect the graviton contribution to the spectrum of cosmological perturbations.

Finally, the field fluctuations can be translated to the temperature-temperature correlation function as [113],

$$\begin{aligned}\left\langle \frac{\delta T(\hat{n}_1)\delta T(\hat{n}_2)}{T_0^2} \right\rangle &= \int \frac{d^3k d^3k'}{(2\pi)^6} \sum_{l,l'} \frac{(2l+1)(2l'+1)}{(4\pi)^2}(-i)^{l+l'} \\ &\quad \times P_l(\vec{k}\cdot\hat{n}_1/k) P_{l'}(\vec{k'}\cdot\hat{n}_2/k')\mathcal{R}(\vec{k})\Theta_l(\vec{k})\mathcal{R}(\vec{k'})\Theta_{l'}(\vec{k'})\,,\end{aligned} \tag{5.34}$$

where $P_l(x)$ denotes a Legendre polynomial, and $\Theta_l(\vec{k}\,)$ and $\Theta_{l'}(\vec{k'})$ denote the appropriate transfer functions, which relate $\mathcal{R}(\vec{k}\,)$ to $\delta T(\vec{k}\,)$, and which are obtained by solving the Boltzmann equation for the photon fluid.

5.5 A small black hole in a de Sitter universe

Keeping in mind the procedure of the previous section for the derivation of cosmological perturbations from scalar fluctuations we have to pay special attention to use gauge invariant fields also in the inhomogeneous case. We split the metric into the Schwarzschild-de Sitter background (5.7) and a perturbation $h_{\mu\nu}$. The spatial part of the perturbation h_{ij} can be decomposed as

$$h_{ij} = 2\psi\gamma_{ij} - 2\overline{\nabla}_{(i}\overline{\nabla}_{j)}E + 2\overline{\nabla}_{(i}F_{j)} + h_{ij}^{TT}\,, \tag{5.35}$$

where γ_{ij} is the induced metric on the spatial slices for the metric (5.7) and $\overline{\nabla}$ is the covariant derivative compatible with γ_{ij}. The vector ξ^μ that generates the gauge transformation $x^\mu \to x^\mu + \xi^\mu(x)$ can be written as $\xi^\mu = (\xi^0, \xi^i)$, with $\xi^i = \xi^i_\mathrm{T} + \overline{\nabla}^i\xi$ and $\overline{\nabla}_i\xi^i_\mathrm{T} = 0$. The metric perturbation transforms as

$$\begin{aligned} h_{ij} \to h'_{ij} &= h_{ij} - 2\nabla_{(i}\xi_{j)} \\ &= 2\psi\gamma_{ij} - 2\overline{\nabla}_{(i}\overline{\nabla}_{j)}(E+\xi) + 2\overline{\nabla}_{(i}(F_{j)} - \xi^\mathrm{T}_{j)}) + h_{ij}^{TT} + 2\Gamma^0_{ij}\xi_0 \end{aligned} \tag{5.36}$$

with the Christoffel symbols of the metric (5.7)

$$\Gamma^0_{ij} = \frac{H_0}{a}\gamma^\mathrm{dS}_{ij} - \frac{3H_0}{2a}\delta\gamma_{ij} \tag{5.37}$$

and

$$\gamma^\mathrm{dS}_{ij} = a^2\begin{pmatrix} 1 & 0 & 0 \\ 0 & r^2 & 0 \\ 0 & 0 & r^2\sin^2\theta \end{pmatrix}, \qquad \delta\gamma_{ij} = \frac{4a^2\mu^3\eta^3}{3r^3}\begin{pmatrix} -2 & 0 & 0 \\ 0 & r^2 & 0 \\ 0 & 0 & r^2\sin^2\theta \end{pmatrix}. \tag{5.38}$$

Moreover, we observe that $\delta\gamma_{ij}$ is traceless to the relevant order in μ, showing that ξ_0 generates also transformations of F_j and h_{ij}^{TT}. The transformation properties of the two scalars ψ and E are

$$\psi \to \psi + \frac{H_0}{a}\xi_0 + \mathcal{O}(\mu^6), \qquad E \to E + \xi + \mathcal{O}(\mu^6). \tag{5.39}$$

Together with the gauge transformation of the scalar field, $\phi \to \phi + (\phi_0'/a^2)\xi_0$, we find that

$$\psi - \frac{H_0 a}{\phi_0'}\phi \to \psi - \frac{H_0 a}{\phi_0'}\phi + \mathcal{O}(\mu^6). \tag{5.40}$$

We conclude that the Sasaki-Mukhanov field $\mathcal{R}$ in Eq. (5.29) is gauge invariant (to order μ^3) also when the inhomogeneity caused by a small black hole is taken into account.

The fact that ξ_0 generates gauge transformations of F_j and h_{ij}^{TT} suggests a mixing of the scalar, vector and tensor sectors in inhomogeneous cosmology. Therefore, for a completely rigorous treatment one should look at the quadratic action on the SdS background and take into account the couplings of the modes.

Furthermore, we make use of the slow-roll paradigm. This means that, even though strictly speaking our results will be derived in SdS space, we shall assume that they hold in quasi-de Sitter space endowed with a small (decaying) black hole, provided one demands the replacements: $H \to H(t)$ and $M \to M(t)$. This is justified when both the Hubble parameter and the black hole mass change adiabatically in time, in the sense that $\dot{H} \ll H_0^2$ ($\epsilon \ll 1$) and $\dot{M} \ll MH_0$.

5.6 The propagators

To study scattering experiments one typically calculates the S-matrix elements. In cosmology, on the other hand, one is primarily interested in expectation values of operators with respect to some definite vacuum state. For this purpose the `in-in` or Schwinger-Keldysh formalism [125, 126, 127, 128, 97] is suitable, in which time evolution of an operator is described in terms of the perturbation theory based on the Keldysh propagator and the `in-in` vertices. Since here we are primarily interested in the spectrum of a scalar field on SdS space, which can be obtained from any equal time two-point correlator, for our purpose it suffices to calculate the corresponding Keldysh propagator.

The Keldysh propagator is a 2×2-matrix of the form,

$$i\mathbf{G}(x;x') = \begin{pmatrix} iG_{++}(x;x') & iG_{+-}(x;x') \\ iG_{-+}(x;x') & iG_{--}(x;x') \end{pmatrix}, \tag{5.41}$$

whose components are the Wightman functions iG_{+-}, iG_{-+} and (anti-)time ordered Feynman propagators iG_{++}, iG_{--}, defined as,

$$\begin{aligned} iG_F(x;x') \equiv iG_{++}(x;x') &= \langle\Omega|T\phi(x)\phi(x')|\Omega\rangle && \text{(Feynman)} \\ iG_{+-}(x;x') &= \langle\Omega|\phi(x')\phi(x)|\Omega\rangle && \text{(Wightman)} \\ iG_{-+}(x;x') &= \langle\Omega|\phi(x)\phi(x')|\Omega\rangle && \text{(Wightman)} \\ iG_{--}(x;x') &= \langle\Omega|\overline{T}\phi(x)\phi(x')|\Omega\rangle && \text{(anti}-\text{Feynman)}\,, \end{aligned} \tag{5.42}$$

where $|\Omega\rangle$ is a suitably chosen vacuum state. The time ordering is defined as

$$\begin{aligned} T\phi(x)\phi(x') &= \theta(x_0-x_0')\phi(x)\phi(x') + \theta(x_0'-x_0)\phi(x')\phi(x) \\ \overline{T}\phi(x)\phi(x') &= \theta(x_0-x_0')\phi(x')\phi(x) + \theta(x_0'-x_0)\phi(x)\phi(x')\,, \end{aligned} \tag{5.43}$$

i.e. later times are to the left for T and early times are to the left for $\overline{T}$. The propagator $i\mathbf{G}$ satisfies the equation

$$\sqrt{-g(x)}\left(\Box_x - m_{\rm eff}^2\right) i\mathbf{G}(x;x') = i\sigma^3\delta^4(x-x')\,, \tag{5.44}$$

where σ^3 is the Pauli matrix

$$\sigma^3 = \begin{pmatrix} 1 & 0 \\ 0 & -1 \end{pmatrix} \tag{5.45}$$

and $m_{\rm eff}^2 = d^2V(\phi_0)/d\phi_0^2$ is the effective mass-squared of the field, which in the following we neglect. In slow-roll inflation $m_{\rm eff}$ can be expressed in terms of the second slow-roll parameter $\eta_V = M_P^2V''/V$, i.e. $m_{\rm eff}^2 = \eta_V V(\phi_0)/M_P^2$, such that setting $m_{\rm eff} \to 0$ is equivalent to $\eta_V \to 0$.

5.6.1 The de Sitter case

In analogy to the graviton case in the previous chapter, we can solve the equation of motion for the massless scalar field (5.3–5.4) in de Sitter space explicitly. Taking advantage of spatial homogeneity of de Sitter space, the following mode decomposition of the free field is convenient,

$$\phi(\eta,\vec{x}) = \int \frac{d^3\vec{k}}{(2\pi)^3}\left[u_k(\eta)b(\vec{k}\,)\mathrm{e}^{i\vec{k}\cdot\vec{x}} + u_k^*(\eta)b^\dagger(\vec{k}\,)\mathrm{e}^{-i\vec{k}\cdot\vec{x}}\right], \tag{5.46}$$

where $b(\vec{k}\,)$ and $b^\dagger(\vec{k}\,)$ are the annihilation and creation operators and obey the commutation relation, $[b(\vec{k}\,), b^\dagger(\vec{k}\,')] = (2\pi)^3\delta^3(\vec{k}-\vec{k}\,')$. The mode functions $u_k(\eta)$ in (5.46) satisfy the equation

$$\left(\partial_\eta^2 + k^2 - \frac{2}{\eta^2}\right)[au_k(\eta)] = 0\,. \tag{5.47}$$

We obtained this result by making use of (5.8) and noting that $a(\eta) = -1/(H_0\eta)$ implies $a''/a = 2/\eta^2$. Imposing the boundary condition that the mode functions behave like in the conformal vacuum in the asymptotic past yields

$$u_k(\eta) = \frac{1}{a}\frac{1}{\sqrt{2k}}\left(1 - \frac{i}{k\eta}\right)\mathrm{e}^{-ik\eta}\,. \tag{5.48}$$

The operators $b(\vec{k}\,)$ annihilate the Bunch-Davies (BD) vacuum $|\Omega\rangle$ (cf. section 4.5). The fact that in the ultraviolet ($k/a \gg H_0$) the BD vacuum minimizes the energy in the field fluctuations has led to the belief that this vacuum represents a sensible physical choice [129] for the inflationary vacuum. However, it is also true that the BD vacuum yields a singular energy in the infrared (where $k/a \ll H_0$). While this implies abundant particle creation and is very welcome in cosmology, since the amplified vacuum fluctuations provide a beautiful explanation for the structure formation in the universe, one has to take proper care to regulate the IR. One way of doing that is to replace the BD vacuum by a more general state, characterized by the following generalization of the mode functions (5.48),

$$u_k(\eta) \to \tilde{u}_k(\eta) = \alpha(k)u_k(\eta) + \beta(k)u_k^*(\eta)\,; \qquad |\alpha(k)|^2 - |\beta(k)|^2 = 1\,. \tag{5.49}$$

By suitably choosing $\beta(k)$ one can then make the infrared part of the vacuum state finite [130]. A concrete working realization of this proposal has been investigated in Refs. [131, 132]. Alternatively, one can remove the infrared problems by placing the universe in a large comoving box of size L. This leads to a discretized reciprocal (momentum) space $\vec{k} = \vec{n}k_0$ [$\vec{n} = (n_1, n_2, n_3)$, with n_i integers], with the comoving lattice size $k_0 = 2\pi/L$. Since k_0 corresponds to the minimum allowed momentum, this cures the infrared problem simply by disallowing the deeply infrared modes. In the limit when $L \to \infty$, the lattice constant $k_0 \to 0$, and the sum over the momenta can be replaced with increasing accuracy by an integral, which has k_0 as the IR cut-off, thus regulating the infrared.

To see how this works in practice, we shall now calculate the regulated Feynman propagator in de Sitter space. In order to do that, we need to relate the direct space propagator to its mode functions (5.48). Because de Sitter space is spatially homogeneous, it is convenient to write the components $i\Delta_{ab}(x;x')$ of the Keldysh propagator (5.41) for de Sitter space in terms of its Fourier space counterparts,

$$i\Delta_{ab}(x;x') = \int \frac{d^3\vec{k}}{(2\pi)^3}\mathrm{e}^{i\vec{k}\cdot(\vec{x}-\vec{x}')}i\Delta_{ab}(k,\eta,\eta')\,. \tag{5.50}$$

Making use of Eqs. (5.46) and (5.48), one finds for the momentum space propagators,

$$\begin{aligned}
i\Delta_{+-}(k,\eta,\eta') &= u_k^*(\eta)u_k(\eta') \\
i\Delta_{-+}(k,\eta,\eta') &= u_k(\eta)u_k^*(\eta') = (i\Delta_{+-}(k,\eta,\eta'))^* \\
i\Delta_{++}(k,\eta,\eta') &= \Theta(\eta-\eta')i\Delta_{-+}(k,\eta,\eta') + \Theta(\eta'-\eta)i\Delta_{+-}(k,\eta,\eta') \\
i\Delta_{--}(k,\eta,\eta') &= \Theta(\eta-\eta')i\Delta_{+-}(k,\eta,\eta') + \Theta(\eta'-\eta)i\Delta_{-+}(k,\eta,\eta')\,.
\end{aligned} \tag{5.51}$$

The corresponding spectrum $\mathcal{P}_\phi^{dS}$, defined by

$$\langle\Omega|\phi(\vec{x},\eta)\phi(\vec{x}',\eta)|\Omega\rangle = \int \frac{dk}{k}\mathcal{P}_\phi^{dS}(k,\eta)\frac{\sin\left(k\|\vec{x}-\vec{x}'\|\right)}{k\|\vec{x}-\vec{x}'\|}\,, \tag{5.52}$$

is obtained straightforwardly from the equal time limit ($\eta' \to \eta$) of the propagator,

$$\mathcal{P}_\phi^{dS}(k,\eta) = \frac{k^3}{2\pi^2}i\Delta_{+-}(k,\eta,\eta) = \frac{H_0^2}{4\pi^2}\left(1+k^2\eta^2\right)\,. \tag{5.53}$$

It is scale invariant at future infinity, $\eta \to 0$.

Based on (5.51) one can calculate the position space de Sitter propagator by performing the momentum integral (5.50) over $k \geq k_0$, where a natural scale for the IR cut-off is set by the size of the horizon, $k_0 \sim H_0$. The resulting Feynman propagator is [133, 134],

$$i\Delta_F(x;x') = \frac{H_0^2}{4\pi^2}\left(\frac{\eta\eta'}{\Delta x^2} - \frac{1}{2}\Big[\log\left(k_0^2\Delta x^2\right) + 2(\gamma_{\rm E}-1)\Big] + \mathcal{O}(k_0)\right), \tag{5.54}$$

where $\Delta x^2 = -(|\eta-\eta'|-i\epsilon)^2 + \|\vec{x}-\vec{x}'\|^2$ is the conformal space distance function. Two comments are in order. Firstly, apart from the standard Hadamard contribution $\propto 1/\Delta x^2$, which is singular on the lightcone (on-shell) and quickly decays off-shell, the de Sitter propagator (5.54) acquires a logarithmic term which contributes both within the past and future light cones. Secondly, the logarithm grows without a limit as $k_0 \to 0$. This is a manifestation of the IR singularity of the Bunch-Davies vacuum. We will see below that a black hole in de Sitter space 'sees' this logarithmic singularity in the corrected SdS propagator as a logarithmic singularity in the mixed space propagator and hence also in the (mixed space) SdS spectrum. This dependence on the IR regulator poses a unique opportunity to investigate the black hole contribution to the spectrum dependent on the IR regularization.

5.6.2 The Schwarzschild-de Sitter case

For the case that a primordial black hole is present in de Sitter space we shall derive only the first order correction in μ to the Schwinger-Keldysh propagator. We start by writing

$$\Box = \Box^{dS} + \delta\Box\,; \qquad \sqrt{-g} = \sqrt{-g_{dS}} + \delta\sqrt{-g}\,; \qquad i\mathbf{G} = i\mathbf{\Delta} + i\delta\mathbf{G}\,, \tag{5.55}$$

with $i\mathbf{\Delta}$ being the propagator on de Sitter space (5.50–5.51), (5.54). By plugging this into (5.44) we find that the correction to $i\delta\mathbf{G}$ satisfies:

$$\sqrt{-g_{dS}(x)}\left(\Box_x^{dS} - m_{\rm eff}^2\right) i\delta\mathbf{G}(x;x') = \\ -\left(\sqrt{-g_{dS}(x)}\delta\Box_x i\mathbf{\Delta}(x;x') + i\frac{\delta\sqrt{-g(x)}}{\sqrt{-g_{dS}(x)}}\sigma^3\delta^4(x-x')\right). \tag{5.56}$$

Note that $\delta\sqrt{-g}$ is only $\mathcal{O}(\mu^6)$, and thus we can neglect it from now on. It follows that

$$i\delta\mathbf{G}(x;x') = i\int d^4x''\sqrt{-g_{dS}(x'')}i\mathbf{\Delta}(x;x'')\sigma^3\delta\Box_{x''}i\mathbf{\Delta}(x'';x')\,. \tag{5.57}$$

This solution of (5.56) is given only up to a homogeneous solution of the d'Alembertian operator in (5.56). The unique propagator in (5.57) is obtained upon specifying the boundary conditions for the mode functions, or equivalently, for the vacuum state. Here the unperturbed vacuum state is chosen to be the (pure) Bunch-Davies vacuum of de Sitter space, whereby the deep infrared modes are removed by placing the universe in a comoving box, as explained in section 5.6.1. When Eq. (5.57) is written in its component form we get,

$$i\delta G_{ab}(x;x') = i\sum_{c=+,-} c\int d^4x''\sqrt{-g_{dS}(x'')}i\Delta_{ac}(x;x'')\delta\Box_{x''}i\Delta_{cb}(x'';x')\,, \tag{5.58}$$

with $a,b = +,-$. Writing the propagator $i\Delta$ in momentum space (5.50–5.51) this becomes

$$\begin{aligned} &i\delta G_{ab}(x;x') \\ &= -\frac{4i\mu^3}{3H_0^2}\int\frac{d^3\vec{k}d^3\vec{k}'}{(2\pi)^6}\int_{\eta_0}^0 d\eta''\eta''\left(\sum_{c=+,-} c\; i\Delta_{ac}(k,\eta,\eta'')i\Delta_{cb}(k',\eta'',\eta')\right)\mathrm{e}^{i(\vec{k}\cdot\vec{x}-\vec{k}'\cdot\vec{x}')} \\ &\quad\times\int_{-\mu\eta''}^\infty\frac{dr''}{r''}\int_{-1}^1 d\cos\theta''\int_0^{2\pi}d\phi''\left(-k'^2+3\frac{(\vec{k}'\cdot\vec{x}'')^2}{r''^2}\right)\mathrm{e}^{i(\vec{k}'-\vec{k})\cdot\vec{x}''}\,. \end{aligned} \tag{5.59}$$

It turns out that it is easiest to evaluate a (double) momentum space version of $i\delta G_{ab}$. To do that, we first introduce the momenta associated with the positions x and x',

$$i\delta G_{ab}(\vec{p_1},\vec{p_2},\eta,\eta') = \int d^3\vec{x}\,d^3\vec{x}'\,i\delta G_{ab}(\vec{x},\vec{x}',\eta,\eta')\mathrm{e}^{-i\vec{p_1}\cdot\vec{x}}\mathrm{e}^{-i\vec{p_2}\cdot\vec{x}'}, \tag{5.60}$$

and, next, relative and average coordinates in position and momentum space, $\vec{r}=\vec{x}-\vec{x}'$, $\vec{y}=(\vec{x}+\vec{x}')/2$ and $\vec{p}=\vec{p}_1+\vec{p}_2$, $\vec{q}=(\vec{p}_1-\vec{p}_2)/2$. This yields

$$\begin{aligned} i\delta G_{ab}(\vec{p},\vec{q},\eta,\eta') &= \int d^3\vec{y}\,d^3\vec{r}\,i\delta G_{ab}(\vec{x},\vec{x}',\eta,\eta')\mathrm{e}^{-i\vec{p}\cdot\vec{y}}\mathrm{e}^{-i\vec{q}\cdot\vec{r}} \\ &= -\frac{16\pi i\mu^3}{3H_0^2}k'^2(3\cos^2\widetilde{\theta}-1)\sum_{c=+,-} c\left(J_{ac,cb}(0;\vec{p},\vec{q},\eta,\eta') - J_{ac,cb}(\eta_0;\vec{p},\vec{q},\eta,\eta')\right), \end{aligned}$$

where here and in what follows $\vec{k} = \vec{q} + \frac{1}{2}\vec{p}$, $\vec{k}' = \vec{q} - \frac{1}{2}\vec{p}$ and $\widetilde{\theta} = \sphericalangle(\vec{k}' - \vec{k}, \vec{k}') = \sphericalangle(-\vec{p}, \vec{q} - \frac{1}{2}\vec{p})$. Moreover, we defined

$$J_{ab,cd}(\eta''; \vec{p}, \vec{q}, \eta, \eta') = \int d\eta'' \eta'' i\Delta_{ab}(k, \eta, \eta'') i\Delta_{cd}(k', \eta'', \eta') \left(\frac{\cos(\mu p \eta'')}{\mu^2 p^2 \eta''^2} - \frac{\sin(\mu p \eta'')}{\mu^3 p^3 \eta''^3} \right). \tag{5.61}$$

The details of the derivation can be found in Appendix B. From Eq. (5.59) and relations (7.13) for the step functions we find that the corrections to the Feynman and anti-Feynman propagators obey the standard time-ordering relations

$$i\delta G_{++}(\vec{p}, \vec{q}, \eta, \eta') = \Theta(\eta - \eta') i\delta G_{-+}(\vec{p}, \vec{q}, \eta, \eta') + \Theta(\eta' - \eta) i\delta G_{+-}(\vec{p}, \vec{q}, \eta, \eta') \tag{5.62}$$

$$i\delta G_{--}(\vec{p}, \vec{q}, \eta, \eta') = \Theta(\eta - \eta') i\delta G_{+-}(\vec{p}, \vec{q}, \eta, \eta') + \Theta(\eta' - \eta) i\delta G_{-+}(\vec{p}, \vec{q}, \eta, \eta') \,. \tag{5.63}$$

In addition, we have

$$i\delta G_{-+}(\vec{p}, \vec{q}, \eta, \eta') = \Big(i\delta G_{+-}(\vec{p}, \vec{q}, \eta, \eta') \Big)^* . \tag{5.64}$$

Therefore, in order to fully reconstruct the black-hole-corrected Keldysh propagator, we only have to determine $i\delta G_{+-}$, for which we need to know only $J_{+-,+-}$ and $J_{+-,-+}$:

$$\begin{aligned} J_{+-,+-}(\eta''; \vec{p}, \vec{q}, \eta, \eta') &= \frac{H_0^4 \eta \eta' \mathrm{e}^{i(k\eta - k'\eta')}}{4kk'(\mu p)^4} \left(1 + \frac{i}{k\eta}\right) \left(1 - \frac{i}{k'\eta'}\right) \mathrm{e}^{-i(k-k')\eta''} \\ &\times \Bigg\{ \left[-\frac{(\mu p)^2}{kk'} + \frac{i(\mu p)^2 (k-k')\eta'' - \frac{(\mu p)^4}{kk'}}{(k-k')^2 - (\mu p)^2} + \frac{2(\mu p)^4}{((k-k')^2 - (\mu p)^2)^2} \right] \cos(\mu p \eta'') \\ &+ \left[\frac{\mu p}{kk'\eta''} - \frac{(\mu p)^3 \eta'' + \frac{i(\mu p)^3 (k-k')}{kk'} + i(\mu p)(k-k')}{(k-k')^2 - (\mu p)^2} + \frac{2i(\mu p)^3 (k-k')}{((k-k')^2 - (\mu p)^2)^2} \right] \sin(\mu p \eta'') \Bigg\} \end{aligned} \tag{5.65}$$

$$\begin{aligned} J_{+-,-+}(\eta''; \vec{p}, \vec{q}, \eta, \eta') &= \frac{H_0^4 \eta \eta' \mathrm{e}^{i(k\eta + k'\eta')}}{4kk'(\mu p)^4} \left(1 + \frac{i}{k\eta}\right) \left(1 + \frac{i}{k'\eta'}\right) \mathrm{e}^{-i(k+k')\eta''} \\ &\times \Bigg\{ \left[\frac{(\mu p)^2}{kk'} + \frac{i(\mu p)^2 (k+k')\eta'' + \frac{(\mu p)^4}{kk'}}{(k+k')^2 - (\mu p)^2} + \frac{2(\mu p)^4}{((k+k')^2 - (\mu p)^2)^2} \right] \cos(\mu p \eta'') \\ &- \left[\frac{\mu p}{kk'\eta''} + \frac{(\mu p)^3 \eta'' - \frac{i(\mu p)^3 (k+k')}{kk'} + i(\mu p)(k+k')}{(k+k')^2 - (\mu p)^2} - \frac{2i(\mu p)^3 (k+k')}{((k+k')^2 - (\mu p)^2)^2} \right] \sin(\mu p \eta'') \Bigg\}. \end{aligned} \tag{5.66}$$

From Eq. (5.61) we get,

$$\begin{aligned} i\delta G_{+-}(\vec{p}, \vec{q}, \eta, \eta') = -\frac{16\pi i \mu^3}{3H_0^2} k'^2 (3\cos^2\widetilde{\theta} - 1) \big[& J^*_{+-,-+}(\eta) - J_{+-,+-}(\eta) \\ & + J_{+-,+-}(\eta') - J_{+-,-+}(\eta') + J_{+-,-+}(\eta_0) - J^*_{+-,-+}(\eta_0) \big] \,, \end{aligned} \tag{5.67}$$

where here, for brevity, we wrote $J_{ab,cd}(\eta'') \equiv J_{ab,cd}(\eta''; \vec{p}, \vec{q}, \eta, \eta')$. In order to get the complete SdS propagator, we still need to add the de Sitter propagator to the correction (5.67), which in double Fourier space reads,

$$i\Delta_{+-}(\vec{p}, \vec{q}, \eta, \eta') = \frac{H_0^2 \eta\eta'}{2q}\Big(1 + \frac{i}{q\eta}\Big)\Big(1 - \frac{i}{q\eta'}\Big)\mathrm{e}^{-iq(\eta-\eta')}(2\pi)^3\delta^3(\vec{p})\,. \tag{5.68}$$

Together with Eqs. (5.62–5.65) and (5.68), relation (5.67) completely determines the desired SdS propagator in the limit of a small black hole mass, and it constitutes the main result of this chapter. An interesting feature of the propagator (5.67) is that, due to causality, it does not contain any information from future infinity ($\eta'' = 0$). Notice that, although $\mu \ll 1$, we have not expanded the factors $\sin(\mu p\eta'')$ and $\cos(\mu p\eta'')$ in powers of μ in Eqs. (5.65–5.66) since one might still want to consider momenta $\vec{p}$ with $-\mu p\eta'' \gtrsim 1$. Consequently, even though our original expansion parameter was μ^3, the propagator correction is formally suppressed only as $\mu^1 \propto M^{1/3}$, thus, as a fractional power of the black hole mass. Finally, it is worth noting that the pole of $J_{+-,-+}$ at $k + k' = \mu p$ in (5.66) is not physically realized for any $\mu < 1$, because $k + k' = \|\vec{q} + \vec{p}/2\| + \|\vec{q} - \vec{p}/2\| > p$.

5.7 The power spectrum

5.7.1 Double momentum space representation

In section 5.6.1 we derived the spectrum (5.53) for a massless scalar field on de Sitter space. The inhomogeneous case with a primordial black hole is far less trivial to deal with, mainly because out of the 10 symmetries (Killing vectors) of de Sitter space only three symmetries remain in Schwarzschild-de Sitter space. (Recall that the homogeneous cosmology of slow-roll inflation, radiation and matter era has six symmetries.)

In principle, one has to rederive the gauge invariant combinations of the fields, such as the Sasaki-Mukhanov field (5.29) $\mathcal{R}$, for the inhomogeneous background and determine their power spectra. But we have seen in Eq. (5.40) that $\mathcal{R}$ is approximately gauge invariant for weak breaking of translational symmetry. Similarly, the graviton contribution can be neglected, since its power spectrum is expected to be equally suppressed, Eq. (5.33).

With these assumptions the correction to the spectrum from the black hole can be determined from $i\delta G_{+-}$ by taking the equal time limit $\eta' \to \eta$ of the propagator (5.67),

$$\begin{aligned} i\delta G_{+-}(\vec{p}, \vec{q}, \eta, \eta) \;&=\; \frac{32\pi\mu^3}{3H_0^2}k'^2(3\cos^2\widetilde{\theta} - 1) \\ &\quad\times \big[\mathrm{Im}\, J_{+-,-+}(\eta_0; \vec{p}, \vec{q}, \eta, \eta) - \mathrm{Im}\, J_{+-,-+}(\eta; \vec{p}, \vec{q}, \eta, \eta)\big]\,. \end{aligned} \tag{5.69}$$

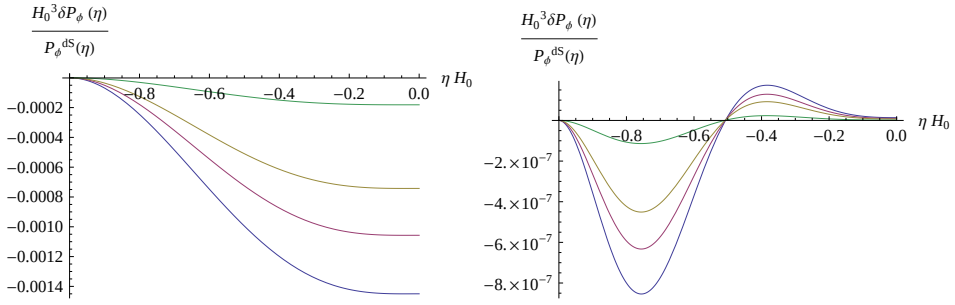

Figure 5.4: The dependence on η of the correction to the power spectrum in (double) momentum space, $\delta\mathcal{P}_\phi(\vec{p},\vec{q},\eta) = (q^3/(2\pi^2))i\delta G_{+-}(\vec{p},\vec{q},\eta,\eta)$, rescaled by the de Sitter spectrum $\mathcal{P}_\phi(\vec{q},\eta) = (H_0^2/(4\pi^2))(1+q^2\eta^2)$, is presented here for fixed momenta $\vec{p}$, $\vec{q}$ and different values of μ (from bottom to top: $\mu = 0.1$ (blue curve), $\mu = 0.09$ (pink), $\mu = 0.08$ (yellow) and $\mu = 0.05$ (green)). The correction is zero at the initial hypersurface, $\eta = -H_0^{-1}$. For small η the spectrum is well described by an expansion to order η^3. The linear order vanishes. It approaches a non-zero value in the limit $\eta \to 0$. Left panel: $p/H_0 = q/H_0 = 1$ and $\sphericalangle(\vec{p},\vec{q}) = 0$, right panel: $p/H_0 = 10$, $q/H_0 = 1/10$ and $\sphericalangle(\vec{p},\vec{q}) = \pi/2$.

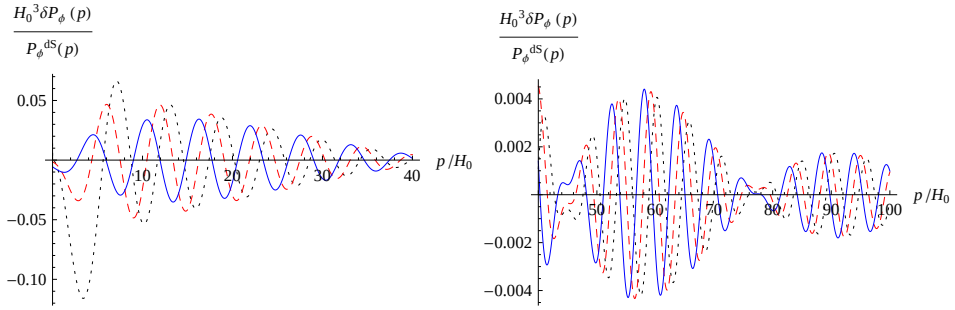

Figure 5.5: In this plot we show the spectrum in (double) momentum space close to the singular region for $\mu = 1/10$ and $\eta = 0$. For this we choose the angle between $\vec{p}$ and $\vec{q}$ to be $\theta = 0.9\pi$ and $q = p/2$ (black curve, dotted), $q = p/2 + H_0$ (red, dashed) and $q = p/2 + 2H_0$ (blue, solid). We observe oscillatory behavior with decaying amplitude. The spectrum diverges for $\vec{q} = -\vec{p}/2$.

The η dependence of the corrected power spectrum $\delta\mathcal{P}_\phi(\vec{p},\vec{q},\eta)$ is displayed in Fig. 5.4. It vanishes at the initial hypersurface $\eta_0 = -H_0^{-1}$ and approaches a non-zero value at $\eta = 0$. This means that by the end of inflation an imprint of a small black hole on the spectrum will remain.

For a homogeneous background the propagator in (double) momentum space contains a delta-peak in the momentum $\vec{p}$ that is associated with the average of the positions. This is seen explicitly in the de Sitter case from Eq. (5.68). In the case of a small inhomogeneity we find a power law divergence at $\vec{k} = \vec{q} + \vec{p}/2 = 0$. The behavior of the spectrum close to this singularity is shown in Fig. 5.5

This observation suggests that an expansion in powers of $\vec{p}\cdot\vec{q}$ and p, which is the basis of the analysis in Ref. [113] is inappropriate for the complete analysis of small black holes in inflation, and, in what follows, we shall not make use of this expansion.

Instead, we shall analyze the mixed space spectrum without making an expansion in powers of $\vec{p}$.

From Eqs. (5.67) and (5.65) it follows that $i\delta G_{+-} = 0$ at the initial hypersurface ($\eta = \eta_0$). In other words, we consider a primordial black hole that was created at a time $\eta = \eta_0$, and we study how it perturbs scalar quantum fluctuations during the subsequent inflationary period.

For $\mu \ll 1$ also $\mu p \ll k + k'$ holds and we can expand $J_{+-,-+}$ in (5.65) to get

$$
\begin{aligned}
J_{+-,-+}(\eta_0;\vec{p},\vec{q},\eta,\eta) = {} & \frac{H_0^4 \mathrm{e}^{i(k+k')(\eta-\eta_0)}}{4kk'(\mu p)^2}\left(\eta^2 - \frac{1}{kk'} + \frac{i(k+k')\eta}{kk'}\right) \\
& \times \Bigg\{ \left(\frac{1}{kk'} + \frac{i\eta_0}{k+k'}\right)\left(\cos(\mu p\eta_0) - \frac{\sin(\mu p\eta_0)}{\mu p\eta_0}\right) \\
& + (\mu p)^2\Bigg[\left(\frac{1}{kk'(k+k')^2} + \frac{2}{(k+k')^4} + \frac{i\eta_0}{(k+k')^3}\right)\cos(\mu p\eta_0) \\
& + \left(\frac{i\eta_0}{kk'(k+k')} - \frac{\eta_0^2}{(k+k')^2} + \frac{i\eta_0}{(k+k')^3}\right)\frac{\sin(\mu p\eta_0)}{\mu p\eta_0}\Bigg]\Bigg\},
\end{aligned}
\tag{5.70}
$$

where we kept sin and cos unexpanded. From this expression we see that there is a contribution that remains finite at future infinity, i.e. at the end of inflation, meaning that this correction to the spectrum is propagated through the radiation and matter dominated epochs of the universe. Taking the limit $\eta \to 0$ one finds

$$
\begin{aligned}
& \mathrm{Im}\, J_{+-,-+}(\eta_0;\vec{p},\vec{q},\eta,\eta) = \\
& -\frac{H_0^4}{4k^2k'^2(\mu p)^2}\Bigg\{\left[\frac{\eta_0\cos((k+k')\eta_0)}{k+k'} - \frac{\sin((k+k')\eta_0)}{kk'}\right]\left(\cos(\mu p\eta_0) - \frac{\sin(\mu p\eta_0)}{\mu p\eta_0}\right) \\
& + (\mu p)^2\Bigg[\frac{\eta_0\cos((k+k')\eta_0)}{(k+k')^3}\cos(\mu p\eta_0) + \left(\frac{1}{kk'} + \frac{1}{(k+k')^2}\right)\frac{\eta_0\cos((k+k')\eta_0)}{(k+k')}\frac{\sin(\mu p\eta_0)}{\mu p\eta_0} \\
& - \left(\frac{1}{kk'} + \frac{2}{(k+k')^2}\right)\frac{\sin((k+k')\eta_0)}{(k+k')^2}\cos(\mu p\eta_0) + \frac{\eta_0^2\sin((k+k')\eta_0)}{(k+k')^2}\frac{\sin(\mu p\eta_0)}{\mu p\eta_0}\Bigg]\Bigg\} \\
& + \mathcal{O}(\eta)\,.
\end{aligned}
\tag{5.71}
$$

Note that $\mathrm{Im}\, J_{+-,-+}(\eta;\vec{p},\vec{q},\eta,\eta) = \mathcal{O}(\eta)$. Therefore, this contribution to the propagator is subdominant at late times and becomes completely negligible by the end of inflation. Since we are primarily interested in late time cosmology, from now on we shall not consider these terms. However, we should keep in mind that these terms become increasingly important at early times when η approaches η_0, since they guarantee that $i\delta G_{ab} \to 0$ when $\eta \to \eta_0$.

5.7.2 Mixed space representation

Rather than working with the momentum $\vec{p}$, we shall mainly consider the mixed space propagator by means of a Fourier transformation of (5.67) with respect to $\vec{p}$. The

mixed space propagator $i\delta G_{+-}(\vec{y},\vec{q},\eta,\eta')$ is a function of the relative momentum $\vec{q}$, the average position $\vec{y}=(\vec{x}+\vec{x}')/2$ and the times η and η'. This makes the physical interpretation easier, because the corresponding equal time statistical propagator

$$\delta F(\vec{y},\vec{q},\eta,\eta)=\mathrm{Re}\, i\delta G_{+-}(\vec{y},\vec{q},\eta,\eta) \tag{5.72}$$

is closely related to the Boltzmann distribution function δf ($\delta f\simeq q\delta F$), cf. [135], and hence allows for a simple statistical interpretation as the phase space density of particles with momentum $\vec{q}$ at position $\vec{y}$ at time η. Likewise, the corresponding spectrum $\delta\mathcal{P}=[q^3/(2\pi^2)]\delta F$ can be given an analogous simple statistical interpretation. The dependence on $\vec{p}$ as well as on $\vec{y}$ in the mixed space propagator signals a breakdown of translational invariance. Furthermore, the mixed space representation is advantageous also because the power law divergence at $\vec{p}=-2\vec{q}$, that plagues the double momentum space propagator, will become a mild logarithmic divergence in the mixed space propagator, whose origin is the IR divergence of the BD vacuum. From the above discussion we know that this divergence is regulated when the IR of the de Sitter state is made finite. Just as we have regulated the de Sitter propagator (5.54), we shall regulate this divergence by placing the universe in a comoving box of size $L=2\pi/k_0$. The mixed space propagator can then be written as

$$\begin{aligned} i\delta G_{+-}(\vec{y},\vec{q},\eta,\eta;k_0) &= \int_{k\geq k_0}\frac{d^3\vec{p}}{(2\pi)^3}i\delta G_{+-}(\vec{p},\vec{q},\eta,\eta)\mathrm{e}^{i\vec{p}\cdot\vec{y}} \\ &= \frac{32\pi\mu^3}{3H_0^2}\int_{k\geq k_0}\frac{d^3\vec{p}}{(2\pi)^3}k'^2(3\cos^2\widetilde{\theta}-1)\mathrm{Im}\, J_{+-,-+}(\eta_0;\vec{p},\vec{q},\eta,\eta)\mathrm{e}^{i\vec{p}\cdot\vec{y}}\,. \end{aligned} \tag{5.73}$$

An inspection of this integral shows that it is indeed logarithmically divergent in the IR when $\vec{p}=-2\vec{q}$, where $k=0$. The divergence is regulated by imposing $k\geq k_0$. The terms in the integrand that cause this logarithmic divergence go as $1/k^3$ for small k in $\mathrm{Im}\, J_{+-,-+}$ (the integral is convergent at $\vec{p}=2\vec{q}$ where $k'=0$). Let us split $i\delta G_{+-}$ into an IR finite part and an IR divergent part. For this we choose the z-axis to point in the direction of $\vec{q}$ and keep $\vec{p}$ general, i.e. $\vec{q}=q(0,0,1)$ and $\vec{p}=p\,(\cos\phi\sin\theta,\sin\phi\sin\theta,\cos\theta)$, and introduce $x=\cos\theta$ and $w=p/(2q)$. The momenta k and k' are then simply

$$k=q\sqrt{1+2wx+w^2},\qquad k'=q\sqrt{1-2wx+w^2}\,. \tag{5.74}$$

Furthermore,

$$3\cos^2\widetilde{\theta}-1=2+\frac{3(x^2-1)}{1-2wx+w^2}\,. \tag{5.75}$$

The IR limit, $k=0$, is then given by the point $w=1$ and $x=-1$ in the $(w-x)$-plane. The other momentum takes the value $k'=p=2q$ there. So, we can split the

propagator as follows

$$
\begin{aligned}
&i\delta G_{+-}(\vec{y},\vec{q},\eta,\eta,k_0) \qquad (5.76)\\
&= \frac{32\pi\mu^3}{3H_0^2}\int\frac{d^3\vec{p}}{(2\pi)^3}\Big[k'^2(3\cos^2\widetilde{\theta}-1)\mathrm{Im}\,J_{+-,-+}(\eta_0;\vec{p},\vec{q},\eta,\eta)\mathrm{e}^{i\vec{p}\cdot\vec{y}} - F^{\mathrm{div}}(\eta,\eta_0,\vec{p},\vec{q},\vec{y})\Big]\\
&\quad + \frac{32\pi\mu^3}{3H_0^2}\int_{k\geq k_0}\frac{d^3\vec{p}}{(2\pi)^3}F^{\mathrm{div}}(\eta,\eta_0,\vec{p},\vec{q},\vec{y})\,,
\end{aligned}
$$

with

$$
\begin{aligned}
F^{\mathrm{div}}(\eta,\eta_0,\vec{p},\vec{q},\vec{y}) &= \frac{H_0^4\mathrm{e}^{-2i\vec{q}\cdot\vec{y}}}{2\mu^2p^2k^3}\Bigg\{\frac{\sin(2q\eta_0)}{2q}\left(\cos(2\mu q\eta_0)-\frac{\sin(2\mu q\eta_0)}{2\mu q\eta_0}\right) \qquad (5.77)\\
&\quad -\mu^2\left[\eta_0\cos(2q\eta_0)\frac{\sin(2\mu q\eta_0)}{2\mu q\eta_0}-\frac{\sin(2q\eta_0)}{2q}\cos(2\mu q\eta_0)\right]\Bigg\}\,.
\end{aligned}
$$

Restricting the momentum k to be above some IR cut-off k_0 translates to

$$
x\geq x_0\left(w,\frac{k_0}{q}\right)=\frac{1}{2w}\left(\frac{k_0^2}{q^2}-(1+w^2)\right) \qquad (5.78)
$$

for $1-k_0/q\leq w\leq 1+k_0/q$. It follows that

$$
\int_{k\geq k_0}\frac{dwdx}{(1+2wx+w^2)^{3/2}}=\log\left(\frac{q^2}{k_0^2}\right)+2+\mathcal{O}(k_0). \qquad (5.79)
$$

We can neglect terms that vanish for $k_0\to 0$. As a result, we obtain an explicit expression for the cut-off dependent part of the propagator

$$
\begin{aligned}
&\frac{32\pi\mu^3}{3H_0^2}\int_{k\geq k_0}\frac{d^3\vec{p}}{(2\pi)^3}F^{\mathrm{div}}(\eta,\eta_0,\vec{p},\vec{q},\vec{y}) \qquad (5.80)\\
&\quad=\frac{8\mu H_0^2\mathrm{e}^{-2i\vec{q}\cdot\vec{y}}}{3\pi q^2}\Bigg\{\frac{\sin(2q\eta_0)}{2q}\left(\cos(2\mu q\eta_0)-\frac{\sin(2\mu q\eta_0)}{2\mu q\eta_0}\right)\\
&\qquad-\mu^2\left[\eta_0\cos(2q\eta_0)\frac{\sin(2\mu q\eta_0)}{2\mu q\eta_0}-\frac{\sin(2q\eta_0)}{2q}\cos(2\mu q\eta_0)\right]\Bigg\}\left(\log\left(\frac{q^2}{k_0^2}\right)+2\right).
\end{aligned}
$$

The power spectrum is defined by [cf. Eq. (5.52)],

$$
\langle\Omega|\phi(\vec{x},\eta)\phi(\vec{x}',\eta)|\Omega\rangle=\int\frac{dq}{q}\mathcal{P}_\phi(\vec{q},\vec{y},\eta)\frac{\sin(qr)}{qr}\,, \qquad (5.81)
$$

with $r=\|\vec{x}-\vec{x}'\|$. We have already derived the power spectrum for the de Sitter background, equation (5.53). Hence, we will only be interested in the correction induced by the black hole,

$$
\delta\mathcal{P}_\phi(\vec{q},\vec{y},\eta)=\frac{q^3}{2\pi^2}\,\mathrm{Re}\,i\delta G_{+-}(\vec{y},\vec{q},\eta,\eta)\,. \qquad (5.82)
$$

Again, we can make a split into IR finite and IR divergent part,

$$\delta\mathcal{P}_\phi(\vec{q},\vec{y},\eta) = \delta\mathcal{P}_\phi^{\rm fin}(\vec{q},\vec{y},\eta) + \delta\mathcal{P}_\phi^{\rm div}(\vec{q},\vec{y},\eta,k_0), \tag{5.83}$$

with

$$\delta\mathcal{P}_\phi^{\rm div}(\vec{q},\vec{y},\eta,k_0) = -\frac{4\mu q H_0\cos(2\vec{q}\cdot\vec{y})}{3\pi^3}\left\{\frac{\sin(2q/H_0)}{2q/H_0}\left(\cos(2\mu q/H_0) - \frac{\sin(2\mu q/H_0)}{2\mu q/H_0}\right)\right.$$
$$\left. - \mu^2\left[\cos(2q/H_0)\frac{\sin(2\mu q/H_0)}{2\mu q/H_0} - \frac{\sin(2q/H_0)}{2q/H_0}\cos(2\mu q/H_0)\right]\right\}\left(\log\left(\frac{q^2}{k_0^2}\right)+2\right).$$

This expression will be added to the numerical results for the finite part to determine the total correction. The finite part is given in terms of an integral in Appendix C, Eq. (7.18).

5.8 Numerical results

5.8.1 The anisotropic case: different angles

For $\vec{y}\neq 0$ we can study the dependence of the spectrum on the angle between $\vec{q}$ and $\vec{y}$. The numerical results are shown in Fig. 5.6. All plots show the correction to the spectrum $\delta\mathcal{P}_\phi$ normalized by the scale invariant de Sitter spectrum, Eq. (5.53),

$$\mathcal{P}_\phi^{\rm dS}\Big|_{\eta=0} = \frac{H_0^2}{4\pi^2}\,. \tag{5.84}$$

Although a good fitting curve has not been found for general angles, it is worth noting that besides the high frequency oscillations a modulation with a much lower frequency is present which is determined by the mass parameter μ. Therefore, the mass of the black hole can, in principle, be inferred directly from the corrections to the scale invariant de Sitter spectrum.

The anisotropic case, $\vec{y}\neq 0$, with the vectors $\vec{y}$ and $\vec{q}$ being perpendicular ($\theta=\pi/2$) turns out to be identical within numerical precision to the isotropic case, $\vec{y}=0$. From the point of view of observations it is hence impossible to associate data to the one case or the other. On the level of the integral expressions (7.18, Appendix C) for the two cases one can argue that, because of the pole at $(w,x)=(1,-1)$, the Bessel function $J_0(2qyw\sqrt{1-x^2})$ that is present in the anisotropic case is effectively evaluated to unity, yielding the same result as the isotropic case. We demonstrate this in Fig. 5.7. Small values of q (large scales) are relevant for black holes that formed at a later stage of inflation. This can be seen by following the modes that are stretched into today's observable scales back in time (see also Fig. 5.11 in section 5.9). However, due to

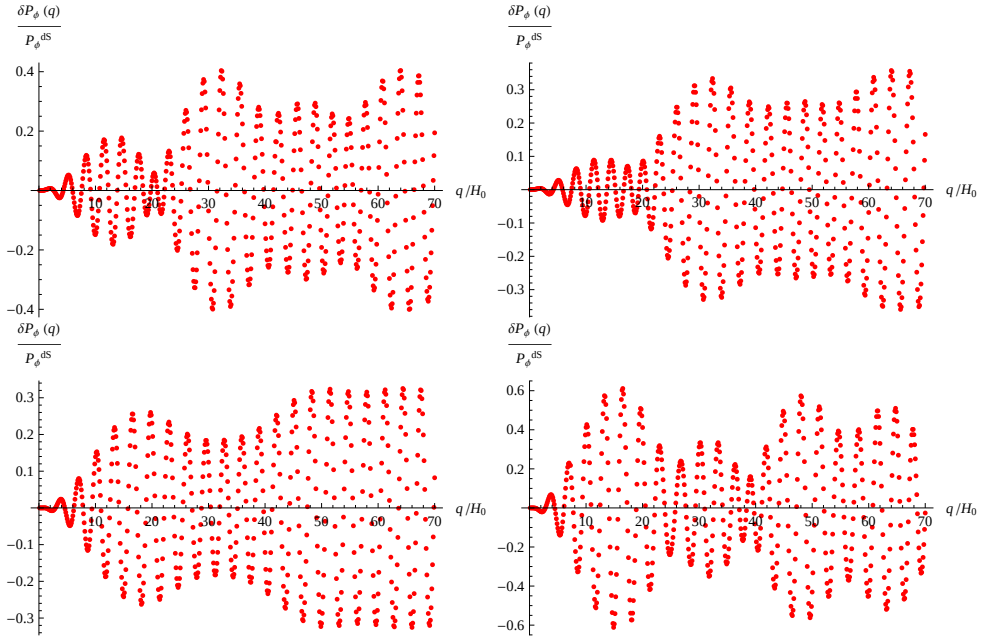

Figure 5.6: The correction to the spectrum is plotted as a function of the momentum q for fixed $qy = 1$, $\mu = 1/10$ and cut-off $k_0/H_0 = 1/10$ but different angles between $\vec{q}$ and $\vec{y}$. Upper left panel: $\theta = 0$, upper right: $\theta = \pi/8$, lower left: $\theta = \pi/4$ and lower right: $\theta = \pi/4$. The case $\theta = \pi/2$ is treated separately (Fig. 5.7). This is the result of a numerical integration with a discretization of eight points per unit. For general angles we could not find a good fitting curve. Nevertheless, we observe $\cos(2q/H_0)$ oscillations modulated with $\cos(2\mu q/H_0)$.

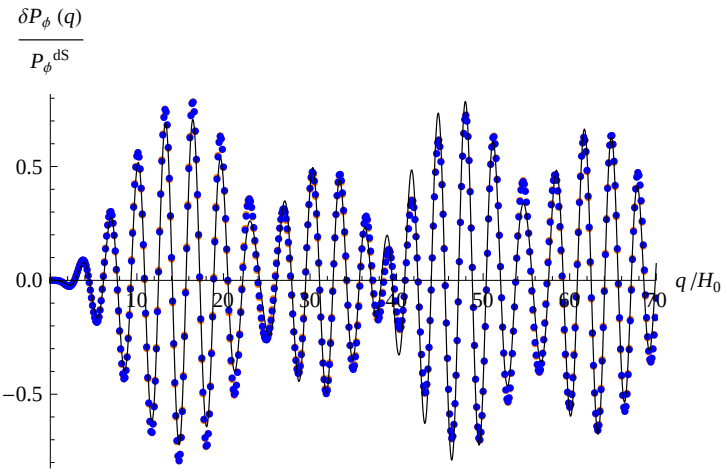

Figure 5.7: It is shown that the anisotropic case (blue dots, dark) with vectors $\vec{q}$ and $\vec{y}$ being perpendicular, $\theta = \pi/2$, coincides with the isotropic case, $\vec{y} = 0$ (orange dots, light, mostly covered by blue dots). This is illustrated for mass parameter $\mu = 1/10$, cut-off $k_0/H_0 = 1/10$ and $qy = 1$. The black fitting curve is given explicitly in Appendix D.

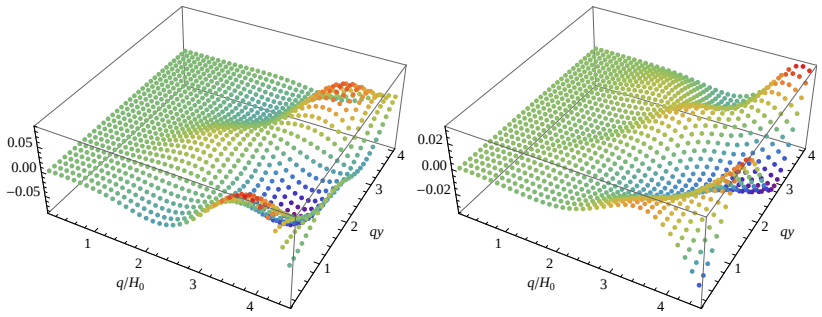

Figure 5.8: This plot shows the numerical result for the spectrum for small values of the two variables q and qy for $\mu = 1/10$ and $\sphericalangle(\vec{q}, \vec{y}) = 0$. A discretization of eight points per unit was used. The momentum cut-off is $k_0/H_0 = 1/10$ for the left panel and $k_0/H_0 = 1$ for the right one. There is a significant cut-off dependence.

the rapid expansion of space-time, the probability for creation of such black holes is expected to be strongly suppressed. We present numerical results for the spectrum in the region of small qy and q in Fig. 5.8. Furthermore, for $q/H_0 \ll 1$ we can expand $\delta\mathcal{P}_\phi(\vec{q}, \vec{y})$ and find that

$$\delta\mathcal{P}_\phi(\vec{q}, \vec{y}, k_0) = \frac{16\mu^5 q^3}{9\pi^3 H_0} F(qy, \theta) + \frac{16\mu^5 q^3}{9\pi^3 H_0} \left(\log\left(\frac{q^2}{k_0^2}\right) + 2 \right) \cos(2qy\cos\theta), \tag{5.85}$$

with $\theta = \sphericalangle(\vec{q}, \vec{y})$. This means that the cut-off dependent and cut-off independent part of the correction to the spectrum factorize individually for low momenta. The integral expression of the functions F is given in Appendix C, Eq. (7.20). In Fig. 5.9 we plot the corrected spectrum for different angles and small q/H_0. We find that the function F is very well approximated by

$$F(qy, \theta) = \begin{cases} -4.8(\log(qy) + 1.2)\cos\left(2qy\cos(\theta)\right) & \text{for } qy \lesssim 0.5, \\ -2.0(\log(qy) + 1.3)\cos\left(2qy\cos(\theta)\right) & \text{for } qy \gtrsim 2.0. \end{cases} \tag{5.86}$$

for any angle θ. The fit is not very good in the intermediate region $0.5 < qy < 2.0$. Thus, we have found an analytic expression that describes the correction to the spectrum very well for large scales. Moreover, the mass parameter μ for the black hole can be found from the amplitude of the spectrum and the IR cut-off k_0 from the enveloping curve.

5.8.2 The isotropic case: cut-off and mass dependence

We pointed out in the previous section that the isotropic case virtually coincides with the case that the vectors $\vec{q}$ and $\vec{y}$ are perpendicular but non-zero. Yet, we can study the dependence of the spectrum on μ and the cut-off k_0. The results are summarized in Fig. 5.10 with general fitting curves (cf. Appendix D) that approximate the numerical

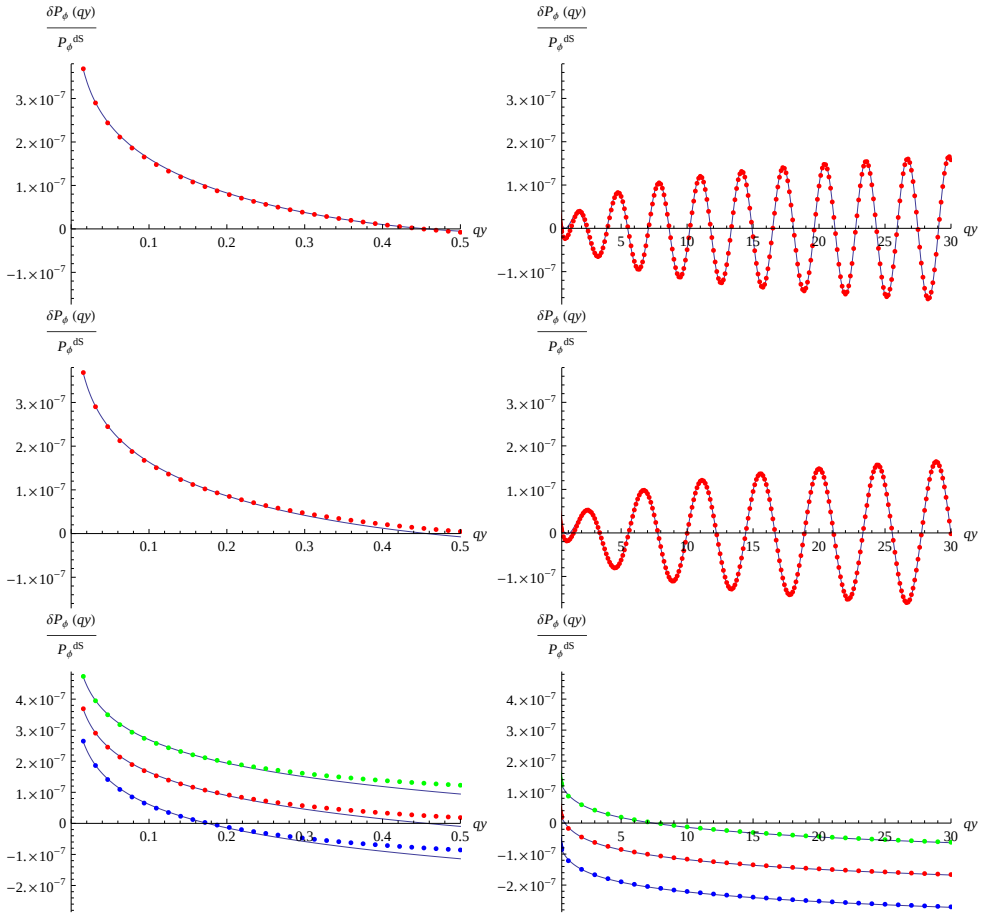

Figure 5.9: The correction to the spectrum as a function of qy is plotted for different angles θ between $\vec{q}$ and $\vec{y}$ in the limit $q/H_0 \to 0$. Upper panels: $\theta = 0$, middle panels: $\theta = \pi/4$ and lower panels: $\theta = \pi/2$. For all plots we chose $q/H_0 = 1/10$ and $\mu = 1/10$. The upper and middle panels have a cut-off $k_0/H_0 = 1/10$. The lower panels show also the cut-off dependence: green (upper) dots correspond to $k_0/H_0 = 1/100$, red (middle) dots to $k_0/H_0 = 1/10$ and blue (lower) dots to $k_0/H_0 = 1$. The fitting curves are given by Eq. (5.86)

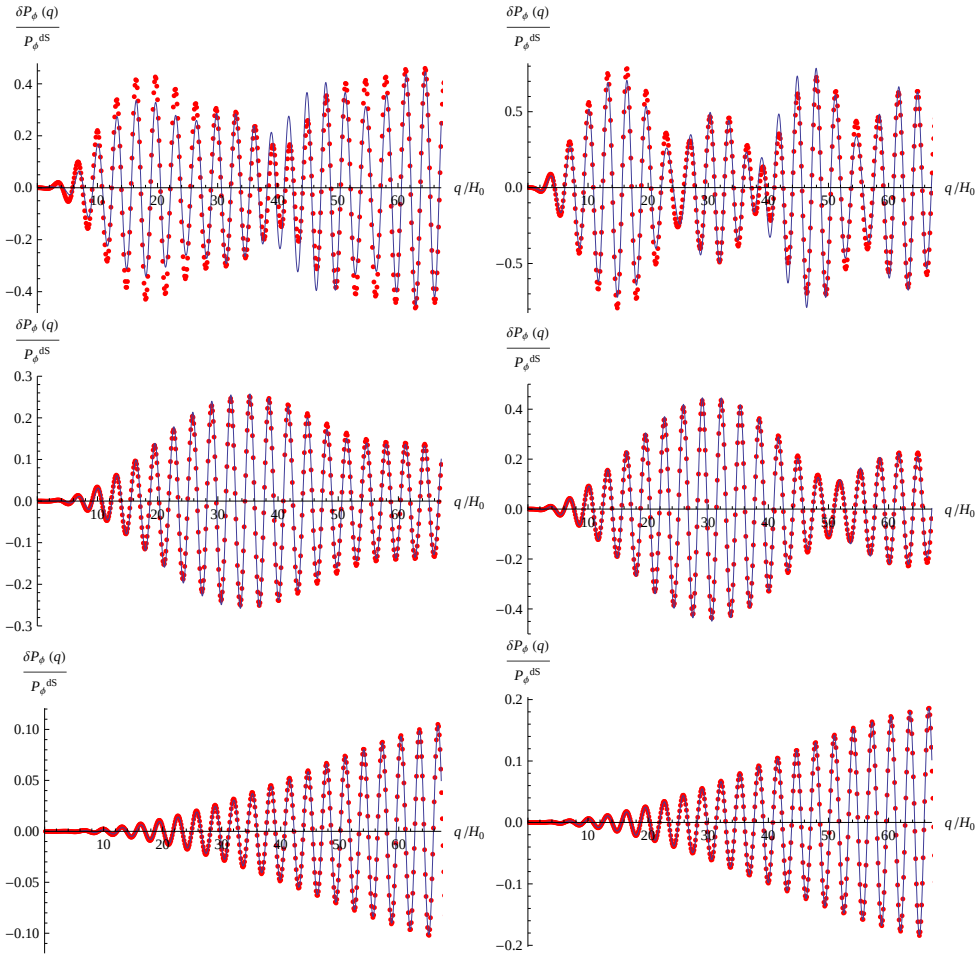

Figure 5.10: We present here the numerical data (red dots) for the correction to the spectrum normalized by the de Sitter spectrum in the isotropic case for cut-off $k_0/H_0 = 1$ (left panels) and $k_0/H_0 = 1/10$ (right panels). Upper panels: $\mu = 1/10$, middle: $\mu = 1/20$ and lower: $\mu = 1/50$. The analytic expression for the fitting function (blue curve) can be found in Appendix D.

data very well, in particular for small μ. Again, the mass parameter determines the modulation frequency.

5.9 Discussion

In this chapter we have derived the correction to the scale invariant power spectrum of a scalar field on de Sitter space from a small primordial black hole to lowest orders in its dimensionless mass parameter $\mu = (GMH/2)^{1/3}$. To this end, we have first analyzed in section 5.3 the probability of black hole formation in the pre-inflationary universe. In order to maximize the formation probability, it was assumed that the pre-inflationary universe is dominated by heavy non-relativistic particles, in which case sub-Hubble perturbations grow. We have found that there is a range for the particle mass $m < m_p$ and the Hubble rate $H_* < m_p$ during that period for which the expected number of sub-Hubble black holes per Hubble volume can be larger than $\mathcal{O}(1)$, as can be seen in Fig. 5.3.

To determine the correction to the spectrum in section 5.6 we have derived an analytic expression for the momentum space propagator of the massless, minimally coupled, scalar field on the Schwarzschild-de Sitter background in the Schwinger-Keldysh formalism. We observe that the propagator diverges in the infrared, demonstrating that, in contrast to a recent proposal [113], an expansion in the momenta is inappropriate, although the breaking of homogeneity is weak. This divergence can be traced to the well known infrared divergence of the massless scalar propagator on de Sitter and was regularized by placing the universe in a large, but finite, comoving box. Furthermore, we have demonstrated that, to leading order in μ, the Sasaki-Mukhanov field (curvature perturbation) remains the correct gauge invariant, dynamical scalar perturbation. By working in the zero curvature gauge, we have then shown how to connect the spectrum in the scalar field fluctuation to the spectrum of the comoving curvature perturbation. Finally, it was shown how to relate the inflationary curvature perturbation to the CMB temperature fluctuations and to the large scale structure of the universe using the appropriate transfer functions. That analysis is yet to be done in detail.

After this preparatory work, in section 5.8 quite some effort has been devoted to the understanding of the scalar field propagator in the mixed representation. This propagator is closely related to the Wigner function, and hence admits a probabilistic interpretation characterizing the Boltzmann distribution function. The mixed space spectrum is a function of not only the relative (comoving) momentum $q = \|\vec{q}\|$, but also of the comoving black hole distance from us, $y = \|\vec{y}\|$, of the angle $\sphericalangle(\vec{q}, \vec{y})$, and finally of the lowest infrared (cut-off) momentum k_0 that can be excited. Our results are mostly analyzed as the black hole contribution to the spectrum relative to the scalar

contribution in de Sitter space. Since the observed spectrum is highly isotropic, and seemingly homogeneous, we were primarily interested in the case when the perturbation induced by a black hole is small, which led us to consider the limit $\mu \ll 1$, or, more precisely, $0.027 < \mu \ll 1$, cf. Eq. (5.12). The lower limit comes from the requirement that, before it evaporates, the black hole must last at least several e-folds during inflation. The effect of the black hole evaporation during inflation is illustrated in Fig. 5.2.

The spectrum was first analyzed in section 5.8.1 for the general anisotropic case, $\vec{y} \neq 0$, with $\vec{y}$ the displacement vector of the black hole with respect to us for different angles between $\vec{y}$ and the momentum vector $\vec{q}$ that is conjugate to the relative distance of two points. Then we considered the large scale region (q/H_0 and qy small) for the special case that $\vec{q}$ and $\vec{y}$ are parallel. Furthermore, by making an expansion for $q \ll H_0$ of the integral expression for the spectrum we showed that it takes a relatively simple form, Eq. (5.85). We presented an explicit expression for fitting functions for the qy dependent part which was determined numerically. In the isotropic case, $\vec{y} = 0$, the dependence on the parameter μ is shown. Unlike the spectrum of scalar homogeneous perturbations in inflation, which is a function of the momentum magnitude q, and depends on two parameters, H and $\epsilon = -\dot{H}/H^2$ at the Hubble crossing, the scalar spectrum in Schwarzschild-de Sitter space depends on q, the distance to the black hole y and the angle between $\vec{q}$ and $\vec{y}$. It can serve as a six dimensional template, whereby the template parameters are the comoving black hole position $\vec{y}$, its mass parameter μ, and H and $\epsilon = -\dot{H}/H^2$ at the first Hubble crossing during inflation. As a summary of the numerical results we can conclude that (i) the spectrum as a function of q is modulated with a lower frequency which is characterized by the mass parameter μ of the black hole; (ii) the enveloping amplitude of the spectrum scales logarithmically with the IR cut-off k_0, and (iii) the isotropic case cannot be distinguished from a particular configuration of the anisotropic case (where $\vec{q} \perp \vec{y}$).

We should point out, however, that a comprehensive analysis of the power spectrum of scalar cosmological perturbations induced by small inflationary black holes should take into account also the degrees of freedom of the graviton and start with the action for the scalar field and the graviton on the unperturbed background. Provided Eq. (5.32) is an accurate expression for the curvature perturbation in terms of the scalar field perturbation in the inhomogeneous case when a small black hole is present, then based on that expression one can calculate the spectrum of comoving curvature perturbation induced by an inflationary black hole. This is the quantity of interest since it sources the CMB temperature fluctuations and the large scale structure. Of course, a more realistic inflationary background is a Schwarzschild black hole in a quasi-de Sitter space (SqdS), in which the Hubble rate and the deceleration parameter are both slowly varying functions of time. In order to make sure that the results presented here

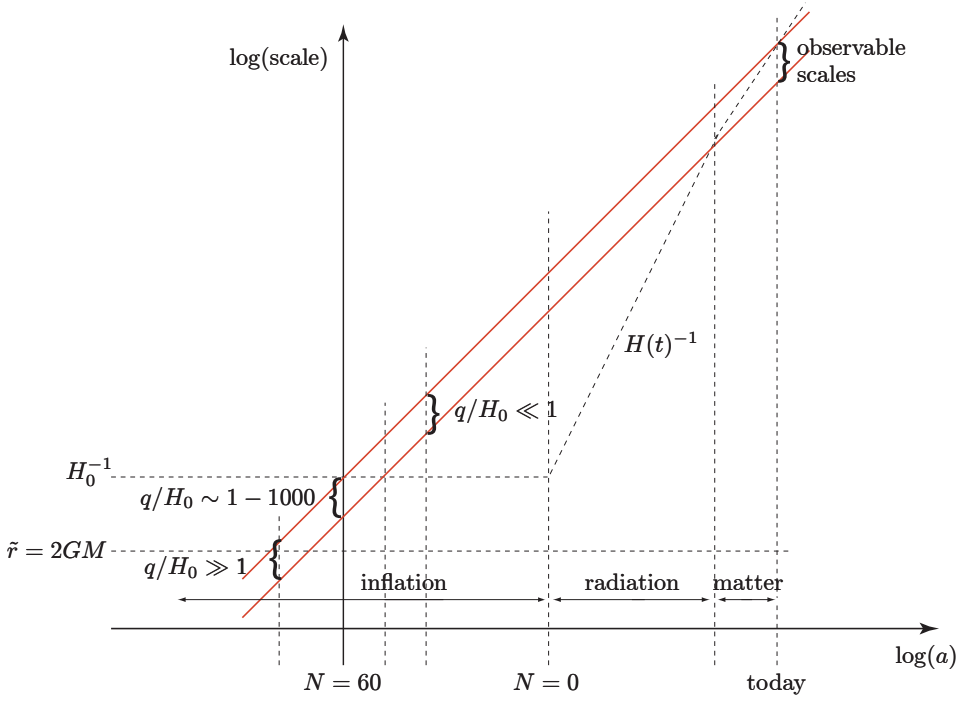

Figure 5.11: The stretching of modes during the evolution of the universe is displayed. The time axis is $\log(a/a_{\rm end}) = -N$ with N the number of e-foldings before the end of inflation. During matter domination the Hubble rate is given by $H(t) \propto a^{-3/2}$, during the radiation era it is $H(t) \sim a^{-2}$. A constant Hubble rate H_0 during inflation (slow-roll approximation) is assumed. The upper diagonal line (red) shows the stretching of the mode that re-enters the Hubble volume today, thereby defining the largest observable scale. That mode crossed the horizon approximately $N_0 \simeq 60$ e-foldings before the end of inflation (sometimes a value of $N_0 = 50$ is assumed). The smallest observable scales depend on the maximum resolution of the apparatus used for the measurement. Today's best resolution is $l \sim \pi/\theta(\text{rad}) \sim 10^2$. The lower diagonal line (red) marks this mode, it exited the Hubble horizon at $N = 50$.

hold also for that case, one would have to make a complete analysis of cosmological perturbations on a SqdS space, which is beyond the scope of this thesis.

Corrections to the power spectrum from primordial black holes are potentially relevant for observations. To assess this possibility more carefully, we have to establish a relationship between the probability of pre-inflationary black hole formation from section 5.3 and the expected number of black holes that leave an imprint on today's CMB sky. A first step in doing that is to trace physical wavelengths, $\lambda_{\rm ph} = a/q$, back in time and check which modes correspond to today's observable scales. In Fig. 5.11 it is shown how physical scales are stretched during the evolution of the universe. The time axis is given in terms of the scale factor $\log(a)$. We are interested in the modes which cross for the first time during inflation the Hubble scale at $t_{1\rm x}$ when $q = a_{1\rm x}H_{1\rm x}$, evolve on super-Hubble scales until some time in matter (or radiation) era, when they cross the Hubble scale for the second time at $q = a_{2\rm x}H_{2\rm x}$. At the end of inflation the

ratio of the physical wave length to the Hubble scale will be, $(a/k)/H^{-1} \propto a^{1-\epsilon}$, where we assumed that $H \propto a^{-\epsilon}$ and $\epsilon \ll 1$ and constant. Since during radiation and matter era, $H^{-1} \propto a^2$ and $H^{-1} \propto a^{3/2}$, the following relation holds,

$$\left(\frac{a_{\rm end}}{a_{\rm 1x}}\right)^{1-\epsilon} = \frac{a_{\rm eq}}{a_{\rm end}} \times \left(\frac{a_{\rm 2x}}{a_{\rm eq}}\right)^{1/2}, \tag{5.87}$$

where $a_{\rm eq}$ is the scale factor at radiation-matter equality. Neglecting $\epsilon \ll 1$ and taking account of the definition, $N_{\rm 1x} = \log(a_{\rm end}/a_{\rm 1x})$, Eq. (5.87) yields

$$N_{\rm 1x} \approx \log\left(\frac{a_{\rm eq}}{a_{\rm end}}\right) + \frac{1}{2}\log\left(\frac{a_{\rm 2x}}{a_{\rm eq}}\right). \tag{5.88}$$

Now, recalling that $a_{\rm eq}/a_{\rm end} \sim 3200$, and $\log(a_{\rm eq}/a_{\rm end}) = (1/2)\log(H_{\rm end}/H_{\rm eq})$, $H_0 = 1.5 \times 10^{-42}$ GeV, $H_{\rm eq} \simeq 3 \times 10^{-37}$ GeV, Eq. (5.88) can be recast as

$$N_{\rm 1x} \simeq 61 + \frac{1}{2}\log\left(\frac{H_{\rm end}}{10^{13}\ {\rm GeV}}\right) - \frac{1}{2}\log(1+z_{\rm 2x}), \tag{5.89}$$

where $z_{\rm 2x} = (a_0/a_{\rm 2x}) - 1$ is the redshift at the second Hubble crossing and a_0 is the scale factor today, such that the last term in (5.89) drops out for modes of the Hubble length today [7].

The black holes that we consider formed during a pre-inflationary era ($N > 60$). Their imprint on the power spectrum measured today corresponds to modes $q/H_0 \gg 1$ at the time of creation and from our numerical results in Figs. 5.6–5.10 we see that the amplitude can be quite large ($\mathcal{O}(0.1)$) when compared to the de Sitter spectrum.

From Figs. 5.9 and 5.11 we see that the black holes which form later during inflation (corresponding to $N \leq 50$) are observed as $q/H_0 \ll 1$ and induce only small fluctuations in the CMB. According to the mechanism described in section 5.3, the probability for formation of these black holes during inflation is small. Yet, at the moment we do not understand enough about this process to be able to make a definite conclusion about their formation probability and observability.

[7] The absence of the graviton signal in the CMB limits $H_{\rm end} \leq 3\times10^{13}$ GeV ($V_{\rm end}^{1/4} < 1.1\times10^{16}$ GeV), and hence $N_{\rm 1x} \simeq 61.6$ is an upper limit for the modes with $z_{\rm 2x} \simeq 0$. In Fig. 5.11 $N_{\rm 1x} = 60$ e-folds corresponds to about $H_{\rm end} \simeq 10^{12}$ GeV ($V_{\rm end}^{1/4} \simeq 2 \times 10^{15}$ GeV).

Chapter 6

Curvature perturbations from primordial monopoles

6.1 Primordial monopoles

The work on small black holes presented in the previous chapter can be extended to localized objects such as primordial magnetic monopoles or heavy particles whose mass is between the GUT and the Planck scale. In this chapter we will focus on magnetic monopoles and study their effect on scalar cosmological perturbations. We expect this effect to be smaller than that of primordial black holes because they are much lighter, but a large number of magnetic monopoles might nevertheless have an impact. It is an interesting question how the spectrum of cosmological perturbations is changed due to the presence of such relics during inflation. This will yield another template for the spectrum which, compared to the black hole case (cf. section 5.9), contains two additional parameters, namely, the magnetic charge and a combination of coupling constants. With this result, their role in inflation can be determined from experimental data.

Magnetic monopoles were studied by Dirac in [136, 137], where a quantization condition,

$$\frac{qe}{\hbar c} = 2\pi n, \qquad n = 0, \pm 1, \pm 2, \ldots \tag{6.1}$$

was derived[1], with q the magnetic and e the electric charge. The theoretical concept of a magnetic monopole has experienced renewed interest in the context of non-Abelian gauge theories. In 1974 the 't Hooft-Polyakov monopole solution was found [138, 139] which, in contrast to the Dirac monopole, carries finite total energy and is a regular solution of the classical field equations. In the light of the symmetry between the electric and magnetic charge in Maxwell's equations one would expect both to

[1]Note that we wrote the quantization condition in rationalized units.

appear in nature, but elementary magnetic monopoles have to date not been detected experimentally [140].

Taking into account the backreaction of the 't Hooft-Polyakov monopole on the geometry, we will see that there is a natural way to define an interior and an exterior region. We will address the question of which of these two regions provides the most relevant contribution to the correction to the spectrum of scalar cosmological perturbations by perturbing around the de Sitter background. In addition, we will compare the contribution from the charge to the contribution of the mass.

6.2 The 't Hooft-Polyakov monopole

6.2.1 Backreaction of the monopole

Before discussing the influence of the 't Hooft-Polyakov monopole on cosmological perturbations, let us review the background geometry that it generates (cf. [64] for details). To this end, we consider an $SU(2)$ Yang-Mills field A^a_μ coupled to a scalar (Higgs) triplet ϕ^a with a non-zero vacuum expectation value v ($a = 1, 2, 3$ is an $SU(2)$ label) which breaks the symmetry. The total action including gravitational interactions is given by

$$S = -\frac{1}{16\pi G}\int d^4x\sqrt{-g}\,R + \int d^4x\sqrt{-g}\,\mathcal{L}_m \tag{6.2}$$

with the matter Lagrangian

$$\mathcal{L}_m = -\frac{1}{4}F^a_{\mu\nu}F^a_{\rho\sigma}g^{\mu\rho}g^{\nu\sigma} - \frac{1}{2}\left(D_\mu\phi\right)^a\left(D_\nu\phi\right)^a g^{\mu\nu} - \frac{\lambda}{2}\left(\phi^a\phi^a - v^2\right)^2 \tag{6.3}$$

and

$$\begin{aligned}\left(D_\mu\phi\right)^a &= \partial_\mu\phi^a - e\epsilon^{abc}A^b_\mu\phi^c \\ F^a_{\mu\nu} &= \partial_\mu A^a_\nu - \partial_\nu A^a_\mu - e\epsilon^{abc}A^b_\mu A^c_\nu\,.\end{aligned} \tag{6.4}$$

The backreaction is determined by making a radially symmetric ansatz for the matter fields and the background metric. Hence, we can write the line element as

$$ds^2 = -B(\tilde{r})d\tilde{t}^2 + A(\tilde{r})d\tilde{r}^2 + \tilde{r}^2 d\Omega^2, \tag{6.5}$$

with a time coordinate $\tilde{t}$ whose relation to the Schwarzschild time coordinate t will become clear later. It is useful to introduce the function $\mathcal{M}(\tilde{r})$ by setting

$$A(\tilde{r}) = \left(1 - \frac{2G\mathcal{M}(\tilde{r})}{\tilde{r}}\right)^{-1}. \tag{6.6}$$

For the matter fields we write

$$\phi^a(\tilde{r}) = v\hat{\tilde{r}}^a h(\tilde{r}), \quad A^a_i(\tilde{r}) = \epsilon^{iak}\hat{\tilde{r}}^k\frac{1-u(\tilde{r})}{e\tilde{r}}, \quad A^a_0(\tilde{r}) = 0, \tag{6.7}$$

where $\hat{\tilde{r}}^k$ are the components of the radial unit vector in a Cartesian coordinate frame ($i = x, y, z$) and the functions $h(\tilde{r})$ and $u(\tilde{r})$ have to be determined from Einstein's equations. Together with the unit vectors in the angular directions $\hat{\theta}^a$ and $\hat{\phi}^a$ a spatial dreibein is defined that is given in Cartesian coordinates as

$$\hat{\tilde{r}}^k = \begin{pmatrix} \sin\theta\sin\phi \\ \sin\theta\cos\phi \\ \cos\theta \end{pmatrix}, \quad \hat{\theta}^k = \begin{pmatrix} \cos\theta\sin\phi \\ \cos\theta\cos\phi \\ -\sin\theta \end{pmatrix}, \quad \hat{\phi}^k = \begin{pmatrix} \cos\phi \\ -\sin\phi \\ 0 \end{pmatrix}. \tag{6.8}$$

Moreover, the time components of the gauge fields A_0^a were set to zero by gauge fixing. For the stress-energy tensor of the matter fields we find

$$\begin{aligned} T_{\mu\nu} &= -\frac{2}{\sqrt{-g}}\frac{\delta S_m}{\delta g^{\mu\nu}} \\ &= \left(\delta_\mu{}^\alpha\delta_\nu{}^\beta g^{\rho\sigma} - \frac{1}{4}g_{\mu\nu}g^{\alpha\beta}g^{\rho\sigma}\right)F^a_{\alpha\rho}F^a_{\beta\sigma} + \left(\delta_\mu{}^\alpha\delta_\nu{}^\beta - \frac{1}{2}g_{\mu\nu}g^{\alpha\beta}\right)(D_\alpha\phi)^a\,(D_\beta\phi)^a \\ &\quad - \frac{\lambda}{2}g_{\mu\nu}\left(\phi^a\phi^a - v^2\right)^2. \end{aligned} \tag{6.9}$$

Plugging the ansatz for the metric (6.5) and the matter fields (6.7) into Einstein's equations with the stress-energy tensor (6.9) and using its conservation equation, $\nabla^\mu T_{\mu\nu} = 0$, yields a system of four ordinary differential equations

$$\begin{aligned} &\text{(i)} && \frac{u''}{A} - \frac{u'A'}{A^2} + \frac{u'}{2A}\frac{(AB)'}{AB} = \frac{u(u^2-1)}{\tilde{r}^2} + e^2v^2uh^2 \\ &\text{(ii)} && \frac{h''}{A} - \frac{h'A'}{A^2} + \frac{2h'}{\tilde{r}A} + \frac{h'(AB)'}{2A^2B} = \frac{2hu^2}{\tilde{r}^2} + 2\lambda v^2h(h^2-1) \\ &\text{(iii)} && \frac{(AB)'}{AB} = 16\pi G\tilde{r}\left(\frac{u'^2}{e^2\tilde{r}^2} + \frac{1}{2}v^2h'^2\right) \\ &\text{(iv)} && \mathcal{M}' = 4\pi\tilde{r}^2\left(\frac{u'^2}{e^2\tilde{r}^2} + \frac{1}{2}v^2h'^2 + \frac{(u^2-1)^2}{2e^2\tilde{r}^4} + \frac{u^2h^2v^2}{\tilde{r}^2} + \frac{\lambda}{2}v^4(h^2-1)^2\right) \\ &&& \quad - 8\pi G\tilde{r}\left(\frac{u'^2}{e^2\tilde{r}^2} + \frac{1}{2}v^2h'^2\right)\mathcal{M}. \end{aligned} \tag{6.10}$$

Primes denote here a derivative with respect to $\tilde{r}$ and the function $\mathcal{M}$ in Eq. (iv) was defined in (6.6). Note that Eq. (iii) can be used to eliminate $B(\tilde{r})$ from the other equations. One can rewrite (6.10) to show that u, h and $\mathcal{M}$ are functions of $ev\tilde{r}$ and that there are only two independent parameters, namely, λ/e^2 and $8\pi Gv^2$.

The first important conclusion that can be drawn from these equations is that for $u(\tilde{r}) = 0$ and $h(\tilde{r}) = 1$ the Reissner-Nordström solution is found,

$$B(\tilde{r}) = A(\tilde{r})^{-1} = 1 - \frac{2GM}{\tilde{r}} + \frac{4\pi G}{e^2\tilde{r}^2} \tag{6.11}$$

with a constant of integration M. Although the cosmological constant has been set to zero for convenience, it is clear that in the same way the Reissner-Nordström-de

Sitter solution is obtained for a non-zero cosmological constant in (6.2). While (6.11) is the correct solution for the 't Hooft-Polyakov monopole in the asymptotic regime, non-singular solutions at the origin can be found by requiring that up to higher orders in $\tilde{r}$,

$$u(\tilde{r}) = 1 - C_u \tilde{r}^2, \quad h(\tilde{r}) = C_h \tilde{r}, \quad \mathcal{M}(\tilde{r}) = \frac{4\pi}{3}\left(\frac{6C_u^2}{e^2} + \frac{3}{2}C_h^2 v^2 + \frac{\lambda}{2}v^4\right)\tilde{r}^3 \,. \tag{6.12}$$

Note that the constants C_u and C_h are specified by the requirements that $u(\tilde{r}) \to 0$ and $h(\tilde{r}) \to 1$ for $\tilde{r} \to \infty$. In particular, solving the system (6.10) numerically with these boundary conditions involves the 'shooting method' to find the correct values of C_u and C_h.

6.2.2 Physical scales of a primordial magnetic monopole

In [64] it was shown that there is a critical vacuum expectation value v_c of the Higgs field for which the monopole becomes a black hole. This can be seen by plotting the metric component $g^{\tilde{r}\tilde{r}} = 1/A(\tilde{r})$ for increasing values of v and noting that for a certain value v_c an event horizon forms at some intermediate radius $\tilde{r}_H$ with $1/A(\tilde{r}_H) = 0$. However, taking the vacuum expectation value v of the Higgs field to be at the GUT scale, $v \simeq 2.4 \times 10^{16}\,\text{GeV}$, yields $8\pi G v^2 = 10^{-4}$ which is far below the critical value. We assumed that $8\pi G v^2 = 10^{-4}$ and $\lambda/e^2 = 1$ to solve (6.10) numerically. The resulting curves are presented in Fig. 6.1. It is seen from the plot for $A(\tilde{r})$ that there is an exterior and interior region of the monopole, which we separated by a vertical line. In the exterior, the solution is approximated well by the Reissner-Nordström solution with the best fit obtained by

$$\mathcal{M}(\tilde{r}) = 17\,\frac{v}{e} - \frac{2\pi}{e^2\tilde{r}}\,. \tag{6.13}$$

Hence, it follows that

$$M = \lim_{\tilde{r}\to\infty} \mathcal{M}(\tilde{r}) \simeq 17\sqrt{\frac{8\pi G v^2}{4\pi\alpha}}M_P\,. \tag{6.14}$$

with the fine structure constant $\alpha = e^2/(4\pi)$. In the limit of small $\tilde{r}$ we have found the best fit to be $A(\tilde{r}) \simeq (1 - 10^{-4}(ev\tilde{r})^2)^{-1}$. For the function $B(\tilde{r})$ the best fit is $B(\tilde{r}) \simeq 1.0001/A(\tilde{r})$ in the exterior region (where the fourth decimal of the constant in the numerator is indeed important to get a good fit). In addition, we took $B(\tilde{r}) \simeq 1 + 10^{-5}(ev\tilde{r})^2$ in the interior region to make the approximate metric continuous. Obviously, these numerical values depend on the choice we made for the parameters $8\pi G v^2$ and λ/e^2.

In order to determine the mass of a typical primordial monopole, we have to take into account that the fine structure constant α in (6.14) grows with the energy scale

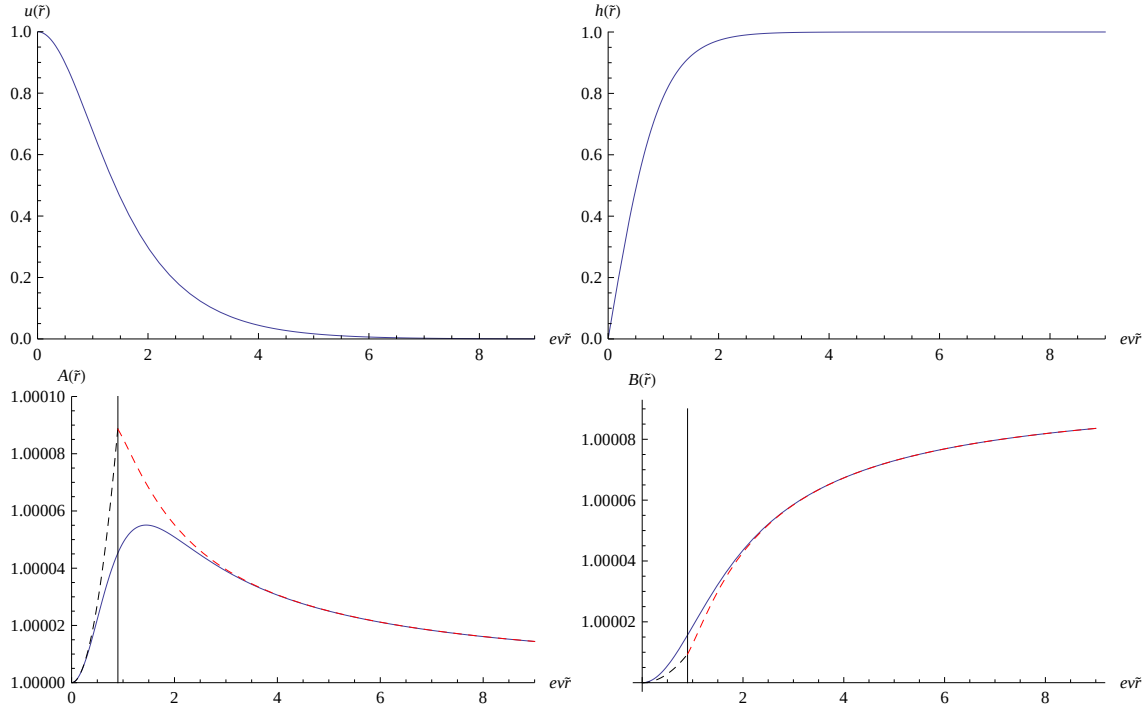

Figure 6.1: In this figure the solution to the system of ODEs (6.10) for the field configuration of the 't Hooft-Polyakov monopole is plotted (u, h and A, B as functions of the Schwarzschild radial coordinate $\tilde{r}$, solid blue curves). The two parameters that specify the solution were chosen to be $\lambda/e^2 = 1$ and $8\pi G v^2 = 10^{-4}$. Moreover, the boundary conditions are such that $u(\tilde{r}) \to 0$ and $h(\tilde{r}) \to 1$ (by 'shooting') and regularity in the center was required. The two lower plots contain fits for the exterior and interior region (separated by the vertical line at $\tilde{r} = 0.9/(ev)$). In the exterior region the fit is obtained from the Reissner-Nordström solution (red curve, dashed) and in the interior the curves are approximated by a quadratic polynomial (black, dashed).

and, roughly, reaches a value of $\alpha \simeq 1/30$ at the GUT scale which corresponds to $e \simeq 0.65$. Therefore, we conclude that a typical mass is $M \simeq 0.05\, m_P$. A monopole that contains a black hole necessarily has a mass which is larger than the Planck mass, namely, $M \simeq 7\, m_P$. The dimensionless mass parameter that we introduced in the previous chapter can then be estimated to be $\mu = (GMH_0/2)^{1/3} \simeq 3 \times 10^{-3}$ in the case of a monopole, where we used that the Hubble rate during inflation is $H_0 \simeq 10^{13}\,\text{GeV}$. Furthermore, from Schwinger's quantization condition [141] in rationalized units, $qe = 4\pi n$ for an integer n, which is more restrictive than Dirac's condition in Eq. (6.1), we find that the smallest non-zero magnetic charge is $q \simeq 19$.

6.2.3 Cosmological coordinates for RNdS exterior region

In the previous chapter we have found it convenient to work with coordinates on the Schwarzschild-de Sitter space that are suited to inflationary cosmology [cf. Eq. (5.2)]. More specifically, the starting point for the computation of the correction to the

Keldysh propagator (5.41) from a small black hole was to make an expansion of the metric written in these 'cosmological coordinates' in the small dimensionless parameter $\mu = (GMH_0/2)^{1/3}$ with M the mass of the black hole. In the case of the magnetic monopole we have seen that asymptotically the gravitational field is well described by the Reissner-Nordström-de Sitter metric (RNdS). The goal is now to determine the generalization of the cosmological coordinates in order to include the correction from the charge.

Let us start with the static form of the RNdS solution,

$$\begin{aligned} ds^2 &= -f(\tilde{r})dt^2 + f(\tilde{r})^{-1}d\tilde{r}^2 + \tilde{r}^2 d\Omega^2 \\ f(\tilde{r}) &= 1 - 2GM/\tilde{r} + Gq^2/(4\pi\tilde{r}^2) - \Lambda\tilde{r}^2/3\,, \end{aligned} \tag{6.15}$$

where the term with the magnetic charge q follows from (6.11) and Schwinger's quantization condition. Note that there are two black hole horizons[2] in the RNdS geometry in addition to the cosmological horizon. This fact is important from the point of view of black hole physics but will not play any role in the analysis that follows since it is the limit of large $\tilde{r}$ that we are interested in. In order to switch to cosmological coordinates we first introduce the cosmological proper time coordinate τ by

$$d\tau = dt - \frac{\sqrt{1 - f(\tilde{r})}}{f(\tilde{r})} d\tilde{r} \tag{6.16}$$

and, as an intermediate step, the comoving radial coordinate $R = \tilde{r}/a(\tau)$. As usual, $a(\tau) = \mathrm{e}^{H_0\tau}$ denotes the scale factor and $H_0 = \sqrt{\Lambda/3}$ is the Hubble rate. In these comoving coordinates the metric becomes

$$ds^2 = -d\tau^2 + a^2(\tau)\left[(dR + F(\tau, R)d\tau)^2 + R^2 d\Omega^2\right]\,, \tag{6.17}$$

where

$$F(\tau, R) = \frac{R\dot{a} - \sqrt{1 - f(Ra)}}{a} = RH_0\left(1 - \sqrt{\frac{2GM}{a^3R^3H_0^2} - \frac{Gq^2}{4\pi a^4R^4H_0^2} + 1}\right) \tag{6.18}$$

and $\dot{a} = da/dt$. It might be difficult, however, to work with the comoving coordinates because of the off-diagonal components of the metric. We can diagonalize the metric (6.17) by solving the partial differential equation

$$\frac{\partial R(\tau, r)}{\partial \tau} = -F(\tau, R)\,, \tag{6.19}$$

[2]Depending on the values of M, q and Λ there might actually be no horizon (which means that the singularity is naked) or just one horizon (which means that the black hole is extremal). However, the first case is excluded by the weak cosmic censorship conjecture [142] and the second is not generic.

where the new radial coordinate r will be determined by specifying the constant of integration. One has to make the choice in such a way that homogeneous cosmology is recovered in the limit of zero mass and charge. Integration of (6.19) yields

$$\int \frac{udu}{\sqrt{P(u)}} = H_0\left(\tau + \tau_0(r)\right), \qquad P(u) = u^4 + 2GMH_0u - GH_0^2q^2/(4\pi) \tag{6.20}$$

with the dimensionless variable $u = aRH_0$ and an integration constant $\tau_0(r)$. Introducing the dimensionless charge parameter $\kappa = 3GH_0^2q^2/(4\pi)$ we can write $P(u) = u^4 + 4\mu^3u - \kappa/3$. From the estimates made in section 6.2.2 we find that $\kappa \simeq 8.8 \times 10^{-11}$.

In contrast to the Schwarzschild-de Sitter case (cf. Appendix A), where the integral that defines the coordinate transformation can be written in terms of the simple elementary function (7.6), the solution of (6.20) involves elliptic functions. For this reason we shall not attempt to derive the exact form of the RNdS metric in cosmological coordinates, but only compute the relevant correction from the charge to lowest order in the dimensionless parameter κ. In fact, this correction to the metric is the only information that we need in order to determine later how the spectrum of scalar perturbations is modified. In view of the values of μ and κ for the primordial magnetic monopole, estimated in section 6.2.2, we can neglect terms of order κ^2, μ^6 and $\kappa\mu^3$. Thus, the expansion of (6.20) gives

$$H_0\left(\tau + \tau_0(r)\right) = \int \frac{udu}{\sqrt{u^4 + 4\mu^3u}} + \frac{\kappa}{6}\int \frac{udu}{\left(u^4 + 4\mu^3u\right)^{3/2}} + \mathcal{O}(\kappa^2) \tag{6.21}$$

$$= \log(u) + \frac{2\mu^3}{3u^3} - \frac{\kappa}{24u^4} + \mathcal{O}(\mu^6, \kappa^2, \mu^3\kappa)\,. \tag{6.22}$$

The correct limit of homogenous cosmology is obtained by setting $\tau_0(r) = H_0^{-1}\log(r/R_0)$ because then it follows that $R(\tau, r) = r$. Inverting this relation to the relevant order in the perturbation parameters we find that

$$R(\tau, r) = r\left(1 - \frac{2\mu^3}{3(arH_0)^3} + \frac{\kappa}{24(arH_0)^4}\right) + \mathcal{O}(\mu^6, \kappa^2, \mu^3\kappa)\,. \tag{6.23}$$

Now, solving (6.19) perturbatively yields

$$F(\tau, R(\tau, r)) = RH_0\left(-\frac{2\mu^3}{u^3} + \frac{\kappa}{6u^4} + \mathcal{O}(\mu^6, \kappa^2, \mu^3\kappa)\right) \tag{6.24}$$

$$= rH_0\left(-\frac{2\mu^3}{(arH_0)^3} + \frac{\kappa}{6(arH_0)^4}\right) + \mathcal{O}(\mu^6, \kappa^2, \mu^3\kappa)\,.$$

With this result we can reexpress the metric in the cosmological coordinates. From

$$dR + F(\tau, R(\tau, r))d\tau = \left(1 + \frac{4\mu^3}{3(arH_0)^3} - \frac{\kappa}{8(arH_0)^4}\right)dr \tag{6.25}$$

we see that the metric becomes indeed diagonal. Hence, the metric assumes the final form

$$ds^2 = a^2(\eta)\Bigg\{ -d\eta^2 + \left(1 + \frac{8\mu^3}{3(arH_0)^3} - \frac{\kappa}{4(arH_0)^4}\right) dr^2 + r^2\left(1 - \frac{4\mu^3}{3(arH_0)^3} + \frac{\kappa}{12(arH_0)^4}\right) d\Omega^2 \Bigg\}. \tag{6.26}$$

On this perturbed background we are going to study the fluctuations of the inflaton field $\phi(x)$ and eventually calculate the amplitude of scalar cosmological perturbations. The equation of motion of a massless inflaton field is the Klein-Gordon equation

$$\Box\phi(x) = g_{\mu\nu}\nabla^\mu\nabla^\nu\phi(x) = \frac{1}{\sqrt{-g}}\partial_\mu\sqrt{-g}g^{\mu\nu}\partial_\nu\phi(x) = 0\,. \tag{6.27}$$

Neglecting again higher orders in μ and κ we find that

$$\sqrt{-g} = a^4 r^2 \sin\theta\left(1 - \frac{\kappa}{24(arH_0)^4}\right) + \mathcal{O}(\mu^6, \kappa^2, \mu^3\kappa)\,. \tag{6.28}$$

The scalar d'Alembertian is therefore given by

$$\Box_S = \Box^{dS} - \frac{4\mu^3 H_0^2\eta^5}{3r^3}\left(\nabla^2 - 3\partial_r^2\right) + \frac{\kappa H_0^2\eta^6}{12r^4}\left(\frac{2}{\eta}\partial_\eta - \nabla^2 + 4\partial_r^2 - \frac{2}{r}\partial_r\right), \tag{6.29}$$

where, besides the de Sitter background contribution, also the mass correction and the correction from the charge are now taken into account. This result obviously reduces to (5.9) for $\kappa = 0$. Note that the operator that is multiplied by κ in (6.29) is more complicated than the one that is multiplied by μ. Indeed, we shall see that many more terms have to be computed to determine the correction to the spectrum of scalar perturbations as compared to the case of a small black hole without charge.

6.2.4 Monopole interior in cosmological coordinates

Let us introduce 'cosmological coordinates' also in the interior region in analogy to the procedure that led to the line element (6.26). As a starting point, we integrate Eq. (iii) of (6.10) which yields

$$B(\tilde{r}) = \frac{1}{A(\tilde{r})}\exp\left\{16\pi G v^2\int_0^{ev\tilde{r}} d\rho\left[\frac{\dot{u}^2}{\rho} + \frac{1}{2}\rho\dot{h}^2\right]\right\} \equiv \frac{C^2(\tilde{r})}{A(\tilde{r})}\,, \tag{6.30}$$

with a dot denoting a derivative with respect to the dimensionless variable $\rho = ev\tilde{r}$. From the analysis in section 6.2.2 (where we assumed that $8\pi G v^2 = 10^{-4}$) it follows that $C_\infty^2 - 1 \equiv \lim_{\tilde{r}\to\infty}(C^2(\tilde{r}) - 1) \simeq 10^{-4}$. Thus, for an observer at infinity, the time in the interior runs slower by a factor of $1/C_\infty$. In order to match the interior region with

the exterior RNdS solution, however, we must use the same time coordinate globally. This is achieved by introducing

$$dt^2 = C_\infty^2 d\tilde{t}^2 \equiv (1+\varepsilon^2) d\tilde{t}^2 \tag{6.31}$$

with a small parameter $\varepsilon \simeq 0.01$. Making the approximation $A(\tilde{r}) \simeq 1 + \alpha^2 \tilde{r}^2$ and $B(\tilde{r}) \simeq 1 + \beta^2 \tilde{r}^2$, we find that, close to the origin, the metric (6.5) is given by

$$ds^2 \simeq -(1 - \varepsilon^2 + \beta^2 \tilde{r}^2) dt^2 + \left(1 + \alpha^2 \tilde{r}^2\right) d\tilde{r}^2 + \tilde{r}^2 d\Omega^2 \,, \tag{6.32}$$

where here and in the following we neglected higher-order terms in ε, $\alpha\tilde{r}$ and $\beta\tilde{r}$ since $ev\tilde{r} \lesssim 1$. Note that ε is dimensionless but α and β have dimension of inverse length. In fact, from the estimates that were made in section 6.2.2 one obtains $\alpha \simeq 16\, H_0$ and $\beta \simeq 5\, H_0$.

Having established the values of the parameters we proceed to the coordinate transformations. First, it follows from (6.32) that for small $\tilde{r}$ we have $f(\tilde{r}) \equiv g^{\tilde{r}\tilde{r}} \simeq 1 - \alpha^2 \tilde{r}^2$. Then the definition of the proper time τ yields

$$d\tau = dt - \frac{\sqrt{1 - f(\tilde{r})}}{f(\tilde{r})} d\tilde{r} = dt - \alpha \tilde{r} d\tilde{r} \,, \tag{6.33}$$

and the comoving radial coordinate is defined as $r = \tilde{r}/a(\tau)$ with the scale factor $a(\tau) = \mathrm{e}^{\alpha\tau}$. From this we immediately find the final form for the metric in the interior,

$$ds^2 = a^2(\eta) \Big\{ -\Big(1 - \varepsilon^2 + (\alpha^2 + \beta^2)(ar)^2\Big) d\eta^2 + dr^2 + r^2 d\Omega^2 \Big\} \,. \tag{6.34}$$

The conformal time η is obtained, as usual, by setting $d\tau^2 = a^2 d\eta^2$ which implies that $a = -1/(\alpha\eta)$. Finally, the Klein-Gordon equation for the inflaton field on the background (6.34) can be determined by expanding the d'Alembertian in the small parameters. We find that

$$\sqrt{-g} = a^4 r^2 \sin\theta \left(1 - \frac{1}{2}\varepsilon^2 + \frac{1}{2}(\alpha^2 + \beta^2) a^2 r^2\right) , \tag{6.35}$$

and, hence,

$$\Box = \Box^{dS_\alpha} + \left(\frac{2\varepsilon^2}{a^2} - 3(\alpha^2 + \beta^2) r^2\right) \frac{1}{\eta} \partial_\eta + \left(-\frac{\varepsilon^2}{a^2} + (\alpha^2 + \beta^2) r^2\right) \partial_\eta^2 + \left(\alpha^2 + \beta^2\right) r \partial_r \,, \tag{6.36}$$

where the operator $\Box^{dS_\alpha}$ is the scalar d'Alembertian on de Sitter space with the Hubble parameter $H = \alpha$.

6.3 Corrections to the Keldysh propagator

The derivation of the Keldysh propagator in this section resembles the work presented in section 5.6 of the previous chapter for the case of a primordial black hole. As before, the correction to the propagator for small perturbation parameters will be computed. Determining these corrections for the monopole, however, turns out to be more involved than for the black hole for the following reason. We have seen in the previous sections that the background of a magnetic monopole is approximated well by an interior region with metric (6.34) and an exterior RNdS region with metric (6.26). Therefore, in total, there are six parameters that characterize the monopole, namely, α, β, ε for the interior, μ, κ for the exterior and the effective monopole radius $\tilde{r}_M = 0.9/(ev)$. Recall that only ε, μ and κ are dimensionless and small. The other two parameters were estimated to be $\alpha \approx 16H_0$ and $\beta \simeq 5H_0$.

The full Keldysh propagator $i\mathbf{G}$ is given in terms of the Feynman propagators iG_{++}, iG_{--} and the Wightman functions iG_{+-}, iG_{-+} defined in (5.42) as

$$i\mathbf{G}(x;x') = \begin{pmatrix} iG_{++}(x;x') & iG_{+-}(x;x') \\ iG_{-+}(x;x') & iG_{--}(x;x') \end{pmatrix} \tag{6.37}$$

and satisfies

$$\sqrt{-g(x)}\left(\Box_x - m_{\text{eff}}^2\right) i\mathbf{G}(x;x') = i\sigma^3\delta^4(x-x')\,, \tag{6.38}$$

where σ^3 is one of the Pauli matrices [cf. Eq. (5.45)]. The effective mass m_{eff} of the inflaton field is related to the second slow-roll parameter η_V, as explained in section 5.6, and will be neglected. Expanding this equation around de Sitter space yields

$$\sqrt{-g_{dS}(x)}\,\Box_x^{dS} i\delta\mathbf{G}(x;x') = -\left(\sqrt{-g_{dS}(x)}\delta\Box_x i\mathbf{\Delta}(x;x') + i\frac{\delta\sqrt{-g(x)}}{\sqrt{-g_{dS}(x)}}\sigma^3\delta^4(x-x')\right), \tag{6.39}$$

with the propagator $i\mathbf{\Delta}$ for de Sitter space, the correction to the determinant of the metric $\delta\sqrt{-g(x)}$ [given by (6.28) for the exterior region and by (6.35) for the monopole interior] and the correction to the d'Alembertian $\delta\Box$ [given by (6.29) for the exterior and by (6.36) for the interior]. It follows that

$$i\delta\mathbf{G}(x;x') = i\int d^4x''\sqrt{-g_{dS}(x'')}i\mathbf{\Delta}(x;x'')\sigma^3\delta\Box_{x''}i\mathbf{\Delta}(x'';x') - \frac{\delta\sqrt{-g(x')}}{\sqrt{-g_{dS}(x')}}i\Delta(x;x')\,. \tag{6.40}$$

To this solution any homogeneous solution of (6.39) can be added. As has been discussed in the black hole case in section 5.6.2, we obtain the unique propagator by choosing the mode functions to correspond to the Bunch-Davies vacuum for the de Sitter background. Unlike the black hole case, we will not derive the statistical propagator (5.72) in the 'mixed space' representation for which an IR regularization of the

vacuum state was needed. The integration range in (6.40) has to be separated into an interior and an exterior region before evaluating the integral. Thus, it is convenient to introduce the following notation for the components of $i\delta\mathbf{G}$,

$$i\delta G_{ab}(x;x') = i\delta G^{\rm int}_{ab}(x;x') + i\delta G^{\rm ext}_{ab}(x;x') - \frac{\delta\sqrt{-g(x')}}{\sqrt{-g_{dS}(x')}} i\Delta_{ab}(x;x')\,, \tag{6.41}$$

where

$$\begin{aligned} i\delta G^{\rm int}_{ab}(x;x') &= i\sum_{c=+,-} c \int\limits_{\tilde r\le\tilde r_M} d^4x''\sqrt{-g_{dS}(x'')}i\Delta_{ac}(x;x'')\delta\Box_{x''}i\Delta_{cb}(x'';x')\,, \\ i\delta G^{\rm ext}_{ab}(x;x') &= i\sum_{c=+,-} c \int\limits_{\tilde r\ge\tilde r_M} d^4x''\sqrt{-g_{dS}(x'')}i\Delta_{ac}(x;x'')\delta\Box_{x''}i\Delta_{cb}(x'';x')\,, \end{aligned} \tag{6.42}$$

and $a, b = +, -$ specify the correlation functions according to (6.37). Note that, compared to the correction of the propagator (5.58) due to a black hole, there is an additional correction proportional to the propagator for de Sitter space (6.41) in the case of a magnetic monopole. This extra term has its origin in the expression for the determinant of the metric tensor [cf. Eqs. (6.28) and (6.35)] and is absent in (5.5) (at the relevant order in μ), where the correction from the mass was determined.

Before we can evaluate the two integrals in (6.42), the boundary of the integration range $\tilde r = \tilde r_M = 0.9/(ev)$ has to be translated into cosmological coordinates (r,η). For this, note that it follows from (6.23) that $\tilde r$ is just a function of r/η,

$$\tilde r = aR \simeq -\frac{r}{\eta H_0}\left(1 + \frac{2\mu^3}{3(r/\eta)^3} + \frac{\kappa}{24(r/\eta)^4}\right)\,. \tag{6.43}$$

Hence, at the monopole boundary we have $r = -\xi\eta$ for some constant ξ and Fig. 6.2 shows that $\xi \simeq 2.8\times10^{-3}$.

The easiest way to evaluate (6.42) is to perform a Fourier transformation of the propagator $i\Delta$,

$$i\Delta_{ab}(x;x') = \int \frac{d^3\vec k}{(2\pi)^3} \mathrm{e}^{i\vec k\cdot(\vec x-\vec x')} i\Delta_{ab}(k,\eta,\eta')\,, \tag{6.44}$$

where the momentum space propagators are given in (5.51) and the mode functions are the ones that define the Bunch-Davies vacuum

$$u_k(\eta) = \frac{1}{a}\frac{1}{\sqrt{2k}}\left(1 - \frac{i}{k\eta}\right)\mathrm{e}^{-ik\eta}\,. \tag{6.45}$$

Now, plugging (6.44), (6.28), (6.29), (6.35) and (6.36) into (6.42), we find

$$
\begin{aligned}
i\delta G^{\rm int}_{ab}(x;x') = \int \frac{d^3\vec{k}d^3\vec{k}'}{(2\pi)^6}{\rm e}^{i(\vec{k}\cdot\vec{x}-\vec{k}'\cdot\vec{x}')} \qquad (6.46)\\
\times\Bigg\{\frac{i\varepsilon^2}{H_0^2}\int_{\eta_0}^0\frac{d\eta''}{\eta''^2}\Bigg(\sum_{c=+,-}c\;i\Delta_{ac}(k,\eta,\eta'')\left[\frac{2}{\eta''}\partial_{\eta''}-\partial^2_{\eta''}\right]i\Delta_{cb}(k',\eta'',\eta')\Bigg)\\
\times\int_0^{-\xi\eta''}dr''\;r''^2\int_{-1}^1 d\cos\theta''\int_0^{2\pi}d\phi''\;{\rm e}^{i(\vec{k}'-\vec{k})\cdot\vec{x}''}\\
+\frac{i(\alpha^2+\beta^2)}{H_0^4}\int_{\eta_0}^0\frac{d\eta''}{\eta''^4}\Bigg(\sum_{c=+,-}c\;i\Delta_{ac}(k,\eta,\eta'')\left[-\frac{3}{\eta''}\partial_{\eta''}+\partial^2_{\eta''}\right]i\Delta_{cb}(k',\eta'',\eta')\Bigg)\\
\times\int_0^{-\xi\eta''}dr''\;r''^4\int_{-1}^1 d\cos\theta''\int_0^{2\pi}d\phi''\;{\rm e}^{i(\vec{k}'-\vec{k})\cdot\vec{x}''}\\
+\frac{i(\alpha^2+\beta^2)}{H_0^4}\int_{\eta_0}^0\frac{d\eta''}{\eta''^4}\Bigg(\sum_{c=+,-}c\;i\Delta_{ac}(k,\eta,\eta'')i\Delta_{cb}(k',\eta'',\eta')\Bigg)\\
\times\int_0^{-\xi\eta''}dr''\;r''^2\int_{-1}^1 d\cos\theta''\int_0^{2\pi}d\phi''\;i\vec{k}'\cdot\vec{x}''{\rm e}^{i(\vec{k}'-\vec{k})\cdot\vec{x}''}\Bigg\},
\end{aligned}
$$

$$
\begin{aligned}
i\delta G^{\rm ext}_{ab}(x;x') = \qquad (6.47)\\
-\frac{4i\mu^3}{3H_0^2}\int\frac{d^3\vec{k}d^3\vec{k}'}{(2\pi)^6}{\rm e}^{i(\vec{k}\cdot\vec{x}-\vec{k}'\cdot\vec{x}')}\int_{\eta_0}^0 d\eta''\eta''\Bigg(\sum_{c=+,-}c\;i\Delta_{ac}(k,\eta,\eta'')i\Delta_{cb}(k',\eta'',\eta')\Bigg)\\
\times\int_{-\xi\eta''}^\infty\frac{dr''}{r''}\int_{-1}^1 d\cos\theta''\int_0^{2\pi}d\phi''\left(-k'^2+3\frac{(\vec{k}'\cdot\vec{x}'')^2}{r''^2}\right){\rm e}^{i(\vec{k}'-\vec{k})\cdot\vec{x}''}\\
+\frac{i\kappa}{12H_0^2}\int\frac{d^3\vec{k}d^3\vec{k}'}{(2\pi)^6}{\rm e}^{i(\vec{k}\cdot\vec{x}-\vec{k}'\cdot\vec{x}')}\\
\times\Bigg\{\int_{\eta_0}^0 d\eta''\eta''^2\Bigg(\sum_{c=+,-}c\;i\Delta_{ac}(k,\eta,\eta'')i\Delta_{cb}(k',\eta'',\eta')\Bigg)\\
\times\int_{-\xi\eta''}^\infty\frac{dr''}{r''^2}\int_{-1}^1 d\cos\theta''\int_0^{2\pi}d\phi''\left(k'^2-4\frac{(\vec{k}'\cdot\vec{x}'')^2}{r''^2}-\frac{2i\vec{k}'\cdot\vec{x}''}{r''^2}\right){\rm e}^{i(\vec{k}'-\vec{k})\cdot\vec{x}''}\\
+2\int_{\eta_0}^0 d\eta''\eta''\Bigg(\sum_{c=+,-}c\;i\Delta_{ac}(k,\eta,\eta'')\partial_{\eta''}i\Delta_{cb}(k',\eta'',\eta')\Bigg)\\
\times\int_{-\xi\eta''}^\infty\frac{dr''}{r''^2}\int_{-1}^1 d\cos\theta''\int_0^{2\pi}d\phi''{\rm e}^{i(\vec{k}'-\vec{k})\cdot\vec{x}''}\Bigg\},
\end{aligned}
$$

where the lower bound η_0 denotes the initial hypersurface. Like in the previous chapter, we obtain the momentum space propagators by first making a Fourier transformation to introduce the momenta $\vec{p}_1$ and $\vec{p}_2$ associated with the positions $\vec{x}$ and $\vec{x}'$,

$$
i\delta G_{ab}(\vec{p_1},\vec{p_2},\eta,\eta') = \int d^3\vec{x}\,d^3\vec{x}'\;i\delta G_{ab}(\vec{x},\vec{x}',\eta,\eta'){\rm e}^{-i\vec{p_1}\cdot\vec{x}}{\rm e}^{-i\vec{p_2}\cdot\vec{x}'}\,. \qquad (6.48)
$$

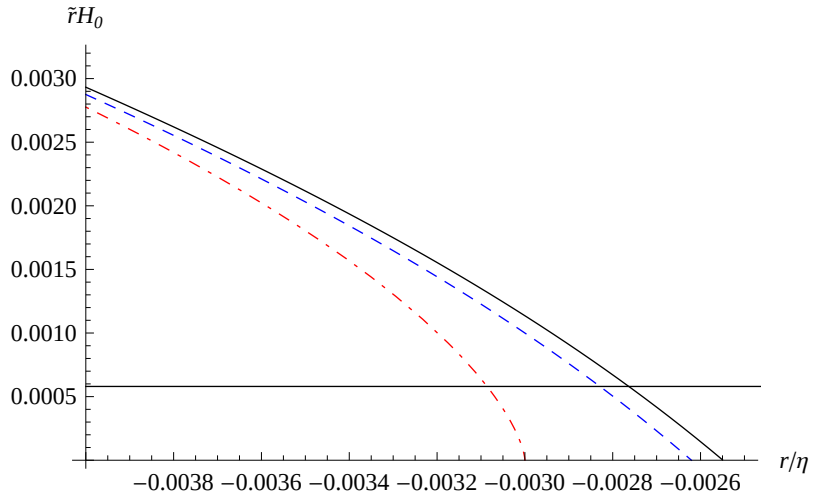

Figure 6.2: This plot shows how the Schwarzschild radial coordinate $\tilde{r}$ is related to the cosmological coordinates (r, η) on RNdS space which were derived in section 6.2.3. It yields a numerical estimate for the effective monopole boundary at $\tilde{r} = \tilde{r}_M$ in terms of r and η. For all the curves, the mass parameter is chosen to be $\mu = 3 \times 10^{-3}$ (cf. estimates in section 6.2.2). The solid (black) curve shows $\tilde{r}$ as a function of r/η for $\kappa = 8.8 \times 10^{-11}$ and is determined from (6.43) which takes into account only the lowest orders in the perturbation parameters μ and κ. The horizontal line marks the boundary of the monopole at $\tilde{r}_M = 0.9/(ev) = 5.8 \times 10^{-4}/H_0$. These two curves intersect approximately at $r/\eta \simeq -2.8 \times 10^{-3}$ which is thus the monopole boundary in cosmological coordinates. In order to get an idea about the error one makes with this perturbative analysis, the curves for $\kappa = 0$ are plotted, too, with the exact coordinate transformation given by the dashed-dotted curve (red) and the approximate result by the dashed (blue) curve. It is seen that the error is roughly 10%.

Then, we define relative and average coordinates in position and momentum space, $\vec{r} = \vec{x} - \vec{x}'$, $\vec{y} = (\vec{x} + \vec{x}')/2$ and $\vec{p} = \vec{p}_1 + \vec{p}_2$, $\vec{q} = (\vec{p}_1 - \vec{p}_2)/2$. It follows that

$$\vec{k} \cdot \vec{x} - \vec{k}' \cdot \vec{x}' - \vec{p} \cdot \vec{y} - \vec{q} \cdot \vec{r} = \vec{r} \cdot \left(-\vec{q} + \frac{1}{2}\vec{k} + \frac{1}{2}\vec{k}' \right) + \vec{y} \cdot \left(-\vec{p} + \vec{k} - \vec{k}' \right) \tag{6.49}$$

which can be used to evaluate

$$i\delta G_{ab}(\vec{p}, \vec{q}, \eta, \eta') = \int d^3\vec{y}\, d^3\vec{r}\, i\delta G_{ab}(\vec{x}, \vec{x}', \eta, \eta')\ \mathrm{e}^{-i\vec{p}\cdot\vec{y}} \mathrm{e}^{-i\vec{q}\cdot\vec{r}}\,. \tag{6.50}$$

It can be seen from (6.46–6.47) that the correction to the propagator obeys

$$i\delta G_{-+}(\vec{p}, \vec{q}, \eta, \eta') = \Big(i\delta G_{+-}(\vec{p}, \vec{q}, \eta, \eta') \Big)^* \tag{6.51}$$

since the integrals over the spatial variables r'', θ'' and ϕ'' in (6.46–6.47) are all real (cf. Appendix E). Moreover, the Feynman and anti-Feynman propagators $i\delta G_{++}$ and $i\delta G_{--}$ must obey the standard time-ordering relations

$$i\delta G_{++}(\vec{p}, \vec{q}, \eta, \eta') = \Theta(\eta - \eta') i\delta G_{-+}(\vec{p}, \vec{q}, \eta, \eta') + \Theta(\eta' - \eta) i\delta G_{+-}(\vec{p}, \vec{q}, \eta, \eta') \tag{6.52}$$

$$i\delta G_{--}(\vec{p}, \vec{q}, \eta, \eta') = \Theta(\eta - \eta') i\delta G_{+-}(\vec{p}, \vec{q}, \eta, \eta') + \Theta(\eta' - \eta) i\delta G_{-+}(\vec{p}, \vec{q}, \eta, \eta')\,. \tag{6.53}$$

This has been checked explicitly for the part of the propagator that is multiplied by the mass parameter μ and is stated in (5.62–5.63) but should be checked for the other terms too. Using these relations and the results presented in Appendix E we find for the interior contribution that

$$\begin{aligned} i\delta G^{\rm int}_{ab}(\vec{p},\vec{q},\eta,\eta') = \frac{4\pi i}{H_0^2}\sum_{c=+,-} c\left\{\frac{\varepsilon^2}{p^3}\left[J^{{\rm int},1}_{ac,cb}(0)-J^{{\rm int},1}_{ac,cb}(\eta_0)\right]\right. \\ \left. + \frac{(\alpha^2+\beta^2)}{H_0^2 p^5}\left[J^{{\rm int},2}_{ac,cb}(0)-J^{{\rm int},2}_{ac,cb}(\eta_0)\right] + \frac{(\alpha^2+\beta^2)}{H_0^2 p^4}k'\cos\widetilde{\theta}\left[J^{{\rm int},3}_{ac,cb}(0)-J^{{\rm int},3}_{ac,cb}(\eta_0)\right]\right\}, \end{aligned} \tag{6.54}$$

where we write here and in what follows $\vec{k}=\vec{q}+\frac{1}{2}\vec{p}$, $\vec{k}'=\vec{q}-\frac{1}{2}\vec{p}$ and $\widetilde{\theta}=\sphericalangle(\vec{k}'-\vec{k},\vec{k}')=\sphericalangle(-\vec{p},\vec{q}-\frac{1}{2}\vec{p})$ for short. Moreover, we introduced

$$J^{{\rm int},1}_{ab,cd}(\tilde{\eta}) = \int^{\tilde{\eta}}\frac{d\eta''}{\eta''^2}\,i\Delta_{ab}(k,\eta,\eta'')\left[\frac{2}{\eta''}\partial_{\eta''}-\partial^2_{\eta''}\right]i\Delta_{cd}(k',\eta'',\eta')\left[\sin\rho-\rho\cos\rho\right] \tag{6.55}$$

$$\begin{aligned} J^{{\rm int},2}_{ab,cd}(\tilde{\eta}) = \int^{\tilde{\eta}}\frac{d\eta''}{\eta''^4}\,i\Delta_{ab}(k,\eta,\eta'')\left[-\frac{3}{\eta''}\partial_{\eta''}+\partial^2_{\eta''}\right]i\Delta_{cd}(k',\eta'',\eta') \\ \times\left[3(\rho^2-2)\sin\rho-\rho(\rho^2-6)\cos\rho\right] \end{aligned}$$

$$J^{{\rm int},3}_{ab,cd}(\tilde{\eta}) = \int^{\tilde{\eta}}\frac{d\eta''}{\eta''^4}\,i\Delta_{ab}(k,\eta,\eta'')i\Delta_{cd}(k',\eta'',\eta')\left[(\rho^2-3)\sin\rho+3\rho\cos\rho\right]$$

with $\rho=-\xi p\eta''$. For convenience, we suppress the dependence of the $J^{{\rm int},i}$ on $\vec{p},\vec{q},\eta,\eta'$ throughout. By specifying the integration range in the indefinite integrals (6.55) to be $\eta_0\le\eta''\le 0$ we find for the exterior contribution

$$\begin{aligned} & i\delta G^{\rm ext}_{ab}(\vec{p},\vec{q},\eta,\eta') \\ &= \frac{\pi i}{12H_0^2}\sum_{c=+,-} c\left\{-64\mu^3 k'^2\left(3\cos^2\widetilde{\theta}-1\right)\left[J^{{\rm ext},1}_{ac,cb}(0)-J^{{\rm ext},1}_{ac,cb}(\eta_0)\right]\right. \\ &\quad + \kappa p k'\cos\widetilde{\theta}\left(p-2k'\cos\widetilde{\theta}\right)\left[J^{{\rm ext},2}_{ac,cb}(0)-J^{{\rm ext},2}_{ac,cb}(\eta_0)\right] \\ &\quad + 2\kappa p k'\left(6k'\cos^2\widetilde{\theta}+p\cos\widetilde{\theta}-2k'\right)\left[J^{{\rm ext},3}_{ac,cb}(0)-J^{{\rm ext},3}_{ac,cb}(\eta_0)\right] \\ &\quad \left. + 4\kappa p\left[J^{{\rm ext},4}_{ac,cb}(0)-J^{{\rm ext},4}_{ac,cb}(\eta_0)\right]\right\} \end{aligned} \tag{6.56}$$

with

$$J^{{\rm ext},1}_{ab,cd}(\tilde{\eta}) = \int^{\tilde{\eta}} d\eta''\eta''\,i\Delta_{ab}(k,\eta,\eta'')i\Delta_{cd}(k',\eta'',\eta')\left[\frac{\cos\rho}{\rho^2}-\frac{\sin\rho}{\rho^3}\right] \tag{6.57}$$

$$J^{{\rm ext},2}_{ab,cd}(\tilde{\eta}) = \int^{\tilde{\eta}} d\eta''\eta''^2\,i\Delta_{ab}(k,\eta,\eta'')i\Delta_{cd}(k',\eta'',\eta')\left[\frac{\cos\rho}{\rho}+\frac{\sin\rho}{\rho^2}+{\rm Si}(\rho)-\frac{\pi}{2}\right]$$

$$J^{{\rm ext},3}_{ab,cd}(\tilde{\eta}) = \int^{\tilde{\eta}} d\eta''\eta''^2\,i\Delta_{ab}(k,\eta,\eta'')i\Delta_{cd}(k',\eta'',\eta')\left[\frac{\sin\rho}{\rho^4}-\frac{\cos\rho}{\rho^3}\right] = \frac{1}{\xi p}J^{{\rm ext},1}_{ab,cd}(\eta'')$$

$$J^{{\rm ext},4}_{ab,cd}(\tilde{\eta}) = \int^{\tilde{\eta}} d\eta''\eta''\,i\Delta_{ab}(k,\eta,\eta'')\partial_{\eta''}i\Delta_{cd}(k',\eta'',\eta')\left[\frac{\cos\rho}{\rho}+\frac{\sin\rho}{\rho^2}+{\rm Si}(\rho)-\frac{\pi}{2}\right].$$

Note that (6.51) and (6.52–6.53) imply that the knowledge of the correction to the Wightman function $i\delta G_{+-}$ completely specifies the correction to the whole Keldysh propagator. Furthermore, in order to determine δG_{+-} we only need to know $J_{+-,+-}$ and $J_{+-,-+}$ because for all J's we have

$$J_{-+,+-} = J^*_{+-,-+}\,. \tag{6.58}$$

It is also easily seen that each $J_{+-,-+}$ can be obtained from the corresponding $J_{+-,+-}$ by a formal substitution[3] in k' [see e.g. (5.65–5.66)],

$$J_{+-,-+} = -J_{+-,+-}\Big|_{k'\to -k'}\,. \tag{6.59}$$

Thus, all the ingredients for the construction of the correction to the Keldysh propagator from the magnetic monopole have been collected. By evaluating these contributions we can determine the spectrum of the scalar field fluctuations and make a link to the gauge invariant scalar cosmological perturbations. The individual contributions to the propagator are not presented in this thesis because they do not provide any immediate physical insight.

6.4 The power spectrum

We have seen in section 5.4.1 of the previous chapter that the gauge invariant Sasaki-Mukhanov field $\mathcal{R}$ that describes scalar cosmological perturbations is related in a simple way to inflaton fluctuations ϕ in the zero curvature gauge [cf. Eq. (5.31)]. In particular, using this gauge, the spectrum of scalar cosmological perturbations can be expressed as

$$\mathcal{P}_{\mathcal{R}} = \frac{1}{2\epsilon M_P^2}\mathcal{P}_\phi \tag{6.60}$$

with the slow-roll parameter $\epsilon = -\dot{H}/H^2$. It was also shown that the field $\mathcal{R}$ is gauge invariant even when corrections from the mass of a small black hole are taken into account. In this chapter we additionally considered the corrections from the charge of a magnetic monopole. Although the dimensionless charge parameter is tiny, $\kappa = 8.8\times 10^{-11}$, one should check if $\mathcal{R}$ is gauge invariant under gauge transformations for the perturbed RNdS background.

The amplitude of the spectrum of inflaton fluctuations on de Sitter space is given by $\mathcal{P}_\phi = H_0^2/(4\pi^2)$. For the correction to this spectrum one finds that [cf. Eq. (5.82)]

$$\delta\mathcal{P}_\phi(\vec{p},\vec{q},\eta,\eta) = \frac{q^3}{2\pi^2}\,\mathrm{Re}\, i\delta G_{+-}(\vec{p},\vec{q},\eta,\eta)\,, \tag{6.61}$$

[3]No physical meaning should be attached to this substitution since it is the *magnitude* of the momentum that changes sign.

where the full expression for $i\delta G_{+-}$ is obtained from the Eqs. (6.41), (6.54) and (6.56). We shall only consider the limit $\eta \to 0$ which denotes the end of inflation. First note that the last term in (6.41) is immediately seen to be suppressed by $\kappa = 8.8 \times 10^{-11}$ from (6.28) for the exterior region. In the interior region it is suppressed by $\varepsilon^2 = 10^{-4}$, $(\alpha\tilde{r})^2 \leq 5 \times 10^{-5}$ and $(\beta\tilde{r})^2 \leq 2 \times 10^{-5}$ which follows from (6.35) and Fig. 6.1. For the contributions $i\delta G^{\mathrm{int}}_{+-}$ and $i\delta G^{\mathrm{ext}}_{+-}$ in (6.54) and (6.56) we find that they greatly simplify in the limit $\eta' = \eta = 0$ [cf. also Eq. (5.69)],

$$
\begin{aligned}
i\delta G^{\mathrm{int}}_{+-}(\vec{p},\vec{q},0,0) = \frac{8\pi}{H_0^2}\Bigg\{ & \frac{\varepsilon^2}{p^3}\left[\mathrm{Im}\, J^{\mathrm{int},1}_{+-,-+}(0) - \mathrm{Im}\, J^{\mathrm{int},1}_{+-,-+}(\eta_0)\right] \\
& + \frac{(\alpha^2+\beta^2)}{H_0^2 p^5}\left[\mathrm{Im}\, J^{\mathrm{int},2}_{+-,-+}(0) - \mathrm{Im}\, J^{\mathrm{int},2}_{+-,-+}(\eta_0)\right] \\
& + \frac{(\alpha^2+\beta^2)}{H_0^2 p^4} k' \cos\widetilde{\theta}\left[\mathrm{Im}\, J^{\mathrm{int},3}_{+-,-+}(0) - \mathrm{Im}\, J^{\mathrm{int},3}_{+-,-+}(\eta_0)\right]\Bigg\},
\end{aligned}
\tag{6.62}
$$

$$
\begin{aligned}
& i\delta G^{\mathrm{ext}}_{+-}(\vec{p},\vec{q},0,0) \\
& = \frac{\pi}{6H_0^2}\Bigg\{ -64\mu^3 k'^2\left(3\cos^2\widetilde{\theta} - 1\right)\left[\mathrm{Im}\, J^{\mathrm{ext},1}_{+-,-+}(0) - \mathrm{Im}\, J^{\mathrm{ext},1}_{+-,-+}(\eta_0)\right] \\
& \quad + \kappa p k' \cos\widetilde{\theta}\left(p - 2k'\cos\widetilde{\theta}\right)\left[\mathrm{Im}\, J^{\mathrm{ext},2}_{+-,-+}(0) - \mathrm{Im}\, J^{\mathrm{ext},2}_{+-,-+}(\eta_0)\right] \\
& \quad + 2\kappa p k'\left(6k'\cos^2\widetilde{\theta} + p\cos\widetilde{\theta} - 2k'\right)\left[\mathrm{Im}\, J^{\mathrm{ext},3}_{+-,-+}(0) - \mathrm{Im}\, J^{\mathrm{ext},3}_{+-,-+}(\eta_0)\right] \\
& \quad + 4\kappa p\left[\mathrm{Im}\, J^{\mathrm{ext},4}_{+-,-+}(0) - \mathrm{Im}\, J^{\mathrm{ext},4}_{+-,-+}(\eta_0)\right]\Bigg\}.
\end{aligned}
\tag{6.63}
$$

In particular, it is seen that we only have to determine $\mathrm{Im}\, J_{+-,-+}$ from all the possible $J_{ab,cd}$ in (6.55) and (6.57). Solving these integrals, we find that for the interior region there is no contribution from future infinity[4] $\eta'' = 0$,

$$
\mathrm{Im}\, J^{\mathrm{int},1}_{+-,-+}(0) = \mathrm{Im}\, J^{\mathrm{int},2}_{+-,-+}(0) = \mathrm{Im}\, J^{\mathrm{int},3}_{+-,-+}(0) = 0\,. \tag{6.64}
$$

However, not all the corresponding terms vanish for the contributions from the exterior region,

$$
\begin{aligned}
& \mathrm{Im}\, J^{\mathrm{ext},1}_{+-,-+}(0) = \mathrm{Im}\, J^{\mathrm{ext},3}_{+-,-+}(0) = 0\,, \\
& \mathrm{Im}\, J^{\mathrm{ext},2}_{+-,-+}(0) = -\frac{\pi H_0^4}{k^2 k'^2}\left(\frac{3}{(k+k')^5} + \frac{1}{kk'(k+k')^3}\right), \\
& \mathrm{Im}\, J^{\mathrm{ext},4}_{+-,-+}(0) = -\frac{\pi H_0^4}{4k^2 k'}\left(\frac{3}{(k+k')^4} + \frac{1}{k(k+k')^3}\right).
\end{aligned}
\tag{6.65}
$$

The contributions to the spectrum from the initial hypersurface $\eta'' = \eta_0$ turn out to be rather lengthy expressions and are therefore presented in Appendix F. Here, we shall

[4] These results are obtained from the expressions in Appendix F by considering $\eta'' = 0$ instead of $\eta'' = \eta_0$.

only discuss their qualitative features. More specifically, we are interested in the powers of the perturbation parameters that control the magnitude of the individual terms. Collecting the leading orders in the perturbation parameters, the exterior contribution can be written as

$$\begin{aligned} &i\delta G^{\text{ext}}_{+-}(\vec{p},\vec{q},0,0) \\ &\quad = \frac{\pi H_0^2}{6}\left\{\frac{64\mu^3}{\xi^2} f_1^{\text{ext}}(\vec{p},\vec{q}) + \frac{\kappa}{4\xi} f_2^{\text{ext}}(\vec{p},\vec{q}) + \frac{\kappa}{2\xi^3} f_3^{\text{ext}}(\vec{p},\vec{q}) + \frac{\kappa}{\xi} f_4^{\text{ext}}(\vec{p},\vec{q})\right\}, \end{aligned} \tag{6.66}$$

with functions $f_i^{\text{ext}}(\vec{p},\vec{q})$ that have the dimension of p^{-6} and result from $\text{Im}\, J^{\text{ext},i}_{+-,-+}$. Note that, as expected, the contributions from future infinity (6.65) do not contribute at the leading order. Although the momentum dependence of the functions f_i^{ext} should be studied carefully to be rigorous, we can get an idea about the relevance of these terms by evaluating the dimensionless prefactors. The estimates in section 6.2.2 yielded $\mu = 3\times 10^{-3}$, $\kappa = 8.8\times 10^{-11}$ and from Fig. 6.2 we found $\xi = 2.8\times 10^{-3}$. Hence,

$$\frac{64\mu^3}{\xi^2} \simeq 0.2, \quad \frac{\kappa}{\xi} \simeq 3\times 10^{-8}, \quad \frac{\kappa}{2\xi^3} \simeq 2\times 10^{-3}\,. \tag{6.67}$$

This shows that the charge parameter greatly suppresses the terms $\text{Im}\, J^{\text{ext},\{2,3,4\}}_{+-,-+}$ and the largest contribution results from the mass term. But, again, it is important to check whether the effect of the charge can be neglected for all momenta $\vec{p},\vec{q}$.

Since $\xi \simeq \mu$, it seems that the primordial magnetic monopole causes the same effect as a primordial black hole of the same mass but this is not so for two reasons. Firstly, the primordial black holes that we studied in the previous chapter had a mass parameter μ above a critical value $\mu_{\text{crit}} \simeq 0.027$. This guaranteed that they do not evaporate during inflation. Indeed, a black hole with a mass corresponding to $\mu = 3\times 10^{-3}$, i.e. $M = 0.05\, m_P$ would decay within a fraction of the Planck time (see also Fig. 5.2). Secondly, there is an additional contribution from the monopole interior region which appears to have a non-negligible effect. To see this, we write the interior contribution in analogy to (6.66) as

$$i\delta G^{\text{int}}_{+-}(\vec{p},\vec{q},0,0) = 2\pi H_0^2\left\{\varepsilon^2\xi f_1^{\text{int}}(\vec{p},\vec{q}) + \frac{(\alpha^2+\beta^2)\xi}{H_0^2}\Big(f_2^{\text{int}}(\vec{p},\vec{q}) + f_3^{\text{int}}(\vec{p},\vec{q})\Big)\right\}. \tag{6.68}$$

Now, using that $\varepsilon = 0.01$ and $\alpha = 16H_0$, $\beta = 5H_0$, we find

$$\varepsilon^2\xi \simeq 3\times 10^{-7}, \quad \frac{(\alpha^2+\beta^2)\xi}{H_0^2} \simeq 0.8\,. \tag{6.69}$$

Based on this estimate for the contribution from the interior region we are led to conclude that it is comparable to the contribution from the exterior. However, this should be regarded only as an indication as long as the functions f_i^{int} have not been analyzed.

Furthermore, it would be interesting to investigate the correction from the magnetic monopole to the Keldysh propagator in the mixed space representation because of its relation to the Boltzmann distribution function [cf. Eq. (5.72)], but this analysis is beyond the scope of the work presented in this chapter. It is important to emphasize that also in the case of the magnetic monopole presented here we made the assumption that the possible coupling of scalar, vector and tensor modes on the inhomogeneous background we worked with does not play a role. This should be checked by expanding the action to quadratic order in the field fluctuations. Finally, the suppression of the spectrum of tensor modes by the slow-roll parameter ϵ shown in (5.33) is expected to hold when homogeneity is weakly broken but should be established rigorously.

Chapter 7

Conclusions

It has been a longstanding goal to unify general relativity with quantum theory. One approach to this problem is to proceed via a lattice regularization of the gravitational path integral, of the kind developed in Quantum Regge Calculus. The discretized geometries used in this approach are piecewise flat and differ from each other only by the edge lengths of the individual flat simplicial building blocks. An alternative to this lattice formulation of quantum gravity is the method of dynamical triangulations in which the edge lengths of the simplices are fixed and different geometries are described by different triangulations. Imposing causality by excluding certain ill-behaved geometries in this model defines Causal Dynamical Triangulations (CDT). Using CDT, it was shown in [38] that, in the pure gravity case, there is a phase in which extended four-dimensional universes are generated in the continuum limit. This allows the conclusion that the model has a good classical limit. Of course, there exist several other approaches to quantum gravity. Most prominently, a lot of work has been invested into research in string theory which is considered to be a possible unified theory of all forces of nature, including gravity.

In the first part of the thesis (chapters 2 and 3) we took an important step in validating the classical limit of the matter-coupled CDT model in four dimensions by considering the coupling to a point-like mass. Without matter, the geometry of the background obtained from the quantum superposition appears to be that of a (Euclidean) de Sitter space. On the classical level, inserting a point like mass into the empty space endowed with a positive cosmological constant generates a Schwarzschild-de Sitter (SdS) background geometry. For this type of matter-coupling, the quantization procedure defined by the non-perturbative sum over causal Euclidean geometries in CDT is thus expected to yield a modified ground state that has the properties of Euclidean SdS space on large scales. The classical limit of the quantum gravity model can be tested by studying the properties of suitable observables which can be measured using Monte

Carlo simulations. The main result of the work presented in chapter 3 is the derivation of classical volume profiles which are modified by the mass. More specifically, it was shown in Fig. 3.8(b) that, after rescaling to the same amplitude, the profiles obtained for different masses all collapse to a single universal curve. This can be seen as an opportunity to establish the presence of a SdS ground state by measuring the expectation value of the volume profiles of geometries generated by CDT coupled to a point-like mass and comparing the resulting curves to the classical volume profiles presented in this thesis. It should be stressed, however, that these results were found only in the limit of small masses with an upper bound set by parameters used in computer simulations. The main reason for this restriction is that the Gaussian normal coordinates that we used do not cover the entire Euclidean SdS manifold. Another important result concerns the implementation of the mass-line in the triangulated geometry with topology $S^1 \times S^3$ used in CDT simulations. In fact, the mass-line is required to form a contractible loop in order to be consistent with the classical Euclidean SdS solution. This has been visualized in Fig. 3.5.

Establishing the correct behavior of the CDT model in the presence of a point-like mass would mean that the model can be used to study quantum properties of the Schwarzschild-de Sitter space non-perturbatively. This is similar in spirit to the fuzzball proposal in string theory (see [143] for a review) which is also a quantum description of a black hole. The method of dynamical triangulations, however, offers the possibility to measure the expectation values of suitable observables directly. For instance, it would be interesting to see how fluctuations in the volume and in the curvature are affected by the black hole. The implementation of the coupling of a point-like mass to quantum gravity in CDT is not a simple task. Above all, the moves used in the Monte Carlo simulations have to be generalized to update the mass-line together with the geometry. Furthermore, one has to explore the phase structure of the matter-coupled model to find the correct classical limit. The condition for the mass-line to form a contractible loop poses another difficulty. Some work has already been put into the problem of including a point-like mass into CDT but no conclusion has been reached so far.

The second part of this thesis (chapters 4, 5 and 6) deals with the inclusion of objects of a similar type into inflationary cosmology. Namely, the effect of small primordial black holes (PBHs) and magnetic monopoles on the spectrum of scalar cosmological perturbations during inflation was discussed. Such small deviations from the ΛCDM model might provide a physical explanation for anomalies in the cosmic microwave background (CMB) and the large scale structure of the universe which have been the subject of recent debates [102, 105]. In particular, it is possible that the large scale (dark) flows [105] are related to the presence of PBHs moving with respect to the CMB

rest frame. This proposal offers an alternative to the suggestions put forward in [144] and [145] which are based on extra dimensions and string theory. However, the analysis presented in chapter 4 should be regarded only as a first step in the investigation of the role of PBHs in the context of such anomalies since (i) we considered a black hole that is *stationary* with respect to the CMB, and (ii) we ignored the possible coupling of scalar, vector and tensor modes which is absent for a homogeneous background but might play a role in inhomogeneous cosmology. In spite of point (ii), we expect our results for the spectrum to be valid for small masses for which homogeneity is only weakly broken and the Sasaki-Mukhanov variable that describes scalar cosmological perturbations is gauge-invariant to the leading order in the small mass parameter [cf. Eq. (5.40)]. The resulting correction to the spectrum of these perturbations from PBHs defines a six-parameter template with the amplitude and the slope that fully characterize perturbations on a homogeneous background and additional parameters for the mass of the black hole and the vector specifying its comoving distance from us. Using this template, the relevance of PBHs for anomalies can be determined from CMB data and from observations of the large scale structure.

In order to establish the results mentioned above, we started by studying fluctuations of the metric on a homogeneous background in chapter 4. Specializing to de Sitter space, the graviton spectrum, Eq. (4.47), was derived in three steps. First, the Einstein-Hilbert action was expanded to quadratic order in the fluctuations, then the two gauge-invariant tensor modes were separated from the other (unphysical) degrees of freedom and, finally, the tensor modes were quantized. This derivation allowed us to conclude in chapter 5 that the graviton spectrum is suppressed in slow-roll inflation when compared to scalar curvature perturbations induced by fluctuations of the inflaton field [cf. Eq. (5.33)]. We made the assumption that the tensor and vector modes play a subdominant role also in the case that the homogeneity of the background is broken by a small black hole. The probability of creation of such small PBHs from Gaussian density fluctuations during a pre-inflationary phase dominated by heavy particles was shown in Fig. 5.3. It is an important result that there is a range of parameters for which several PHBs per Hubble volume are expected. Having established this, the corrections to the spectrum of scalar cosmological perturbations from these PBHs were determined. To this end, we derived the Keldysh propagator of the inflaton field on SdS space since, in the zero curvature gauge, the spectrum of scalar cosmological perturbations is directly related to the spectrum of inflaton fluctuations [cf. (5.32)]. The Keldysh propagator was computed to first order in the dimensionless mass parameter and analyzed in the mixed space (position/momentum) representation. It was found that it has a logarithmic IR divergence that we regulated by putting the universe in a large comoving box. This divergence is due to the choice of the Bunch-Davies vacuum

state for the propagator. In fact, with this choice of the vacuum state, already the propagator on de Sitter space is IR divergent, as was shown in Eq. (5.54). Fixing the IR cut-off parameter and the position of the black hole, we studied the scale dependence of the spectrum. We observed that the oscillations in the spectrum are modulated by a low frequency set by the mass parameter of the black hole, thus making it possible, in principle, to deduce the black hole mass from observational data.

In the case of the primordial magnetic monopole, presented in chapter 6, we first studied the background geometry that it generates. It was found that the monopole can be naturally divided into an interior and an exterior region (see Fig. 6.1). We approximated the interior gravitational field by a quadratic polynomial and showed that it is very well described by the Reissner-Nordström-de Sitter solution in the exterior. Estimating the physical scales for a primordial magnetic monopole it was seen that the typical mass is $M = 0.05\, m_P$. For such small deviations from homogeneity we can study the correction to the spectrum of scalar cosmological perturbations by expanding the Keldysh propagator in small parameters. In addition to the correction from the mass, which was also present in the black hole case, the propagator receives a correction from the charge and from parameters characterizing its interior. The analysis of the spectrum has provided evidence that the effect of the charge is subdominant compared to the mass. However, in order to make a definite conclusion, the spectrum should be fully evaluated in momentum space using Eq. (6.66). Curiously, we have also found that the contribution from the interior is similar in magnitude to the exterior contribution which means that the interior structure of the monopole appears to affect the correction to the spectrum. The results presented in the last chapter define another template which makes it possible to determine the relevance of primordial magnetic monopoles from observational data.

Appendices

Appendix A

The coordinate transformations that give rise to the line element in cosmological form, Eq. (5.2), are presented here. In its static form the Schwarzschild de Sitter (SdS) solution is given by the line element

$$\begin{aligned} ds^2 &= -f(\tilde{r})dt^2 + f(\tilde{r})^{-1}d\tilde{r}^2 + \tilde{r}^2 d\Omega^2 \\ f(\tilde{r}) &= 1 - 2GM/\tilde{r} - \tilde{r}^2/R_0^2\,, \end{aligned} \tag{7.1}$$

with $R_0 = \sqrt{3/\Lambda}$ being the Hubble radius and Λ the cosmological constant. If we take

$$\tau(t,\tilde{r}) = t - \int \frac{\sqrt{1-f(\tilde{r})}}{f(\tilde{r})}d\tilde{r}, \quad R(\tau,\tilde{r}) = \tilde{r}/a(\tau) \tag{7.2}$$

for $a(\tau) = \mathrm{e}^{\tau/R_0}$ then the metric becomes

$$ds^2 = -d\tau^2 + a^2(\tau)\left[(dR + F(\tau,R)d\tau)^2 + R^2 d\Omega^2\right] \tag{7.3}$$

with

$$F(\tau,R) = \frac{R}{R_0}\left(1 - \sqrt{\frac{2GMR_0^2}{R^3 a^3(\tau)} + 1}\right). \tag{7.4}$$

In order to make the metric diagonal, we have to solve a differential equation for a function $R(\tau, r)$

$$\frac{\partial R}{\partial \tau} = -F(\tau,R)\,, \tag{7.5}$$

which has the solution

$$R(\tau,r) = (2GMR_0^2)^{1/3}\mathrm{e}^{-\tau/R_0}\sinh^{2/3}\left(\frac{3}{2}\frac{\tau+\tau_0(r)}{R_0}\right), \tag{7.6}$$

where $\tau_0(r)$ is a τ-independent integration constant. This constant can be determined by the requirement that $R(\tau, r) = r$ for $M = 0$, i.e. homogeneous cosmology is recovered. One finds that

$$\tau_0(r) = R_0 \log\left(\left(\frac{2}{GMR_0^2}\right)^{1/3} r\right), \tag{7.7}$$

and hence,

$$R(\tau, r) = r\left(1 - \frac{GMR_0^2}{2a^3r^3}\right)^{2/3} .$$

The metric then becomes

$$\begin{aligned} ds^2 &= -d\tau^2 + a^2(\tau)\left[\left(\frac{\partial R}{\partial r}(\tau, r)\right)^2 dr^2 + R^2(\tau, r)d\Omega^2\right] \qquad (7.8)\\ &= -d\tau^2 + \frac{(2GMR_0^2)^{2/3}}{r^2}\sinh^{4/3}\left(\frac{3}{2}\frac{\tau+\tau_0(r)}{R_0}\right)\left[\coth^2\left(\frac{3}{2}\frac{\tau+\tau_0(r)}{R_0}\right)dr^2 + r^2d\Omega^2\right]\\ &= -d\tau^2 + a^2(\tau)\left(1 - \frac{GMR_0^2}{2a^3r^3}\right)^{4/3}\left[\left(\frac{1+\frac{GMR_0^2}{2a^3r^3}}{1-\frac{GMR_0^2}{2a^3r^3}}\right)^2 dr^2 + r^2d\Omega^2\right] , \end{aligned}$$

which is recast in the main text, Eq. (5.2), in conformal time η, $d\eta = dt/a(t)$. Note that the metric is singular at

$$r_0(\tau) = \left(\frac{GMR_0^2}{2}\right)^{1/3}\frac{1}{a(\tau)} , \qquad (7.9)$$

and regular for all values $r > r_0(\tau)$. As a check, $R_{\mu\nu} - \Lambda g_{\mu\nu} = 0$, and the Kretschmann invariant is

$$R_{\mu\nu\rho\sigma}R^{\mu\nu\rho\sigma} = \frac{48GM^2}{\tilde{r}^6} + \frac{8\Lambda^2}{3} = \frac{48GM^2}{a^6r^6\left(1-\frac{GMR_0^2}{2a^3r^3}\right)^4} + \frac{8\Lambda^2}{3} , \qquad (7.10)$$

with $\tilde{r}$ denoting as previously the Schwarzschild radial coordinate. This proves that r_0 corresponds to the curvature singularity at $\tilde{r} = 0$. Since $\partial\tilde{r}/\partial r > 0$ for $r > r_0(\tau)$, we conclude that $\tilde{r} \to \infty$ when $r \to \infty$ without any double-valued regions.

Appendix B

For the derivation of (5.61) from (5.59) we have to evaluate first

$$\begin{aligned} I_1(\vec{k}, \vec{k}', \eta'') &\equiv \int_{-\mu\eta''}^{\infty}\frac{dr''}{r''}\int_{-1}^{1}d\cos\theta''\int_0^{2\pi}d\phi''\mathrm{e}^{i(\vec{k}'-\vec{k})\cdot\vec{x}''} = 4\pi\left(\frac{\sin\rho}{\rho} - \mathrm{Ci}(\rho)\right) \qquad (7.11)\\ I_2(\vec{k}, \vec{k}', \eta'') &\equiv \int_{-\mu\eta''}^{\infty}\frac{dr''}{r''}\int_{-1}^{1}d\cos\theta''\int_0^{2\pi}d\phi''\frac{(\vec{k}'\cdot\vec{x}'')^2}{r''^2}\mathrm{e}^{i(\vec{k}'-\vec{k})\cdot\vec{x}''}\\ &= \frac{4\pi k'^2}{3}\left(\left(\frac{\sin\rho}{\rho} - \mathrm{Ci}(\rho)\right) + \left(3\cos^2\widetilde{\theta} - 1\right)\left(\frac{\cos\rho}{\rho^2} - \frac{\sin\rho}{\rho^3}\right)\right) , \end{aligned}$$

with the cosine integral function $\mathrm{Ci}(z) = -\int_z^\infty dt\cos(t)/t$, $\widetilde{\theta} = \sphericalangle(\vec{k}'-\vec{k},\vec{k}')$ and $\rho = -\mu\|\vec{k}-\vec{k}'\|\eta''$. Then, it follows that

$$\begin{aligned} I(\vec{k},\vec{k}',\eta'') &\equiv \int_{-\mu\eta''}^{\infty}\frac{dr''}{r''}\int_{-1}^{1}d\cos\theta''\int_0^{2\pi}d\phi''\left(-k'^2+3\frac{(\vec{k}'\cdot\vec{x}'')^2}{r''^2}\right)\mathrm{e}^{i(\vec{k}'-\vec{k})\cdot\vec{x}''} \\ &= -k'^2 I_1(\vec{k},\vec{k}',\eta'')+3I_2(\vec{k},\vec{k}',\eta'') \\ &= 4\pi k'^2\left(3\cos^2\widetilde{\theta}-1\right)\left(\frac{\cos(\mu\|\vec{k}-\vec{k}'\|\eta'')}{\mu^2\|\vec{k}-\vec{k}'\|^2\eta''^2}-\frac{\sin(\mu\|\vec{k}-\vec{k}'\|\eta'')}{\mu^3\|\vec{k}-\vec{k}'\|^3\eta''^3}\right). \end{aligned} \tag{7.12}$$

To establish (5.62) and (5.63) we used the following relations for the step function:

$$\begin{aligned} &\Theta(\eta-\eta'')\Theta(\eta''-\eta') = \Theta(\eta-\eta')\left[\Theta(\eta''-\eta')-\Theta(\eta''-\eta)\right] \\ &\Theta(\eta-\eta'')\Theta(\eta'-\eta'') = \Theta(\eta-\eta')\Theta(\eta'-\eta'')+\Theta(\eta'-\eta)\Theta(\eta-\eta'') \\ &\Theta(\eta''-\eta)\Theta(\eta''-\eta') = \Theta(\eta-\eta')\Theta(\eta''-\eta)+\Theta(\eta'-\eta)\Theta(\eta''-\eta') \\ &\Theta(\eta''-\eta)\Theta(\eta'-\eta'') = \Theta(\eta'-\eta)\left[\Theta(\eta''-\eta)-\Theta(\eta''-\eta')\right]. \end{aligned} \tag{7.13}$$

The final form for $J_{+-,+-}$ and $J_{+-,-+}$, Eqs. (5.65) and (5.66), can be obtained by solving the following integral, for real parameters A, B, α and $\alpha \neq 1$ and $\rho = -\mu\eta''p$ with $A+\alpha B = 0$,

$$\begin{aligned} &\int d\rho\left(\rho^3+iA\rho^2+B\rho\right)\left(\frac{\cos\rho}{\rho^2}-\frac{\sin\rho}{\rho^3}\right)\mathrm{e}^{i\alpha\rho} \\ &= \left[\left(\frac{2}{(\alpha^2-1)^2}+\frac{\alpha(A-i\rho)}{\alpha^2-1}\right)\cos\rho+\left(\frac{i(\alpha-A)-\rho}{\alpha^2-1}-\frac{2i\alpha}{(\alpha^2-1)^2}+\frac{B}{\rho}\right)\sin\rho\right]e^{i\alpha\rho}. \end{aligned} \tag{7.14}$$

Appendix C

We present here the general integral expression for the finite part of the spectrum. For this we write

$$\begin{aligned} \vec{q} &= q(0,0,1) \\ \vec{p} &= p(\cos\phi\sin\theta,\sin\phi\sin\theta,\cos\theta) \\ \vec{y} &= y(\cos\phi_y\sin\theta_y,\sin\phi_y\sin\theta_y,\cos\theta_y). \end{aligned} \tag{7.15}$$

Introducing $x = \cos\theta$ and $w = p/(2q)$, as in the main text, we find that

$$\int_0^{2\pi}d\phi\cos(\vec{p}\cdot\vec{y}) = 2\pi J_0(2qyw\sqrt{1-x^2}\sin\theta_y)\cos(2qywx\cos\theta_y). \tag{7.16}$$

In terms of the variables κ and κ',

$$\kappa = k/q = \sqrt{1+2wx+w^2}, \qquad \kappa' = k'/q = \sqrt{1-2wx+w^2}, \tag{7.17}$$

the integral form of the spectrum, in Eqs. (5.76) and (5.82–5.83), becomes

$$\delta\mathcal{P}^{\rm fin}(q,y,\eta) = \frac{2\mu q H_0}{3\pi^3}\int_0^\infty dw\int_{-1}^1 \frac{dx}{\kappa^2}\left(2+\frac{3(x^2-1)}{\kappa'^2}\right) \tag{7.18}$$
$$\times\left\{\frac{\cos((\kappa+\kappa')q/H_0)}{\kappa+\kappa'}\left(\cos(2\mu wq/H_0)-\frac{\sin(2\mu wq/H_0)}{2\mu wq/H_0}\right)\right.$$
$$+(2\mu w)^2\left[\frac{\cos((\kappa+\kappa')q/H_0)}{(\kappa+\kappa')^3}\left(\cos(2\mu wq/H_0)+\frac{\sin(2\mu wq/H_0)}{2\mu wq/H_0}\right)\right.$$
$$\left.\left.-\frac{2\sin((\kappa+\kappa')q/H_0)}{(q/H_0)(\kappa+\kappa')^4}\cos(2\mu wq/H_0)+\frac{(q/H_0)\sin((\kappa+\kappa')q/H_0)}{(\kappa+\kappa')^2}\frac{\sin(2\mu wq/H_0)}{2\mu wq/H_0}\right]\right\}$$
$$\times J_0(2qyw\sqrt{1-x^2}\sin\theta_y)\cos(2qywx\cos\theta_y)$$
$$-\frac{2\mu q H_0}{3\pi^3}\int_0^\infty dw\int_{-1}^1\frac{dx}{\kappa^3}\left[\left(2+\frac{3(x^2-1)}{\kappa'^2}\right)\right.$$
$$\times\left\{\frac{\sin((\kappa+\kappa')q/H_0)}{(q/H_0)\kappa'}\left(\cos(2\mu wq/H_0)-\frac{\sin(2\mu wq/H_0)}{2\mu wq/H_0}\right)\right.$$
$$\left.-(2\mu w)^2\left[\frac{\cos((\kappa+\kappa')q/H_0)}{\kappa'(\kappa+\kappa')}\frac{\sin(2\mu wq/H_0)}{2\mu wq/H_0}-\frac{\sin((\kappa+\kappa')q/H_0)}{(q/H_0)\kappa'(\kappa+\kappa')^2}\cos(2\mu wq/H_0)\right]\right\}$$
$$\times J_0(2qyw\sqrt{1-x^2}\sin\theta_y)\cos(2qywx\cos\theta_y)$$
$$-2\left\{\frac{\sin(2q/H_0)}{2q/H_0}\left(\cos(2\mu q/H_0)-\frac{\sin(2\mu q/H_0)}{2\mu q/H_0}\right)\right.$$
$$\left.\left.-\mu^2\left[\cos(2q/H_0)\frac{\sin(2\mu q/H_0)}{2\mu q/H_0}-\frac{\sin(2q/H_0)}{2q/H_0}\cos(2\mu q/H_0)\right]\right\}\cos(2qy\cos\theta_y)\right].$$

For $q/H_0 \ll 1$ one finds

$$\delta\mathcal{P}_\phi(q,y,\eta) = \frac{16\mu^5 q^3}{9\pi^3 H_0}F(qy,\theta_y)+\frac{16\mu^5 q^3}{9\pi^3 H_0}\left(\log\left(\frac{q^2}{k_0^2}\right)+2\right)\cos(2qy\cos\theta_y) \tag{7.19}$$

with

$$F(qy,\theta_y) = \tag{7.20}$$
$$+\int_0^\infty dw\ w^4\int_{-1}^1\frac{dx}{\kappa^2(\kappa+\kappa')^3}$$
$$\times\left(2+\frac{3(x^2-1)}{\kappa'^2}\right)2J_0(2qyw\sqrt{1-x^2}\sin\theta_y)\cos(2qywx\cos\theta_y)$$
$$+\int_0^\infty dw\ \int_{-1}^1\frac{dx}{\kappa^3}\left[\left(2+\frac{3(x^2-1)}{\kappa'^2}\right)\frac{2w^4 J_0(2qyw\sqrt{1-x^2}\sin\theta_y)\cos(2qywx\cos\theta_y)}{\kappa'(\kappa+\kappa')}\right.$$
$$\left.-\cos(2qy\cos\theta_y)\right].$$

Appendix D

This appendix contains the fitting functions for the numerical data. In the isotropic case $\vec{y} = 0$, the correction to the spectrum normalized by the scale invariant de Sitter spectrum $4\pi^2/H_0^2$ has been fitted in Fig. 5.10 with the following function:

$$
\begin{aligned}
f(q,\mu,k_0) = \mu A(\mu)\log(q/H_0)\Big[&(1-\cos(2\mu q/H_0))\sin(2q/H_0-1/4) \\
&+\mu^2 B(\mu)(q/H_0)\cos(2q/H_0-\pi/4)\Big] \\
+\frac{16\mu q/H_0}{3\pi}\Bigg\{&\frac{\sin(2q/H_0-1/4)}{2q/H_0}\left(\cos(2\mu q/H_0)-\frac{\sin(2\mu q/H_0)}{2\mu q/H_0}\right) \\
&-\mu^2\left[\cos(2q/H_0-1/4)\frac{\sin(2\mu q/H_0)}{2\mu q/H_0}-\frac{\sin(2q/H_0-1/4)}{2q/H_0}\cos(2\mu q/H_0)\right]\Bigg\} \\
&\times\Big(\log(3q^2)+2\Big) \\
-\frac{16\mu q/H_0}{3\pi}\Bigg\{&\frac{\sin(2q/H_0)}{2q/H_0}\left(\cos(2\mu q/H_0)-\frac{\sin(2\mu q/H_0)}{2\mu q/H_0}\right) \\
&-\mu^2\left[\cos(2q/H_0)\frac{\sin(2\mu q/H_0)}{2\mu q/H_0}-\frac{\sin(2q/H_0)}{2q/H_0}\cos(2\mu q/H_0)\right]\Bigg\}\left(\log\left(\frac{q^2}{k_0^2}\right)+2\right).
\end{aligned}
\tag{7.21}
$$

We have no analytic expression for the functions A and B but we observe that the dependence on μ is weak,

$$
\begin{aligned}
A(1/50) &= 0.76, \qquad B(1/50) = -1.0. \\
A(1/20) &= 0.87, \qquad B(1/20) = -0.7, \\
A(1/10) &= 0.80, \qquad B(1/10) = -1.3\,.
\end{aligned}
\tag{7.22}
$$

Obviously, setting $A = 0.8$ and $B = -1.0$ for all μ results in reasonable fits, too.

Appendix E

The integrals over the spatial variables r'', θ'', ϕ'' appearing in (6.46) and (6.47) are evaluated to

$$I_1^{\rm int}(\vec{k},\vec{k}',\eta'') \equiv \int_0^{-\xi\eta''} dr''\; r''^2 \int_{-1}^{1} d\cos\theta'' \int_0^{2\pi} d\phi''\; \mathrm{e}^{i(\vec{k}'-\vec{k})\cdot\vec{x}''} \tag{7.23}$$
$$= \frac{4\pi}{p^3}\Big[\sin\rho - \rho\cos\rho\Big]$$
$$I_2^{\rm int}(\vec{k},\vec{k}',\eta'') \equiv \int_0^{-\xi\eta''} dr''\; r''^4 \int_{-1}^{1} d\cos\theta'' \int_0^{2\pi} d\phi''\; \mathrm{e}^{i(\vec{k}'-\vec{k})\cdot\vec{x}''} \tag{7.24}$$
$$= \frac{4\pi}{p^5}\Big[3(\rho^2-2)\sin\rho - \rho(\rho^2-6)\cos\rho\Big]$$
$$I_3^{\rm int}(\vec{k},\vec{k}',\eta'') \equiv \int_0^{-\xi\eta''} dr''\; r''^2 \int_{-1}^{1} d\cos\theta'' \int_0^{2\pi} d\phi''\; i\vec{k}'\cdot\vec{x}''\; \mathrm{e}^{i(\vec{k}'-\vec{k})\cdot\vec{x}''} \tag{7.25}$$
$$= \frac{4\pi k'\cos\widetilde{\theta}}{p^4}\Big[(\rho^2-3)\sin\rho + 3\rho\cos\rho\Big]\,,$$

$$I_1^{\rm ext}(\vec{k},\vec{k}',\eta'') \tag{7.26}$$
$$\equiv \int_{-\xi\eta''}^{\infty} \frac{dr''}{r''} \int_{-1}^{1} d\cos\theta'' \int_0^{2\pi} d\phi'' \left(-k'^2 + 3\frac{(\vec{k}'\cdot\vec{x}'')^2}{r''^2}\right) \mathrm{e}^{i(\vec{k}'-\vec{k})\cdot\vec{x}''}$$
$$= 4\pi k'^2\left(3\cos^2\widetilde{\theta} - 1\right)\left[\frac{\cos\rho}{\rho^2} - \frac{\sin\rho}{\rho^3}\right]$$

$$I_2^{\rm ext}(\vec{k},\vec{k}',\eta'') \tag{7.27}$$
$$\equiv \int_{-\xi\eta''}^{\infty} \frac{dr''}{r''^2} \int_{-1}^{1} d\cos\theta'' \int_0^{2\pi} d\phi'' \left(k'^2 - 4\frac{(\vec{k}'\cdot\vec{x}'')^2}{r''^2} - \frac{2i\vec{k}'\cdot\vec{x}''}{r''^2}\right) \mathrm{e}^{i(\vec{k}'-\vec{k})\cdot\vec{x}''}$$
$$= \pi p k'\cos\widetilde{\theta}\left(p - 2k'\cos\widetilde{\theta}\right)\left[\frac{\cos\rho}{\rho} + \frac{\sin\rho}{\rho^2} + \mathrm{Si}(\rho) - \frac{\pi}{2}\right]$$
$$+ 2\pi p k'\left(6k'\cos^2\widetilde{\theta} + p\cos\widetilde{\theta} - 2k'\right)\left[\frac{\sin\rho}{\rho^4} - \frac{\cos\rho}{\rho^3}\right]$$

$$I_3^{\rm ext}(\vec{k},\vec{k}',\eta'') \equiv \int_{-\xi\eta''}^{\infty} \frac{dr''}{r''^2} \int_{-1}^{1} d\cos\theta'' \int_0^{2\pi} d\phi'' \mathrm{e}^{i(\vec{k}'-\vec{k})\cdot\vec{x}''} \tag{7.28}$$
$$= 2\pi p\left[\frac{\cos\rho}{\rho} + \frac{\sin\rho}{\rho^2} + \mathrm{Si}(\rho) - \frac{\pi}{2}\right]\,,$$

with $\rho = -\xi\|\vec{k}-\vec{k}'\|\eta''$, $p = \|\vec{k}-\vec{k}'\|$, the sine integral function $\mathrm{Si}(z) = \int_0^z dt\,\sin(t)/t$ and $\widetilde{\theta} = \sphericalangle(\vec{k}'-\vec{k},\vec{k}')$.

Appendix F

In this Appendix the contributions to the spectrum of inflaton fluctuations from the interior and exterior region are presented. The following expressions are derived from the integral expressions (6.55) and (6.57) evaluated at $\eta'' = \eta_0$ and $\eta = \eta' = 0$.

$$\begin{aligned}
&\mathrm{Im}\, J^{\mathrm{int},1}_{+-,-+}(\eta_0) = \qquad (7.29)\\
&-\frac{H_0^4}{4k^2k'}\Bigg\{\left(\frac{k'\xi p\eta_0}{k+k'}+\frac{k'(\xi p)^3\eta_0}{(k+k')^3}\right)\left(\frac{\sin(\xi p\eta_0)}{\xi p\eta_0}-\cos(\xi p\eta_0)\right)\cos[(k+k')\eta_0]\\
&\quad+\left(\frac{2k'(\xi p)^3}{(k+k')^4}+\frac{(\xi p)^3}{k(k+k')^2}+\frac{\xi p}{k}\right)\cos(\xi p\eta_0)\sin[(k+k')\eta_0]\\
&\quad-\left(\frac{(\xi p)^3\eta_0}{k(k+k')}+\frac{2k'(\xi p)^3\eta_0}{(k+k')^4}\right)\frac{\sin(\xi p\eta_0)}{\xi p\eta_0}\cos[(k+k')\eta_0]\\
&\quad-\left(\frac{\xi p}{k}+\frac{k'(\xi p)^3\eta_0^2}{(k+k')^2}\right)\frac{\sin(\xi p\eta_0)}{\xi p\eta_0}\sin[(k+k')\eta_0]\Bigg\},
\end{aligned}$$

$$\begin{aligned}
&\mathrm{Im}\, J^{\mathrm{int},2}_{+-,-+}(\eta_0) = \qquad (7.30)\\
&\frac{H_0^4}{4k^2k'}\Bigg\{\left[\frac{4\xi p\sin[(k+k')\eta_0]}{k\eta_0^2}-\frac{\xi p}{\eta_0}\left(4+\frac{k'}{k}\right)\cos[(k+k')\eta_0]\right]\left(\cos(\xi p\eta_0)-\frac{\sin(\xi p\eta_0)}{\xi p\eta_0}\right)\\
&+\left(\frac{k'(\xi p)^3\eta_0}{k+k'}+\frac{k'(\xi p)^5\eta_0}{(k+k')^3}\right)\cos(\xi p\eta_0)\cos[(k+k')\eta_0]\\
&+\left(\frac{(3kk'+k'^2)(\xi p)^3}{k(k+k')^2}-\frac{2(\xi p)^3}{k}+\frac{k'(\xi p)^5}{k(k+k')^3}-\frac{2(\xi p)^5}{k(k+k')^2}\right)\cos(\xi p\eta_0)\sin[(k+k')\eta_0]\\
&+\left(-\frac{k'(\xi p)^5\eta_0}{(k+k')^3}-\frac{3k'(\xi p)^3\eta_0}{k+k'}+\frac{2(\xi p)^5\eta_0}{(k+k')^2}+\frac{k'(\xi p)^5\eta_0}{k(k+k')^2}\right)\frac{\sin(\xi p\eta_0)}{\xi p\eta_0}\cos[(k+k')\eta_0]\\
&+\left(-4k\xi p+k'\xi p-\frac{k'^2\xi p}{k}+\frac{2(\xi p)^3}{k}+\frac{k'(\xi p)^5\eta_0^2}{(k+k')^2}\right)\frac{\sin(\xi p\eta_0)}{\xi p\eta_0}\sin[(k+k')\eta_0]\\
&+\frac{(k+k')(4k^2-kk'+k'^2)}{2k}\mathrm{Im}\left[\mathrm{Ei}(-i\,(k+k'-\xi p)\,\eta_0)-\mathrm{Ei}(-i\,(k+k'+\xi p)\,\eta_0)\right]\Bigg\},
\end{aligned}$$

$$\begin{aligned}
&\mathrm{Im}\, J^{\mathrm{int},3}_{+-,-+}(\eta_0) = \qquad (7.31)\\
&-\frac{H_0^4\xi p}{4k^2k'^2}\Bigg\{\left(\frac{(k+k')\cos[(k+k')\eta_0]}{kk'\eta_0}-\frac{\sin[(k+k')\eta_0]}{kk'\eta_0^2}\right)\left(\cos(\xi p\eta_0)-\frac{\sin(\xi p\eta_0)}{\xi p\eta_0}\right)\\
&\quad-\frac{(\xi p)^2}{(k+k')^2}\cos(\xi p\eta_0)\sin[(k+k')\eta_0]-\left(3-\frac{(k+k')^2}{kk'}\right)\frac{\sin(\xi p\eta_0)}{\xi p\eta_0}\sin[(k+k')\eta_0]\\
&\quad+\left(\frac{(\xi p)^2\eta_0}{k+k'}+\frac{(\xi p)^4\eta_0}{(k+k')^3}\right)\frac{\sin(\xi p\eta_0)}{\xi p\eta_0}\cos[(k+k')\eta_0]\\
&\quad+\frac{k+k'}{2\xi p}\left(3-\frac{(k+k')^2}{kk'}\right)\mathrm{Im}\left[\mathrm{Ei}(-i\,(k+k'-\xi p)\,\eta_0)-\mathrm{Ei}(-i\,(k+k'+\xi p)\,\eta_0)\right]\Bigg\}
\end{aligned}$$

The contributions from the exterior are

$$
\begin{aligned}
&\mathrm{Im}\, J^{\mathrm{ext},2}_{+-,-+}(\eta_0) = \qquad (7.32)\\
&-\frac{H_0^4}{4k^2k'^2}\Bigg\{\Bigg[\left(-\frac{24}{(k+k')^5}+\frac{12kk'\eta_0^2-8}{kk'(k+k')^3}+\frac{4\eta_0^2}{kk'(k+k')}-\frac{\eta_0^4}{k+k'}\right)\cos[(k+k')\eta_0]\\
&-\left(-\frac{24\eta_0}{(k+k')^4}-\frac{8\eta_0}{kk'(k+k')^2}+\frac{4\eta_0^3}{(k+k')^2}+\frac{\eta_0^3}{kk'}\right)\sin[(k+k')\eta_0]\Bigg]\left(\mathrm{Si}(-\xi p\eta_0)-\frac{\pi}{2}\right)\\
&+\frac{1}{\xi p}\Bigg[\left(\frac{10\eta_0}{(k+k')^3}+\frac{4\eta_0}{kk'(k+k')}-\frac{\eta_0^3}{k+k'}\right)\cos(\xi p\eta_0)\cos[(k+k')\eta_0]\\
&\quad+\left(\frac{2\eta_0}{(k+k')^3}+\frac{2\eta_0}{kk'(k+k')}-\frac{\eta_0^3}{k+k'}\right)\frac{\sin(\xi p\eta_0)}{\xi p\eta_0}\cos[(k+k')\eta_0]\\
&\quad+\left(-\frac{12}{(k+k')^4}-\frac{6}{kk'(k+k')^2}+\frac{\eta_0^2}{kk'}+\frac{4\eta_0^2}{(k+k')^2}\right)\cos(\xi p\eta_0)\sin[(k+k')\eta_0]\\
&\quad+\left(\frac{2\eta_0^2}{(k+k')^2}+\frac{\eta_0^2}{kk'}\right)\frac{\sin(\xi p\eta_0)}{\xi p\eta_0}\sin[(k+k')\eta_0]\Bigg]\\
&-\left(\frac{12}{(k+k')^5}+\frac{4}{kk'(k+k')^3}\right)\mathrm{Im}\left[\mathrm{Ei}(-i\,(k+k'-\xi p)\,\eta_0)-\mathrm{Ei}(-i\,(k+k'+\xi p)\,\eta_0)\right]\Bigg\},
\end{aligned}
$$

$$
\begin{aligned}
&\mathrm{Im}\, J^{\mathrm{ext},4}_{+-,-+}(\eta_0) = \qquad (7.33)\\
&-\frac{H_0^4}{4k^2k'}\Bigg\{\Bigg[\left(-\frac{6}{(k+k')^4}-\frac{2}{k(k+k')^3}+\frac{3\eta_0^2}{(k+k')^2}+\frac{\eta_0^2}{k(k+k')}\right)\cos[(k+k')\eta_0]\\
&\quad+\left(-\frac{6\eta_0}{(k+k')^3}-\frac{2\eta_0}{k(k+k')^2}+\frac{\eta_0^3}{k+k'}\right)\sin[(k+k')\eta_0]\Bigg]\left(\mathrm{Si}(-\xi p\eta_0)-\frac{\pi}{2}\right)\\
&\quad-\frac{1}{\xi p}\Bigg[\left(\frac{3\eta_0}{(k+k')^2}+\frac{\eta_0}{k(k+k')}\right)\cos(\xi p\eta_0)\cos[(k+k')\eta_0]\\
&\qquad+\left(\frac{\eta_0}{k(k+k')}+\frac{\eta_0}{(k+k')^2}\right)\frac{\sin(\xi p\eta_0)}{\xi p\eta_0}\cos[(k+k')\eta_0]\\
&\qquad+\left(-\frac{8}{(k+k')^3}-\frac{2}{k(k+k')^2}+\frac{\eta_0^2}{k+k'}\right)\cos(\xi p\eta_0)\sin[(k+k')\eta_0]\\
&\qquad+\frac{\eta_0^2}{k+k'}\frac{\sin(\xi p\eta_0)}{\xi p\eta_0}\sin[(k+k')\eta_0]\Bigg]\\
&\quad+\frac{4k+k'}{k(k+k')^4}\mathrm{Im}\left[\mathrm{Ei}(-i\,(k+k'-\xi p)\,\eta_0)-\mathrm{Ei}(-i\,(k+k'+\xi p)\,\eta_0)\right]\Bigg\},
\end{aligned}
$$

with the exponential integral function $\mathrm{Ei}(z) = -\int_{-z}^{\infty} dt\; e^{-t}/t$ and the sine integral function $\mathrm{Si}(z) = \int_0^z dt \sin(t)/t$. Note that from (6.57) we have $J^{\mathrm{ext},3}_{+-,-+}(\eta_0) = (\xi p)^{-1} J^{\mathrm{ext},1}_{+-,-+}(\eta_0)$.

Moreover, $J^{\mathrm{ext},1}_{+-,-+}(\eta_0)$ is given by (5.71) with μ replaced by ξ,

$$\begin{aligned}
&\mathrm{Im}\, J^{\mathrm{ext},1}_{+-,-+}(\eta_0) = \qquad (7.34)\\
&-\frac{H_0^4}{4k^2k'^2(\xi p)^2}\Bigg\{\left[\frac{\eta_0\cos[(k+k')\eta_0]}{k+k'}-\frac{\sin[(k+k')\eta_0]}{kk'}\right]\left(\cos(\xi p\eta_0)-\frac{\sin(\xi p\eta_0)}{\xi p\eta_0}\right)\\
&+(\xi p)^2\left[\frac{\eta_0\cos[(k+k')\eta_0]}{(k+k')^3}\cos(\xi p\eta_0)+\left(\frac{1}{kk'}+\frac{1}{(k+k')^2}\right)\frac{\eta_0\cos[(k+k')\eta_0]}{(k+k')}\frac{\sin(\xi p\eta_0)}{\xi p\eta_0}\right.\\
&\left.-\left(\frac{1}{kk'}+\frac{2}{(k+k')^2}\right)\frac{\sin[(k+k')\eta_0]}{(k+k')^2}\cos(\xi p\eta_0)+\frac{\eta_0^2\sin[(k+k')\eta_0]}{(k+k')^2}\frac{\sin(\xi p\eta_0)}{\xi p\eta_0}\right]\Bigg\}.
\end{aligned}$$

In order to derive the results presented in (6.64) and (6.65) for the contributions at future infinity $\eta'' \to 0$, we made use of the following expansion of the exponential integral function. For $\rho > 0$,

$$\mathrm{Ei}(\rho) = \gamma_E + \frac{i\pi}{2} + \log(\rho) + i\rho - \frac{\rho^2}{4} + \mathcal{O}\left(\rho^3\right), \qquad (7.35)$$

with Euler's constant $\gamma_E \simeq 0.58$.

Bibliography

[1] C.M. Will. The confrontation between general relativity and experiment. *Living Rev. Rel.*, 9:3, 2005, gr-qc/0510072.

[2] D. Finkelstein. Past-future asymmetry of the gravitational field of a point particle. *Phys. Rev.*, 110:965–967, 1958.

[3] R. Penrose. Gravitational collapse and space-time singularities. *Phys. Rev. Lett.*, 14:57–59, 1965.

[4] S.W. Hawking and R. Penrose. The singularities of gravitational collapse and cosmology. *Proc. Roy. Soc. Lond.*, A314:529–548, 1970.

[5] A. S. Eddington. *The mathematical theory of relativity*. 1923. Cambridge University, London, 2nd Ed.

[6] A.A. Penzias and R.W. Wilson. A measurement of excess antenna temperature at 4080-Mc/s. *Astrophys. J.*, 142:419–421, 1965.

[7] J.C. Mather et al. Measurement of the cosmic microwave background spectrum by the COBE FIRAS instrument. *Astrophys. J.*, 420:439–444, 1994.

[8] R.H. Brandenberger. Lectures on the theory of cosmological perturbations. *Lect. Notes Phys.*, 646:127–167, 2004, hep-th/0306071.

[9] C. Møller. *Les theories relativistes de la gravitation*. 1962. Paris: CNRS.

[10] J.C. Pati and A. Salam. Lepton number as the fourth color. *Phys. Rev.*, D10:275–289, 1974.

[11] H. Georgi and S.L. Glashow. Unity of all elementary particle forces. *Phys. Rev. Lett.*, 32:438–441, 1974.

[12] S.W. Hawking. Particle creation by black holes. *Commun. Math. Phys.*, 43:199–220, 1975.

[13] G. Amelino-Camelia. Quantum gravity phenomenology. 2008, gr-qc/08060339.

[14] G. 't Hooft and M.J.G. Veltman. One loop divergencies in the theory of gravitation. *Annales Poincare Phys. Theor.*, A20:69–94, 1974.

[15] M.J.G. Veltman. Quantum theory of gravitation. In *Les Houches 1975, Proceedings, Methods In Field Theory*, Amsterdam 1976, 265-327.

[16] M.H. Goroff and A. Sagnotti. Quantum gravity at two loops. *Phys. Lett.*, B160:81, 1985.

[17] A.E.M. van de Ven. Two loop quantum gravity. *Nucl. Phys.*, B378:309–366, 1992.

[18] R.P. Woodard. How far are we from the quantum theory of gravity? *Rept. Prog. Phys.*, 72:126002, 2009, gr-qc/09074238.

[19] S. Weinberg. Effective field theory, past and future. *PoS*, CD09:001, 2009, hep-th/09081964.

[20] M.B. Green, J.H. Schwarz and E. Witten. Superstring theory. Vol. 1: Introduction. Cambridge, UK: Univ. Pr. (1987) 469 p.

[21] M.B. Green, J.H. Schwarz and E. Witten. Superstring theory. Vol. 2: Loop amplitudes, anomalies and phenomenology. Cambridge, UK: Univ. Pr. (1987) 596 p.

[22] J. Polchinski. String theory. Vol. 1: An introduction to the bosonic string. Cambridge, UK: Univ. Pr. (1998) 402 p.

[23] J. Polchinski. String theory. Vol. 2: Superstring theory and beyond. Cambridge, UK: Univ. Pr. (1998) 531 p.

[24] A. Ashtekar. New variables for classical and quantum gravity. *Phys. Rev. Lett.*, 57:2244–2247, 1986.

[25] C. Rovelli. Loop quantum gravity. *Living Rev. Rel.*, 1:1, 1998, gr-qc/9710008.

[26] T. Regge. General relativity without coordinates. *Nuovo Cim.*, 19:558–571, 1961.

[27] M. Rocek and R.M. Williams. Quantum Regge calculus. *Phys. Lett.*, B104:31, 1981.

[28] A. Perez. Spin foam models for quantum gravity. *Class. Quant. Grav.*, 20:R43, 2003, gr-qc/0301113.

[29] J.B. Kogut. A review of the lattice gauge theory approach to quantum chromodynamics. *Rev. Mod. Phys.*, 55:775, 1983.

[30] J. Ambjørn, B. Durhuus and J. Fröhlich. Diseases of triangulated random surface models, and possible cures. *Nucl. Phys.*, B257:433, 1985.

[31] F. David. A model of random surfaces with nontrivial critical behavior. *Nucl. Phys.*, B257:543, 1985.

[32] V.A. Kazakov, A.A. Migdal and I.K. Kostov. Critical properties of randomly triangulated planar random surfaces. *Phys. Lett.*, B157:295–300, 1985.

[33] J. Ambjørn, J. Jurkiewicz and R. Loll. Spectral dimension of the universe. *Phys. Rev. Lett.*, 95:171301, 2005, hep-th/0505113.

[34] J. Ambjørn and J. Jurkiewicz. Scaling in four-dimensional quantum gravity. *Nucl. Phys.*, B451:643–676, 1995, hep-th/9503006.

[35] J. Ambjørn and J. Jurkiewicz. Four-dimensional simplicial quantum gravity. *Phys. Lett.*, B278:42–50, 1992.

[36] J. Ambjørn and R. Loll. Non-perturbative Lorentzian quantum gravity, causality and topology change. *Nucl. Phys.*, B536:407–434, 1998, hep-th/9805108.

[37] J. Ambjørn, J. Jurkiewicz and R. Loll. Nonperturbative Lorentzian path integral for gravity. *Phys. Rev. Lett.*, 85:924–927, 2000, hep-th/0002050.

[38] J. Ambjørn, A. Görlich, J. Jurkiewicz and R. Loll. Planckian birth of the quantum de Sitter universe. *Phys. Rev. Lett.*, 100:091304, 2008, hep-th/07122485.

[39] J. Ambjørn, A. Görlich, J. Jurkiewicz and R. Loll. The nonperturbative quantum de Sitter universe. *Phys. Rev.*, D78:063544, 2008, hep-th/08074481.

[40] F. Cianfrani and G. Montani. Matter in loop quantum gravity without time gauge: A nonminimally coupled scalar field. *Phys. Rev.*, D80:084045, 2009.

[41] J. Ambjørn, Z. Burda, J. Jurkiewicz and C.F. Kristjansen. 4-d quantum gravity coupled to matter. *Phys. Rev.*, D48:3695–3703, 1993, hep-th/9303042.

[42] S. Bilke, Z. Burda, A. Krzywicki, B. Petersson, J. Tabaczek and G. Thorleifsson. 4d simplicial quantum gravity interacting with gauge matter fields. *Phys. Lett.*, B418:266–272, 1998, hep-lat/9710077.

[43] J. Ambjørn, K.N. Anagnostopoulos and J. Jurkiewicz. Abelian gauge fields coupled to simplicial quantum gravity. *JHEP*, 08:016, 1999, hep-lat/9907027.

[44] S. Carlip. *Quantum gravity in 2+1 dimensions.* Cambridge University Press, December 2003.

[45] A. Staruszkiewicz. Gravitation theory in three-dimensional space. *Acta Phys. Polon.*, 24:735–740, 1963.

[46] S. Deser, R. Jackiw and G. 't Hooft. Three-dimensional Einstein gravity: Dynamics of flat space. *Ann. Phys.*, 152:220, 1984.

[47] G. 't Hooft. Quantization of point particles in 2+1 dimensional gravity and space-time discreteness. *Class. Quant. Grav.*, 13:1023–1040, 1996, gr-qc/9601014.

[48] H.-J. Matschull and M. Welling. Quantum mechanics of a point particle in 2+1 dimensional gravity. *Class. Quant. Grav.*, 15:2981–3030, 1998, gr-qc/9708054.

[49] K. Noui and A. Perez. Three dimensional loop quantum gravity: Coupling to point particles. *Class. Quant. Grav.*, 22:4489–4514, 2005, gr-qc/0402111.

[50] L. Freidel and D. Louapre. Ponzano-Regge model revisited. I: Gauge fixing, observables and interacting spinning particles. *Class. Quant. Grav.*, 21:5685–5726, 2004, hep-th/0401076.

[51] A.H. Guth. The inflationary universe: A possible solution to the horizon and flatness problems. *Phys. Rev.*, D23:347–356, 1981.

[52] A.D. Linde. A new inflationary universe scenario: A possible solution of the horizon, flatness, homogeneity, isotropy and primordial monopole problems. *Phys. Lett.*, B108:389–393, 1982.

[53] A. Matacz. Inflation and the fine-tuning problem. *Phys. Rev.*, D56:1836–1840, 1997, gr-qc/9611063.

[54] V.F. Mukhanov, H.A. Feldman and R.H. Brandenberger. Theory of cosmological perturbations. Part 1. Classical perturbations. Part 2. Quantum theory of perturbations. Part 3. Extensions. *Phys. Rept.*, 215:203–333, 1992.

[55] A.D. Linde. Coleman-Weinberg theory and a new inflationary universe scenario. *Phys. Lett.*, B114:431, 1982.

[56] A. Albrecht and P.J. Steinhardt. Cosmology for grand unified theories with radiatively induced symmetry breaking. *Phys. Rev. Lett.*, 48:1220–1223, 1982.

[57] S. Dodelson. *Modern cosmology*. Amsterdam, Netherlands: Academic Pr. (2003) 440 p.

[58] H. Kodama and M. Sasaki. Cosmological perturbation theory. *Prog. Theor. Phys. Suppl.*, 78:1–166, 1984.

[59] D. Larson et al. Seven-year Wilkinson microwave anisotropy probe (WMAP) observations: Power spectra and WMAP-derived parameters. 2010, astro-ph/10014635.

[60] V.F. Mukhanov and G.V. Chibisov. Quantum fluctuation and nonsingular universe (in Russian). *JETP Lett.*, 33:532–535, 1981.

[61] T.S. Bunch and P.C.W. Davies. Quantum field theory in de Sitter space: Renormalization by point splitting. *Proc. Roy. Soc. Lond.*, A360:117–134, 1978.

[62] G. Efstathiou and S. Gratton. B-mode detection with an extended Planck mission. *JCAP*, 0906:011, 2009, astro-ph/09030345.

[63] B.J. Carr and S.W. Hawking. Black holes in the early Universe. *Mon. Not. Roy. Astron. Soc.*, 168:399–415, 1974.

[64] K.-M. Lee, V.P. Nair and E.J. Weinberg. Black holes in magnetic monopoles. *Phys. Rev.*, D45:2751–2761, 1992, hep-th/9112008.

[65] J. Ambjørn, J. Jurkiewicz and R. Loll. Emergence of a 4D world from causal quantum gravity. *Phys. Rev. Lett.*, 93:131301, 2004, hep-th/0404156.

[66] J. Ambjørn, J. Jurkiewicz and R. Loll. Reconstructing the universe. *Phys. Rev.*, D72:064014, 2005, hep-th/0505154.

[67] J. Ambjørn, A. Görlich, J. Jurkiewicz and R. Loll. The universe from scratch. *Contemp. Phys.*, 47:103–117, 2006, hep-th/0509010.

[68] J. Ambjørn, A. Görlich, J. Jurkiewicz and R. Loll. Quantum gravity, or the art of building spacetime. In D. Oriti, editor, *Approaches to Quantum Gravity: Toward a New Understanding of Space, Time and Matter*, pages 341–359. Cambridge University Press, 2009, hep-th/0604212.

[69] J. Ambjørn, A. Görlich, J. Jurkiewicz and R. Loll. Quantum gravity as sum over spacetimes. In Booß-Bavnbek, B.; Esposito, G.; Lesch, M., editor, *New Paths Towards Quantum Gravity*, volume 807 of *Lecture Notes in Physics*, pages 59–124. Springer, 2010, gr-qc/09063947.

[70] J. Ambjørn, A. Görlich, J. Jurkiewicz and R. Loll. Causal dynamical triangulations and the quest for quantum gravity. In Ellis, G.; Murugan, J.; Weltman, A., editor, *Foundations of Space and Time*. Cambridge University Press, 2010, hep-th/10040352. (to appear).

[71] R. Loll. The emergence of spacetime, or, quantum gravity on your desktop. *Class. Quant. Grav.*, 25:114006, 2008, gr-qc/07110273.

[72] G.W. Gibbons (ed.) and S.W. Hawking (ed.). *Euclidean Quantum Gravity*. World Scientific, Singapore, Singapore, 1993.

[73] J. Ambjørn, J. Jurkiewicz and R. Loll. Dynamically triangulating Lorentzian quantum gravity. *Nucl. Phys.*, B610:347–382, 2001, hep-th/0105267.

[74] B. Dittrich and R. Loll. Counting a black hole in Lorentzian product triangulations. *Class. Quant. Grav.*, 23:3849–3878, 2006, gr-qc/0506035.

[75] K.S. Thorne, C.W. Misner and J.A. Wheeler. *Gravitation*. Physics Series. W. H. Freeman, 2nd edition, 1973.

[76] C. Teitelboim. Quantum mechanics of the gravitational field. *Phys. Rev.*, D25:3159, 1982.

[77] C. Teitelboim. The proper time gauge in quantum theory of gravitation. *Phys. Rev.*, D28:297, 1983.

[78] R.M. Wald. *General Relativity*. University of Chicago Press, 1st edition, 1984.

[79] R. Gautreau. Geodesic coordinates in the de Sitter universe. *Phys. Rev. D*, 27:764, 1983.

[80] R. Gautreau. On Kruskal-Novikov co-ordinate systems. *Nuovo Cim.*, 56B:49, 1980.

[81] K. Martel and E. Poisson. Regular coordinate systems for Schwarzschild and other spherical spacetimes. *Am. J. Phys.*, 69:476–480, 2001, gr-qc/0001069.

[82] R. Steinbauer and J.A. Vickers. The use of generalised functions and distributions in general relativity. *Class. Quant. Grav.*, 23:R91–R114, 2006, gr-qc/0603078.

[83] S. Deser R. Arnowitt and C.W. Misner. Finite self-energy of classical point particles. *Phys.Rev.Lett.*, 4:375–377, 1960.

[84] H. Nariai. On a new cosmological solution of Einstein's field equations of gravitation. *Sci. Rep. Tohoku Univ.*, 35:46, 1951. reprinted in *Gen. Rel. Grav.* 31:963, 1999.

[85] F.-L. Lin and C. Soo. Quantum field theory with and without conical singularities: black holes with a cosmological constant and the multi-horizon scenario. *Class. Quant. Grav.*, 16(2):551–562, 1999.

[86] E. Hackmann and C. Lämmerzahl. Complete analytic solution of the geodesic equation in Schwarzschild-(anti-) de Sitter spacetimes. *Phys. Rev. Lett.*, 100:171101, 2008.

[87] E. Hackmann and C. Lämmerzahl. Geodesic equation in Schwarzschild-(anti-) de Sitter space-times: Analytical solutions and applications. *Phys. Rev.*, D78:024035, 2008.

[88] I.S. Gradshteyn and I.M. Ryzhik. *Table of integrals, series and products*. Elsevier Inc., 7th edition, 2007.

[89] Z. Stuchlik. Spherically symmetric static configurations of uniform density in spacetimes with a non-zero cosmological constant. *Acta Phys. Slov.*, 50:219–228, 2000, gr-qc/08032530.

[90] O. Lauscher and M. Reuter. Fractal spacetime structure in asymptotically safe gravity. *JHEP*, 10:050, 2005, hep-th/0508202.

[91] P. Hořava. Spectral dimension of the universe in quantum gravity at a Lifshitz point. *Phys. Rev. Lett.*, 102:161301, 2009, hep-th/09023657.

[92] S. Carlip. Spontaneous dimensional reduction in short-distance quantum gravity? In J. Kowalski-Glikman, R. Durka, and M. Szczachor, editors, *The Planck Scale: Proceedings of the XXV Max Born Symposium*, volume 1196, pages 72–80. AIP, 2009, gr-qc/09093329.

[93] J. Ambjørn, A. Görlich, S. Jordan, J. Jurkiewicz and R. Loll. CDT meets Horava-Lifshitz gravity. *Phys. Lett.*, B690:413–419, 2010, hep-th/10023298.

[94] V.F. Mukhanov. Quantum theory of gauge invariant cosmological perturbations. *Sov. Phys. JETP*, 67:1297–1302, 1988.

[95] M. Sasaki. Large scale quantum fluctuations in the inflationary universe. *Prog. Theor. Phys.*, 76:1036, 1986.

[96] M. Zaldarriaga and U. Seljak. An all-sky analysis of polarization in the microwave background. *Phys. Rev.*, D55:1830–1840, 1997, astro-ph/9609170.

[97] T. Prokopec and G. Rigopoulos. Path integral for inflationary perturbations. *Phys. Rev.*, D82:023529, 2010, gr-qc/10040882.

[98] J.C. Mather, D.J. Fixsen, R.A. Shafer, C. Mosier and D.T. Wilkinson. Calibrator design for the COBE far infrared absolute spectrophotometer (FIRAS). *Astrophys. J.*, 512:511–520, 1999, astro-ph/9810373.

[99] G.F. Smoot et al. Structure in the COBE differential microwave radiometer first year maps. *Astrophys. J.*, 396:L1–L5, 1992.

[100] W.J. Percival et al. Baryon acoustic oscillations in the Sloan digital sky survey data release 7 galaxy sample. *Mon. Not. Roy. Astron. Soc.*, 401:2148–2168, 2010, astro-ph/09071660.

[101] B.A. Reid et al. Cosmological constraints from the clustering of the Sloan digital sky survey DR7 luminous red galaxies. *Mon. Not. Roy. Astron. Soc.*, 404:60–85, 2010, astro-ph/09071659.

[102] C.L. Bennett et al. Seven-year Wilkinson microwave anisotropy probe (WMAP) observations: Are there cosmic microwave background anomalies? 2010, astro-ph/10014758.

[103] C.J. Copi, D. Huterer, D.J. Schwarz and G.D. Starkman. Large angle anomalies in the CMB. 2010, astro-ph/10045602.

[104] A. de Oliveira-Costa, M. Tegmark, M. Zaldarriaga and A. Hamilton. The significance of the largest scale CMB fluctuations in WMAP. *Phys. Rev.*, D69:063516, 2004, astro-ph/0307282.

[105] A. Kashlinsky, F. Atrio-Barandela, H. Ebeling, A. Edge and D. Kocevski. A new measurement of the bulk flow of X-ray luminous clusters of galaxies. *Astrophys. J.*, 712:L81–L85, 2010, astro-ph/09104958.

[106] J.-P. Uzan. Dark energy, gravitation and the Copernican principle. 2009, gr-qc/09125452.

[107] T. Buchert. Dark energy from structure - A status report. *Gen. Rel. Grav.*, 40:467–527, 2008, gr-qc/07072153.

[108] S. Rasanen. Evaluating backreaction with the peak model of structure formation. *JCAP*, 0804:026, 2008, astro-ph/08012692.

[109] S. Alexander, T. Biswas, A. Notari and D. Vaid. Local void vs dark energy: Confrontation with WMAP and type Ia supernovae. *JCAP*, 0909:025, 2009, astro-ph/07120370.

[110] P. Zhang and A. Stebbins. Confirmation of the Copernican principle at Gpc radial scale and above from the kinetic Sunyaev Zel'dovich effect power spectrum. 2010, astro-ph/10093967.

[111] B.M. Leith, S.C.C. Ng and D.L. Wiltshire. Gravitational energy as dark energy: Concordance of cosmological tests. *Astrophys. J.*, 672:L91–L94, 2008, astro-ph/07092535.

[112] W. Valkenburg. Swiss cheese and a cheesy CMB. *JCAP*, 0906:010, 2009, astro-ph/09024698.

[113] S.M. Carroll, C.-Y. Tseng and M.B. Wise. Translational invariance and the anisotropy of the cosmic microwave background. *Phys. Rev.*, D81:083501, 2010, astro-ph/08111086.

[114] E. Komatsu et al. Seven-year Wilkinson microwave anisotropy probe (WMAP) observations: Cosmological interpretation. 2010, astro-ph/10014538.

[115] P. Candelas. Vacuum polarization in Schwarzschild space-time. *Phys. Rev.*, D21:2185–2202, 1980.

[116] P. Candelas and B.P. Jensen. The Feynman Green function inside a Schwarzschild black holes. *Phys. Rev.*, D33:1596, 1986.

[117] B.P. Jensen and P. Candelas. The Schwarzschild radial functions. *Phys. Rev.*, D33:1590, 1986.

[118] E. Winstanley and P.M. Young. Vacuum polarization for lukewarm black holes. *Phys. Rev.*, D77:024008, 2008, gr-qc/07083820.

[119] G.C. McVittie. The mass-particle in an expanding universe. *Mon. Not. Roy. Astron. Soc.*, 93:325, 1933.

[120] G.W. Gibbons and S.W. Hawking. Cosmological event horizons, thermodynamics, and particle creation. *Phys. Rev.*, D15:2738–2751, 1977.

[121] H. Saida, T. Harada and H. Maeda. Black hole evaporation in an expanding universe. *Class. Quant. Grav.*, 24:4711–4732, 2007, gr-qc/07054012.

[122] S. Bonometto (ed.), V. Gorini (ed.) and U. Moschella (ed.). Modern cosmology. Bristol, UK: IOP (2002) 480 p.

[123] B.J. Carr. The primordial black hole mass spectrum. *Astrophys. J.*, 201:1–19, 1975.

[124] H.V. Peiris et al. First year Wilkinson microwave anisotropy probe (WMAP) observations: Implications for inflation. *Astrophys. J. Suppl.*, 148:213, 2003, astro-ph/0302225.

[125] J.S. Schwinger. Brownian motion of a quantum oscillator. *J. Math. Phys.*, 2:407–432, 1961.

[126] L.V. Keldysh. Diagram technique for nonequilibrium processes. *Zh. Eksp. Teor. Fiz.*, 47:1515–1527, 1964.

[127] R.D. Jordan. Effective field equations for expectation values. *Phys. Rev.*, D33:444–454, 1986.

[128] S. Weinberg. Quantum contributions to cosmological correlations. *Phys. Rev.*, D72:043514, 2005, hep-th/0506236.

[129] N.D. Birrell and P. C. W. Davies. Quantum fields in curved space. Cambridge, UK, University Press. (1982) 340p.

[130] A. Vilenkin and L.H. Ford. Gravitational effects upon cosmological phase transitions. *Phys. Rev.*, D26:1231, 1982.

[131] T.M. Janssen and T. Prokopec. Regulating the infrared by mode matching: A massless scalar in expanding spaces with constant deceleration. 2009, gr-qc/09060666.

[132] T.S. Koivisto and T. Prokopec. Quantum backreaction in evolving FLRW spacetimes. 2010, gr-qc/10095510.

[133] N.C. Tsamis and R.P. Woodard. The physical basis for infrared divergences in inflationary quantum gravity. *Class. Quant. Grav.*, 11:2969–2990, 1994.

[134] T. Prokopec and E. Puchwein. Photon mass generation during inflation: de Sitter invariant case. *JCAP*, 0404:007, 2004, astro-ph/0312274.

[135] B. Garbrecht, T. Prokopec and M.G. Schmidt. Particle number in kinetic theory. *Eur. Phys. J.*, C38:135–143, 2004, hep-th/0211219.

[136] P.A.M. Dirac. Quantised singularities in the electromagnetic field. *Proc. Roy. Soc. Lond.*, A133:60–72, 1931.

[137] P.A.M. Dirac. The theory of magnetic poles. *Phys. Rev.*, 74:817–830, 1948.

[138] G. 't Hooft. Magnetic monopoles in unified gauge theories. *Nucl. Phys.*, B79:276–284, 1974.

[139] A.M. Polyakov. Particle spectrum in quantum field theory. *JETP Lett.*, 20:194–195, 1974.

[140] K.A. Milton. Theoretical and experimental status of magnetic monopoles. *Rept. Prog. Phys.*, 69:1637–1712, 2006, hep-ex/0602040.

[141] J.S. Schwinger. Magnetic charge and quantum field theory. *Phys.Rev.*, 144:1087–1093, 1966.

[142] R. Penrose. Singulatities and time asymmetry. In *S.W. Hawking, W. Israel: General Relativity*, 581-638.

[143] S.D. Mathur. The fuzzball proposal for black holes: An elementary review. *Fortsch. Phys.*, 53:793–827, 2005, hep-th/0502050.

[144] N. Afshordi, G. Geshnizjani and J. Khoury. Do observations offer evidence for cosmological-scale extra dimensions? *JCAP*, 0908:030, 2009, astro-ph/08122244.

[145] L. Mersini-Houghton and R. Holman. 'Tilting' the universe with the landscape multiverse: The 'dark' flow. *JCAP*, 0902:006, 2009, hep-th/08105388.

Samenvatting

Observaties tonen aan dat de zwaartekracht op macroscopische schaal heel goed door de wetten van de algemene relativiteitstheorie wordt beschreven. In deze theorie wordt aangenomen dat de ruimtetijd een klassieke dynamische grootheid is. Een belangrijke kwestie is hoe dit klassieke beeld in overeenstemming te brengen is met de wetten van de kwantummechanica. Vele pogingen zijn ondernomen om dit fundamentele probleem der theoretische fysica te belichten en daarmee een mogelijkheid te bieden om concrete uitspraken te doen over de structuur van ruimtetijd op de kleinste schalen. Een veelbelovende benadering is de regularisatie van de padintegraal voor de zwaartekracht in de vorm van dynamische triangulaties, hetgeen in dit proefschrift behandeld wordt. De padintegraal is een realisatie van het principe van kwantum superpositie, wat in het geval van zwaartekracht betekent dat ook met geometrieën van ruimtetijd rekening wordt gehouden die geen oplossingen van de klassieke veldvergelijkingen zijn. De regularisatie is gebaseerd op het feit dat elke ruimtetijdgeometrie kan worden benaderd door het in elkaar zetten van kleine gelijkzijdige blokken met nul kromming in het inwendige. Om fysische voorspellingen over de kwantumgeometrie van de ruimtetijd te kunnen doen, moeten observabelen worden bepaald en hun eigenschappen worden geanalyseerd. Het blijkt dat dit in het kader van dynamische triangulaties uitvoerbaar is. Toen het aangetoond was dat de Euclidische triangulaties (zonder causaliteitsrestricties) in vier dimensies en in afwezigheid van materie niet de correcte continuümlimiet hebben, werd een nieuw model ontwikkeld dat causaliteit veronderstelt. In tegenstelling tot de Euclidische versie, heeft het model der Causale Dynamische Triangulaties (CDT) een fase waarin uitgestrekte universa te vinden zijn die op grote schaal de eigenschappen van klassieke ruimtetijd bezitten. In het bijzonder kon worden aangetoond dat de tijdsevolutie van de verwachtingswaarde van het ruimtelijke volume van de universa, die in Monte Carlo simulaties van CDT zijn gegenereerd, op grote schaal overeenkomt met de tijdsevolutie van de Euclidische de Sitter ruimte in een bepaalde ijk. Een discussie van dit resultaat en een algemene inleiding tot CDT zijn te vinden in hoofdstuk 2 van dit proefschrift.

Om het model realistischer te maken wordt in hoofdstuk 3 de koppeling van materie aan geometrie in het niet-perturbatieve kader van CDT behandeld. Het geval van een gelokaliseerde massa in een universum met een positieve kosmologische constante is een fysisch zeer natuurlijke en belangrijke situatie. In dit proefschrift wordt een bijdrage geleverd om de klassieke limiet van het aan materie gekoppelde CDT model in vier dimensies te testen. In de klassieke algemene relativiteitstheorie leidt het inbrengen van een gelokaliseerde massa in een voor de rest lege ruimte tot de Schwarzschild-de Sitter (SdS) achtergrond. Als de dichtheid van het massieve object groot genoeg is ontstaat een zwart gat. We verwachten dat het effect van de introductie van een massa in CDT het gevolg heeft dat de kwantumgeometrie op grote schaal de eigenschappen van de Euclidische SdS ruimte bezit. Om zulke resultaten van computer simulaties met klassieke waarden te vergelijken moeten observabelen worden onderzocht die door de massa worden beïnvloed. Inderdaad blijkt uit het werk dat hier gepresenteerd wordt dat de klassieke tijdsevolutie van het ruimtelijke volume (het *volumeprofiel*) van de Euclidische SdS ruimte voor kleine massa's op een karakteristieke wijze van de tijdsevolutie van de Euclidische de Sitter ruimte afwijkt. Hierbij hebben wij de eigentijdijk moeten gebruiken die ook in het geval zonder massa gebruikt is. Een manier om deze ijk te realiseren is door het invoeren van Gauss normaalcoördinaten. Het is aangetoond dat deze coördinaten voor de Euclidische SdS ruimte niet globaal gedefinieerd zijn. Om het volumeprofiel te bepalen moest een benadering worden gebruikt die eruit bestaat een deel van de Euclidische ruimte uit te snijden en zijn bijdrage tot het totale ruimtelijke volume te verwaarlozen. Wij hebben echter kunnen demonstreren dat dit een goede benadering is voor massa's onder een kritische waarde. Dus kunnen de resultaten uit dit hoofdstuk worden gebruikt om de klassieke limiet van het CDT model met koppeling aan een gelokaliseerde massa te bestuderen.

In het tweede deel van dit proefschrift worden de gevolgen van dergelijke objecten in het kader van kosmologische inflatie behandeld. Er bestaan goede redenen om aan te nemen dat er een korte periode van inflatie in het vroege universum heeft plaatsgevonden waarin de ruimte bijna exponentieel expandeerde. De oorspronkelijke motivatie voor kosmologische modellen van inflatie was de mogelijkheid om drie problemen in de kosmologie op te lossen. Met name, zou men eigenlijk in het huidige universum een grote ruimtelijke kromming, grote inhomogeniteiten en een grote hoeveelheid aan magnetische monopolen verwachten als er nooit een periode van inflatie zou hebben plaatsgevonden. De oplossing die door het paradigma van inflatie wordt geboden is dat het universum dat we tegenwoordig kunnen zien zich vroeger in een gebied binnen een Hubble volume bevond en dus door wisselwerking kon homogeniseren. Bovendien wordt de concentratie van monopolen door een periode van inflatie sterk verdund. Het blijkt echter dat er nog een betere motivatie bestaat om inflatie in ogenschouw te nemen.

Inflatie biedt namelijk een heel elegante verklaring voor de temperatuurfluctuaties in de kosmische achtergrondstraling en voor formatie van structuur in de materieverdeling op grote kosmologische schaal. Men gaat ervan uit dat de oorsprong in beide gevallen in kwantumfluctuaties van velden tijdens de inflatieperiode ligt. De velden die hierbij een rol spelen zijn het inflatonveld en het metriekveld dat de zwaartekracht beschrijft. Het is handig om de fluctuaties in deze velden onder te verdelen naar gelang hun transformatie-eigenschappen onder ruimtelijke rotaties. Het inflatonveld is een scalair veld en het metriekveld bevat zowel scalaire als vector- en tensorvelden. Voor observaties zijn echter alleen velden belangrijk die invariant zijn onder ijktransformaties. Een specifieke combinatie van het inflatonveld en een scalair veld in de metriek kan worden geconstrueerd die ijkinvariant is. Deze wordt de Sasaki-Mukhanov variabele genoemd en beschrijft scalaire kosmologische perturbaties. Er bestaat een zekere ijk waarin het Sasaki-Mukhanov veld eenvoudig gerelateerd is aan het inflatonveld. Behalve de scalaire perturbaties hebben ook de tensorperturbaties belangrijke fysische gevolgen. Daarentegen wordt vermoed dat de invloed van vectorperturbaties in het algemeen ondergeschikt is.

Een belangrijke eigenschap van kosmologische perturbaties is het *spectrum* dat door de tweepuntscorrelatiefunctie in impulsruimte is gegeven. Het spectrum van een scalair veld in een de Sitter ruimte is bijvoorbeeld schaalinvariant. Als het spectrum wel van de schaal afhangt is het nuttig dit door een spectraalindex n_s aan te geven. De waarde van de spectraalindex die voor de kosmische achtergrond straling is gemeten is $n_s = 0.963 \pm 0.014\,(1\sigma)$, dus het spectrum is niet schaalinvariant ($n_s \neq 1$). Een tweede grootheid die het spectrum karakteriseert is zijn amplitude en deze is ook met grote nauwkeurigheid gemeten. Uit kosmologische inflatiemodellen kan dit spectrum worden afgeleid, hetgeen een goede reden geeft om het paradigma van inflatie te beschouwen.

In hoofdstuk 4 van dit proefschrift worden tensorfluctuaties op een homogene achtergrond behandeld. We tonen expliciet aan dat de Einstein-Hilbert actie wat betreft de fluctuaties zich opsplitst in een scalair-, een vector- en een tensorsector. In het bijzonder betekent dit resultaat dat de ijkinvariante tensorfluctuaties apart kunnen worden bestudeerd zonder met de velden in de andere sectoren rekening te houden. Het spectrum van de tensorfluctuaties wordt dan in het geval van een de Sitter achtergrond vastgesteld. Dit kan met het spectrum van scalaire kosmologische fluctuaties worden vergeleken, waaruit volgt dat de amplitude van tensorfluctuaties in slow-roll inflatie sterk onderdrukt is. Daarom wordt in hoofstuk 5 alleen de invloed van primordiale zwarte gaten op de scalaire kosmologische fluctuaties bestudeerd, omdat dit effect vermoedelijk het grootst is. De belangrijkste motivatie voor het analyseren van dit soort inhomogeniteiten is om de mogelijkheid te bieden om anomalieën in de kosmische achtergrond straling te verklaren. Het was belangrijk eerst te schatten hoe veel primordiale zwarte gaten per Hubble volume zouden kunnen ontstaan in een door ma-

terie gedomineerde pre-inflationaire fase. Daarna hebben we de correctie op het spectrum van scalaire kosmologische fluctuaties veroorzaakt door een zwart gat afgeleid en voor verschillende parameters onderzocht. In het bijzonder hebben we aangetoond hoe het spectrum afhangt van de massa van het zwarte gat, van zijn positie en van een afbrekingsparameter. De afbrekingsparameter moest worden ingevoerd om de correlatiefunctie in het infrarode regime te regulariseren. Een iets algemenere situatie wordt in hoofstuk 6 beschreven. We hebben daar het effect van magnetische monopolen op het spectrum van scalaire kosmologische fluctuaties bestudeerd. Daartoe hebben we de achtergrond bepaald die door de 't Hooft-Polyakov monopool wordt veroorzaakt. Binnenin de monopool kan de metriek door kwadratische functies worden benaderd, terwijl erbuiten de metriek heel goed door de Reissner-Nordström-de Sitter geometrie wordt beschreven. Door het gebruik van deze benadering hebben we de correctie op het spectrum in impulsruimte kunnen vaststellen. Bovendien hebben we gezien dat het effect van de magnetische lading van de monopool veel kleiner is dan het effect van zijn massa. Opmerkelijk genoeg blijkt de bijdrage van het inwendige van de monopool niet te kunnen worden verwaarloosd bij het bepalen van de correctie.

Publications

The thesis is based on the following articles:

- I. Khavkine, R. Loll and P. Reska, *Coupling a Point-Like Mass to Quantum Gravity with Causal Dynamical Triangulations*, Class. Quant. Grav. **27**, 185025 (2010).
- T. Prokopec and P. Reska, *Scalar cosmological perturbations from inflationary black holes*, submitted for publication, e-print arXiv: 1007.3851.
- T. Prokopec and P. Reska, *Scalar cosmological perturbations from primordial monopoles*, in preparation.

Other articles to which the author has contributed:

- S. Zohren, P. Reska, R.D. Gill and W. Westra, *A tight Tsirelson inequality for infinitely many outcomes*, Europhys. Lett. **90**, 10002 (2010).

Acknowledgements

First and foremost, I would like to thank my supervisor, Renate Loll, for giving me the possibility to conduct research in the field of quantum gravity, for the guidance, the constant support and the feedback on my scientific work and on my thesis. I am also very grateful to Tomislav Prokopec for fruitful collaboration, for sharing his passion for cosmology with me and for feedback on the manuscript.

Furthermore, it was a great pleasure to work and spend time with Igor Khavkine and Stefan Zohren.

I would like to thank all the people at the ITF for a very friendly and stimulating work environment. In particular, thanks to Anne, Chris, David, Dima, Erik, Jasper, Juliane, Lih-King, Michele, Philipp, Samo and Timothy for common coffee breaks, interesting conversations and comments concerning my work.

Moreover, I am thankful to my former office mates Arnaud, Bas, Daniele, Kevin and Ralph for a nice atmosphere in the office. I also acknowledge the help of the supporting staff, namely, Biene, Els, Geertje, Joost, Olga and Wilma.

During various conferences and workshops I got to know many people. Most notably, I am happy to have met Andrzej and Shiraz who have been working on topics related to my own research.

I wish to thank my friends Alexander H, Angel, Anne M F, Asia, Barbara, Cigdem, Eszter, Felix, Irakli, Karim, Marcin, Marek, Marieke, Neriman, Paresh and Sara for the great time we have spent together in the last years. In addition, I also thank Alexander Q V, José Luis and Slavik for a very pleasant living environment.

Finally, I would like to express my gratitude to my family for encouraging me, giving me advice and being there for me. Thanks to my parents, Kasia, Ania, Tomek and Marcus.

Curriculum Vitae

The author was born on May 4, 1981 in Katowice, Poland. During the years 1992-2001 he attended the Albert-Martmöller-Gymnasium in Witten, Germany. He studied physics and mathematics at the RWTH Aachen University from 2001 to 2004 ('Vordiplom' in physics with highest honors) and was a fellow of the Friedrich-Ebert-Foundation. Subsequently, he followed the Theoretical Physics Master Programme 'Quantum Fields and Fundamental Forces' at Imperial College London and obtained his Master's degree in October 2005 (with distinction). His Master thesis was in the field of quantum chromodynamics and he was supervised by Prof. Dr. Daniel Waldram. In 2006, the author completed a programming internship with Siemens Corporate Research in the United States. In August 2006, he joined the group of Prof. Dr. Renate Loll at the Institute for Theoretical Physics and Spinoza Institute, Utrecht University, as a Marie Curie Fellow in the European Network on Random Geometry. The focus of his research during his PhD was non-perturbative quantum gravity and cosmology. He attended various conferences and workshops where he presented his work. Furthermore, he was teaching assistant of three Master courses at Utrecht University and of several undergraduate courses at RWTH Aachen University.